

ISSN: 0120-1425 • Diciembre de 2022

SERVICIO
GEOLOGICO
COLOMBIANO



bg

Boletín
Geológico

volumen **49**
número 2

<https://revistas.sgc.gov.co/index.php/boletingeo>



Boletín Geológico

Boletín Geológico
Vol. 49, n.º 2, 2022
Periodicidad semestral
ISSN impreso: 0120-1425
ISSN digital: 2711-1318
Servicio Geológico Colombiano

Julio Fierro Morales
Director general

Yenny Paola Casallas
Directora de Geociencias Básicas

John Makario Londoño
Director de Geoamenazas

Marco Antonio Rincón
Director de Recursos Minerales

Hernán Olaya Dávila
Director de Asuntos Nucleares

Juan Manuel Herrera
Director de Hidrocarburos

Hernando Camargo
Director de Laboratorios

Victoria Díaz Acosta
Directora de Gestión de Información

Servicio Geológico Colombiano

Diagonal 53 n.º 34-53
Bogotá, Colombia
Teléfono: (601) 220 0200, ext.: 3048
boletingeologico@sgc.gov.co

Mario Maya
Editor
Boletín Geológico

Comité editorial

Germán Alonso Bayona Chaparro
Cooperación Geológica Ares
Bogotá – Colombia

Matthias Bernet
Université Grenoble Alpes
Francia

Antoni Camprubí Cano
Universidad Nacional Autónoma de México
México

Iván Darío Correa Arango
Consultor
Medellín – Colombia

Thomas Heinrich Cramer
Universidad Nacional de Colombia
Bogotá – Colombia

Tobias Fischer
The University of New Mexico
Estados Unidos

Carlos Jaramillo
Instituto Smithsonian de Investigaciones
Tropicales
Panamá

John Makario Londoño
Servicio Geológico Colombiano
Manizales - Colombia

María Isabel Marín Cerón
Universidad EAFIT
Medellín – Colombia

Camilo Montes Rodríguez
Universidad del Norte
Barranquilla - Colombia

Héctor Mora Páez
Servicio Geológico Colombiano
Manizales - Colombia

Natalia Pardo
Universidad de los Andes
Bogotá – Colombia

Germán A. Prieto
Universidad Nacional de Colombia
Bogotá – Colombia

Yamirka Rojas Agramonte
Universität Kiel
Alemania

John Jairo Sánchez
Universidad Nacional de Colombia
Medellín – Colombia

Luigi Solari
Universidad Nacional Autónoma de México
México

Carlos Augusto Zuluaga Castrillón
Universidad Nacional de Colombia
Bogotá – Colombia

Corrección de estilo en español

Fernando Carretero
Edgar Ordóñez

Traducción y corrección de estilo en inglés

American Journal Experts

Diseño y diagramación

Leonardo Cuéllar V.

Diseño GIS

Cristian Hernández
Jenifer Huertas

Editora general

Carolina Hernández O.

Foto de cubierta

Acuífero San Ignacio asociado a rocas del Complejo Cajamarca Amalfi, Antioquia, Colombia.
Autora: Teresita Betancur V.

Incluida en los siguientes índices y bases de datos:

REDIB
GeoRef
Periódica
Doaj
Dialnet
Google Scholar
Ulrich
Sherpa Romeo

Página web:

<https://revistas.sgc.gov.co/index.php/boletingeo>

Esta obra está bajo licencia internacional Creative Commons Reconocimiento 4.0



Impresión

Imprenta Nacional de Colombia
Carrera 66 N.º 24-09
PBX: (601) 457 8000
www.imprenta.gov.co
Bogotá, D. C., Colombia

Diciembre, 2022

CONTENIDO

3 Editorial

Mario Maya

Data article

5 Macroseismic intensity data and effects of significant earthquakes in Colombia based on historical seismicity studies

Datos de intensidad macrosísmica y efectos de los sismos significativos de Colombia a partir de estudios de sismicidad histórica

Ana Milena **Sarabia Gómez**, Diana Rocío **Barbosa Castro**, María Mónica **Arcila Rivera**

Review article

15 Evolution of arc magmatic cycles from the Carboniferous to the Early Cretaceous in the western paleomargin of Gondwana, north of the Andes

Evolución de los ciclos magmáticos de arco desde el Carbonífero hasta el Cretácico

Temprano, en la paleomargen occidental de Gondwana, norte de los Andes

Gabriel **Rodríguez García**, Ana María **Correa Martínez**, Juan Pablo **Zapata**, Diego Armando **Ramírez**, Carlos Andrés **Sabrica**

Research article

45 Potential and prospects for hydrogeological exploration according to lithostructural criteria in Antioquia department, Colombia

Potencial y perspectivas de exploración hidrogeológica según criterios litoestructurales en Antioquia, Colombia

Teresita **Betancur**, Cristina **Martínez**

Research article

65 Geomechanical characterization of samples in the pilot zone of Bogotá, Colombia, to determine its potential as aggregates for construction

Caracterización geomecánica de muestras en la zona piloto de Bogotá, Colombia, para determinar el potencial como agregados para la construcción

Juan Ricardo **Troncoso Rivera**, Nelly **Páez Fonseca**, Óscar René **Másmela Rodríguez**, Leonardo **Fuentes Aldana** and Roberto **Terraza Melo**

Research article

75 The Upper Cretaceous (Santonian-Maastrichtian) phosphate deposits in the west of the Neiva subbasin, Upper Magdalena Valley, Colombia

El Cretácico Superior con fosfatos (Santoniano-Maastrichtiano) en el occidente de la subcuenca de Neiva, Valle Superior del Magdalena, Colombia

Claudia L. **Martín Rincón**, Roberto **Terraza Melo**, Nadia R. **Rojas Parra**, Germán A. **Martínez Aparicio**, Sandra **Rojas Jiménez**, Juan S. **Hernández González**

97 Corrigendum

Corrigendum to "Interpretation of Palaeozoic geofoms with the use of seismic attributes in a region of the Eastern Plains, Colombia" [*Boletín Geológico*, 49(1), 2022]

Laura Carolina **Esquivel**, Fanny **Villamizar**, Indira **Molina**

98 Editorial Policy and Author Guidelines

EDITORIAL

Boletín *Geológico* publishes Issue 49(2), 2022, with the following articles (Figure 1):

[Sarabia et al.](#) present in a data article the availability of information on the Macro seismic intensities and the effects of earthquakes that have caused considerable damage in Colombia. These data are available to the public through the Historical Seismicity Information System of Colombia (Sistema de Información de Sismicidad Histórica de Colombia [SISHC]), which is an application on the web with free access. There are more than 5000 intensity data points and approximately 4000 reports associated with the effects of historical earthquakes, which can be used in a variety of ways, such as academic, scientific, and institutional studies, historical research, and seismic hazard and risk management evaluations.

[Rodríguez et al.](#) report new and compiled data indicating that arc magmatism in the western paleomargin of Gondwana began in the Carboniferous and continued during the Permian and Early Triassic. Subsequently, the magmatism reactivated during the Early and Middle Jurassic due to the subduction of the Farallon Plate under the continental paleomargin. The arc pluton belts are distributed from the edge of the paleomargin toward the interior of the continent in the same orientation as the slab.

[Betancur and Martínez](#) synthesize useful information to identify potential aquifers for future hydrogeological exploration in Antioquia. This work is based on geological maps of the Servicio Geológico Colombiano (SGC) –scale 1:100 000– and other official sources.

[Troncoso et al.](#) evaluate the potential areas for the exploitation of raw construction materials, considering that these materials are a strategic line for the development of the country. A pilot zone of Bogotá was defined by a radius of 200 km around the city and evaluated, in which lithostratigraphic units with potential for natural aggregates in areas free of mining licenses were studied through geotechnical testing of samples.

[Martín et al.](#) present the results of the geological exploration conducted in the western sector of the Neiva subbasin, Colombia, which included geological mapping at a scale of 1:25 000 and detailed stratigraphic surveys of eleven stratigraphic sections. These works provided a better knowledge regarding the lithostratigraphic units that contain phosphates and their accumulation processes. Additionally, the authors propose an outline of the possible basin paleotopography during the Santonian-Maastrichtian interval.

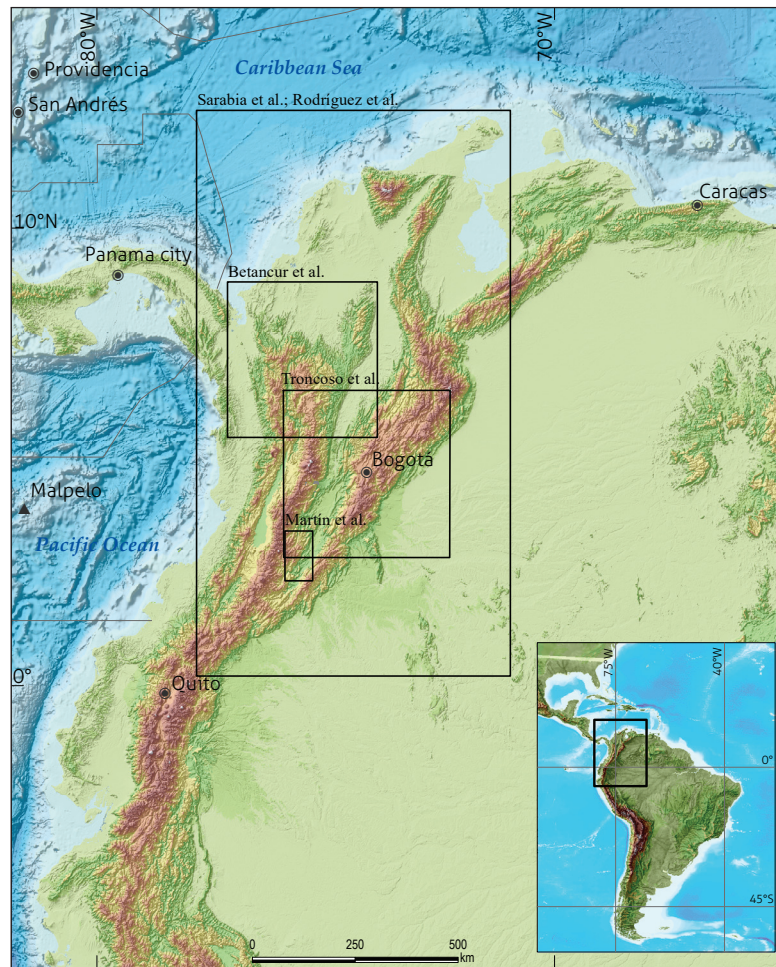


Figure 1. Locations of the areas with contributions presented in *Boletín Geológico*, 49(1), 2022.

Boletín Geológico acknowledges the academic collaboration of the reviewers and their commitment to the peer-reviewed process involved in this issue. The reviewers belong to the following institutions:

- Centro de Desenvolvimento da Tecnologia Nuclear - Brazil
- Defl University, The Netherlands
- Fundación Universitaria Agraria de Colombia
- Universidad de Caldas, Colombia
- Universidad de Sao Paulo, Brazil
- Universidad de Sevilla, Spain
- Universidad EAFIT, Colombia
- Universidad Nacional de Colombia, Colombia
- Universidad Pontificia Bolivariana, Colombia

Mario Maya
Editor

mmaya@sgc.gov.co
boletingeologico@sgc.gov.co



This work is distributed under the Creative Commons Attribution 4.0 License.

Received: November 30, 2021

Revision received: May 30, 2022

Accepted: May 31, 2022

Published online: October 5, 2022

Data article

Macroseismic intensity data and effects of significant earthquakes in Colombia based on historical seismicity studies

Datos de intensidad macrosísmica y efectos de los sismos significativos de Colombia a partir de estudios de sismicidad histórica

Ana Milena Sarabia Gómez¹, Diana Rocío Barbosa Castro¹, María Mónica Arcila Rivera¹

1. Servicio Geológico Colombiano, Bogotá, Colombia.

Corresponding author: Ana Milena Sarabia, asarabia@sgc.gov.co

ABSTRACT

This article presents data on the macroseismic intensities and the effects of earthquakes that have caused significant damage in Colombia, generated in the historical seismicity reports that are prepared for the seismic hazard and risk projects of the Servicio Geológico Colombiano (SGC). These data are the result of research based on the collection, organization and analysis of information related to the effects of earthquakes, according to the methodology of the European Macroseismic Scale of 1998 (EMS-98), which manages descriptions and degrees of intensity according to the effects on people, objects, buildings and nature.

These data are available to the public through the Historical Seismicity Information System of Colombia (Sistema de Información de Sismicidad Histórica de Colombia [SISHC]), which is an application on the web with free access. There are more than 5000 intensity data points and approximately 4000 reports associated with the effects of historical earthquakes, which can be used in a variety of ways, such as academic, scientific and institutional studies, historical research, and seismic hazard and risk management evaluations.

Keywords: earthquake, intensity scale, EMS-98, information system, seismological parameters, seismic hazard.

RESUMEN

En este artículo se presentan los datos de las intensidades macrosísmicas y los efectos de los sismos que han causado daños significativos en Colombia, generados en los informes de sismicidad histórica que se elaboran en los proyectos de amenaza y riesgo sísmico del Servicio Geológico Colombiano (SGC). Estos datos son resultado de la investigación basada en la recopilación, organización y análisis de la información relacionada con los efectos de los sismos, de acuerdo con la metodología de la Escala Ma-

crossísmica Europea de 1998 (EMS-98), que maneja descripciones y grados de intensidad según los efectos ocurridos en personas, objetos, construcciones y naturaleza.

Estos datos se encuentran disponibles al público a través del Sistema de Información de Sismicidad Histórica de Colombia (SISHC), que es un aplicativo en la web de acceso libre, en el cual se encuentran más de 5000 datos de intensidades macrosísmicas y cerca de 4000 datos asociados a efectos de sismos históricos, que pueden ser usados en el ámbito académico, científico e institucional, en investigaciones de historia, amenaza sísmica, gestión del riesgo, entre otros.

Palabras clave: sismo, escala de intensidad, EMS-98, sistema de información, parámetros sismológicos, amenaza sísmica.

1. DESCRIPTION OF THE DATA

The macroseismic intensity data of significant earthquakes, as well as the effects they have caused in different populations of the country, are obtained from historical seismicity studies after the collection and analysis of information by the Seismic Hazard and Risk group of the SGC. These data have national coverage since they were evaluated for populations located in 28 of the 32 departments of Colombia, in addition to the Capital District (Figure 1). However, because earthquakes are continuous phenomena and the political-administrative division of the country has changed throughout history, there are also some estimated data for approximately 80 populations in neighboring countries, such as Venezuela, Ecuador, and Panamá.

The *macroseismic intensity* is defined as a classification of the severity of ground shaking based on observed effects in a limited area. It is independent of instrumental measurements, and it can be applied to both, recent and historical events. To evaluate the intensities, an intensity scale is used that consists of a series of descriptions of the effects produced by a seismic movement, taking into account the *sensors* that define the strength of the earthquake and are easily observable in the environment, such as living creatures, objects, buildings and the natural environment. These scales are numerically closed, generally having 12 ascending degrees, where 1 corresponds to a not felt earthquake and 12 to a completely devastating earthquake, as is the case of the Modified Mercalli scale (MM) and the European Macroseismic Scale of 1998 (EMS-98), both used in the studies of historical seismicity of the SGC.

The *effects* correspond to the perceptions, observations, and damage that occur during a ground shake. These effects are classified into the four *sensors* mentioned, and some examples of them are the loss of balance among people, the vibration or fall of objects, the cracking of walls in buildings and the mass movements triggered by earthquakes.

Historical earthquakes are those that occurred before the implementation of seismological instrumentation that began to operate globally at the beginning of the 20th century and in Colombia, since the 1920s. Even so, the SGC has included in its investigations the study of the intensities of instrumental earthquakes to serve as a comparison to similar historical events. Likewise, the instrumental data of the earthquakes, especially in the first half of the 20th century (except for those of high magnitude), are scarce and of low reliability; for them, the macroseismic intensity data improves the instrumental solutions.

The historical seismicity group of the SGC has studied 81 earthquakes from the 17th century to the present, which have affected the populations of Colombia. The macroseismic data were initially obtained for the most destructive events; that is, those in the seismic catalogs had a maximum intensity ≥ 8 . As these events were studied, the investigation was extended to earthquakes with intensities less than 8.

With this information, reports of macroseismic studies were prepared which are available on the internet in the Geoscientific Information Integration Engine of the SGC (MIIG for its acronym in Spanish). Likewise, to make this information available for free access in a simple, agile and organized way, an application hosted on the web portal called “Historical Seismicity Information System of Colombia” was designed and published (SGC, 2016), which allows the consultation, visualization and download of the historical and macroseismic information of the aforementioned events and is described in the section “Access to the data”.

Before the publication of the application, several authors worked on the collection and analysis of the historical information about the earthquakes, the evaluation of intensities and the seismological analysis, publishing their research in reports, articles, books, and databases (see Ramírez, 1975; Salcedo and Gómez, 2000; Espinosa, 2003; 2012).



Figure1. Populations with macroseismic intensity data on the EMS-98 scale
Source: modified from SGC (2016), <http://sish.sgc.gov.co/visor/>

Currently, 2602 intensity points are stored in the SISHC corresponding to the 81 earthquakes, with an assessment regarding their quality and reliability, and 2447 intensity points, corresponding to evaluations made by other authors for those

same events, which are presented in Table 1. In addition, there is a section with 3934 reports dedicated to the effects that the earthquakes have caused, classified into people, infrastructure, nature and other effects, which are detailed in Table 2.

Table1. Number of intensity points evaluated by the SGC and other authors stored in the SISHC

Date	Local time	Lat.	Long.	Mag.	Depth	SGC IDP	IDP other authors	Imax	Epicentral area
1644/01/16	05:00	7.37	-72.64	6.5	15	5	12	9	Pamplona, Norte de Santander
1644/03/16	12:00	4.46	-74.04	5.5	15	2	12	7	Chipaque, Cundinamarca
1646/04/03	02:00	5.52	-74.13	6.0	15	2	3	8	Muzo, Boyacá
1736/02/02	09:00	2.5	-76.5	6.0	15	1	5	8	Popayán, Cauca
1743/10/18	09:30	4.44	-73.83	6.2	15	13	11	8	Fómeque, Cundinamarca

Date	Local time	Lat.	Long.	Mag.	Depth	SGC IDP	IDP other authors	Imax	Epicentral area
1766/07/09	16:00	3.82	-76.52	6.5	15	5	11	8	Buga, Valle del Cauca
1785/07/12	07:45	2.98	-74.37	7.1	10	17	45	7	Southeast of Cundinamarca
1796/02/15	12:00	7.37	-72.64	5.5	15	1	5	7	Pamplona, Norte de Santander
1805/06/16	03:15	5.37	-74.87	6.1	15	7	14	9	Honda, Tolima
1807/02/17	12:02	6.5	-71.7	5.5	15	1	2	7	Tame, Arauca
1826/06/17	22:30	5.01	-73.59	6.5	15	11	25	8	Úmbita, Boyacá
1827/11/16	18:00	1.8	-75.52	7.1	10	48	141	10	Altamira, Huila
1834/01/20	07:00	1.1	-76.93	6.7	15	29	35	9	Santiago, Putumayo
1834/05/22	03:00	11.5	-74.07	6.4	10	8	4	8	Santa Marta, Magdalena
1869/03/06	06:30	9.0	-74.0	6.0	60	58	0	7/8	El Banco, Magdalena
1875/05/18	11:15	7.86	-72.42	6.8	15	54	50	10	Cúcuta, Norte de Santander
1882/09/07	03:20	10.0	-79.0	6.5	15	17	35	9	Colón, Panamá
1884/11/05	23:45	5.1	-75.5	6.3	120	14	0	8	Hervey, Tolima
1885/05/25	15:05	2.88	-76.54	6.4	15	8	4	8	El Tambo, Cauca
1903/12/01	08:00	6.78	-76.14	5.5	15	2	2	7	Frontino, Antioquia
1906/01/31	10:36	0.99	-79.35	8.8	20	40	51	10	Pacific Coast
1911/04/10	13:42	7.2	-75.3	6.4	120	11	2	7	Yarumal, Antioquia
1917/08/31	06:36	3.78	-74.0	6.7	15	67	44	9	Villavicencio, Meta
1923/12/14	05:31	0.87	-77.78	6.2	10	14	14	9	Cumbal, Nariño
1923/12/22	04:56	4.56	-73.51	5.9	15	29	13	8	Medina, Cundinamarca
1925/06/07	18:41	3.96	-76.31	6.1	120	34	60	7/8	Tuluá, Valle del Cauca
1926/12/18	20:50	0.87	-77.78	6.0	10	9	10	8	Cumbal, Nariño
1928/11/01	11:08	4.95	-73.09	5.9	15	38	23	8	Chinavita, Boyacá
1933/02/10	17:00	1.37	-77.58	5.7	10	5	14	8	Linares, Nariño
1935/08/07	04:00	1.05	-77.31	6.1	10	23	5	8	Tangua, Nariño
1935/09/17	23:58	5.09	-76.08	6.1	15	20	0	8	Pueblo Rico, Risaralda
1935/10/26	20:15	1.07	-77.51	5.9	10	20	0	8	Imues, Nariño
1936/01/09	23:30	1.1	-77.6	5.6	10	16	0	7	Túquerres, Nariño
1936/07/17	12:30	1.17	-77.73	6.3	10	37	3	8	Túquerres, Nariño
1938/02/04	21:23	4.68	-75.69	7.0	150	86	81	8	Colombian Coffee region
1942/05/22	05:30	4.44	-74.64	5.7	15	19	13	7	Girardot, Cundinamarca
1942/12/26	07:30	9.27	-75.52	6.2	15	13	33	8	Lorica, Cordoba
1947/07/14	02:01	1.3	-77.23	6.0	10	60	122	8	Pasto, Nariño
1950/07/08	21:35	7.6	-72.86	6.2	10	41	89	9	Arboledas, Norte de Santander
1952/02/14	16:03	7.36	-76.37	5.9	20	6	10	7	Mutató, Antioquia
1953/12/22	23:45	1.09	-77.59	5.8	10	17	10	8	Guaitarilla, Nariño
1957/04/21	16:12	6.87	-72.09	6.6	25	53	17	7	Malaga, Santander
1957/05/23	21:37	3.7	-76.75	6.1	52.3	16	8	7	Southwest Valle del Cauca
1958/01/19	09:07	1.01	-79.49	7.6	27.5	21	35	8	Esmeraldas, Ecuador
1961/06/16	05:33	8.88	-73.48	6.5	114	20	39	7	Ocaña, Norte de Santander
1961/12/20	08:25	4.49	-75.51	6.8	163	79	75	8	Colombian Coffee Region
1962/02/18	12:25	7.95	-74.81	5.8	46	13	14	7	Maceo, Antioquia
1962/07/30	15:18	5.17	-76.35	6.5	64	107	112	8	Colombian Coffee Region
1966/09/04	17:15	4.62	-73.98	5.3	15	17	16	7	Choachí, Cundinamarca
1967/02/09	10:24	2.85	-74.8	7.0	55	100	158	10	Colombia, Huila
1967/07/29	05:24	6.75	-73.03	6.8	161	123	92	8	Betulia, Santander
1970/09/26	07:02	6.21	-77.49	6.6	15	13	16	8	Bahía Solano, Chocó
1973/04/03	08:53	4.58	-75.57	6.2	150	33	25	7	Salento, Quindío
1973/08/30	13:25	7.14	-72.76	6.3	180	52	58	8	Convención, Norte de Santander
1974/04/17	20:19	6.95	-72.95	5.2	26	9	13	7	Guaca, Santander
1974/07/12	20:18	7.7	-77.58	7.1	10	13	14	8	Pacific Coast
1975/04/05	15:38	10.2	-75.56	5.7	45	14	10	6	Cartagena, Bolívar
1976/04/09	02:09	0.83	-79.57	6.6	17.4	3	45	8	Esmeraldas, Ecuador
1976/07/11	15:41	7.37	-78.11	7.3	17.5	19	11	8	Darién, Panamá
1977/08/30	19:42	7.35	-76.14	6.5	23.3	13	13	7	Apartadó, Antioquia

Date	Local time	Lat.	Long.	Mag.	Depth	SGC IDP	IDP other authors	Imax	Epicentral area
1979/11/23	18:40	4.73	-76.16	7.2	110	99	173	8	Colombian Coffee Region
1979/12/12	02:59	1.56	-79.28	8.1	23.6	56	49	10	Pacific Coast
1981/10/17	23:35	8.14	-72.52	5.9	30	42	150	8	Cúcuta, Norte de Santander
1983/03/31	08:12	2.36	-76.7	5.6	15	10	37	9	Popayán, Cauca
1983/11/22	09:21	0.53	-79.73	6.7	25	7	0	5	Pacific Coast
1988/03/19	23:08	4.41	-73.67	5.0	10	8	0	6	El Calvario, Meta
1991/11/19	15:28	4.52	-77.33	7.2	20	45	25	8	Pacific Coast
1992/10/18	11:12	7.07	-76.8	7.1	10	119	12	10	Murindó, Antioquia
1993/07/21	23:57	6.42	-71.08	6.0	20	7	8	8	Puerto Rondón, Arauca
1994/06/06	15:47	2.89	-75.95	6.8	10	34	0	8	Páez (Belalcázar), Cauca
1995/01/19	10:05	5.1	-72.89	6.5	15	78	95	8	Tauramena, Casanare
1995/02/08	13:40	4.06	-76.56	6.4	71	60	87	8	Calima, Valle del Cauca
1995/02/11	17:45	12.6	-81.52	5.7	15	5	0	6	Archipelago of San Andrés
1995/03/04	18:23	1.25	-77.26	5.0	20	23	11	7	Pasto, Nariño
1999/01/25	13:19	4.43	-75.7	6.1	15	46	12	9	Armenia, Quindío
2004/11/15	04:06	4.69	-77.47	7.2	15	49	4	8	Bajo Baudó, Chocó
2008/05/24	14:20	4.44	-73.81	5.9	10	21	0	8	Quetame, Cundinamarca
2013/02/09	09:16	1.11	-77.56	7.0	162	75	0	7	Guaitarilla, Nariño
2014/10/20	14:33	0.76	-77.95	5.8	10	33	0	6	Chiles, Nariño
2015/03/10	15:55	6.83	-73.13	6.3	157.7	97	0	7	Los Santos, Santander
2016/10/30	19:20	3.41	-74.64	5.2	13.2	62	0	6	Colombia, Huila

Notes: Date: date of the earthquake; Local time: Colombian time (UTC +5); Lat.: Latitude of the epicenter; Long: Longitude of the epicenter; Mag.: Magnitude; Depth: depth in kilometers; SGC IDP: number of intensity data points evaluated by the SGC; IDP other authors: number of intensity data points evaluated by other authors; Imax: maximum intensity evaluated by the SGC; Epicentral area: population or region where the epicenter or the highest intensity was reported.

Source: SGC (2016), <http://sish.sgc.gov.co/visor/>

Table2. Number and description of the effects of earthquakes stored in the SISHC

Category	Effect	Number of associated data
People	Fatalities	204
	Injured people	275
	Victims	9
	Missing	2
Infrastructure	Destruction of public or private buildings	508
	Very heavy damage to public or private buildings	288
	Substantial Damage to public or private buildings	429
	Moderate damage to public or private buildings	829
	Slight damage to public or private buildings	319
	Damage to essential buildings	236
	Damage to road infrastructure	30
	Impact on the provision of public services	46
Nature	Population relocation	15
	Mass movements	192
	Cracks in the ground	97
	Liquefaction	74
	Tsunami/Abnormal waves	76
	Subsidence/Uplift	12
	Hydrological anomalies	13
Other effects	Shaking of trees	5
	Foreshocks	27
	Aftershocks	199
	Waves on the ground	15
	Earthquake sound	33
	Earthquake lights	1

Source: Modified from SGC (2016), <http://sish.sgc.gov.co/visor/>

2. IMPORTANCE OF THE DATA

- » Knowing in detail the intensities and effects of the earthquakes that have caused severe damage in different regions of the country contributes to the evaluation of the seismic hazard on different scales.
- » Obtaining seismological parameters of historical earthquakes allow expansion of the temporal window of earthquake measurement in the country and complement the seismic catalogs.
- » Making evaluations of the intensities available in the two intensity scales most used today in the world: Modified Mercalli and European Macroseismic Scale of 1998.
- » Disseminating appropriate geoscientific knowledge, since the intensity is a qualitative measure based on the damage caused and the extent of the effects, facilitates communication of the seismic risk between the population and the decision-making entities, contributing to the management of the comprehensive risk.
- » Having the data of the intensities and the effects of significant historical earthquakes enables any researcher interested in the subject can make their analyses and interpretations.
- » Investigating historical earthquakes is considered a permanent task since the finding of a new document can modify the intensity data, including the maximum intensity, which

directly affects the evaluation of the seismological parameters; for this reason, the authors are invited to continue with this activity.

3. ACCESS TO DATA

The reports of macroseismic studies that have been carried out during the past 15 years in the SGC are available on the internet through the Geoscientific Information Integration Engine (MIIG), which is part of the web portal of the Servicio Geológico Colombiano. In the supplementary data, the published reports are detailed in chronological order, and a direct link to each document that is available for download is included.

Likewise, to access in a simple and agile way the data of intensities and effects of the most significant earthquakes that have affected the country, an application published on the website of the SGC called “Historical Seismicity Information System of Colombia” was developed. SISHC, presents the interface observed in Figure 2. The system was published in 2012 (decommissioned version) and had significant visualization and performance improvements in 2016, which is the current version. Access to the data is presented in Table 3.

This system allows for five queries through which it is possible to access the specific information on each earthquake, and the results of each are shown on a map and in a table:

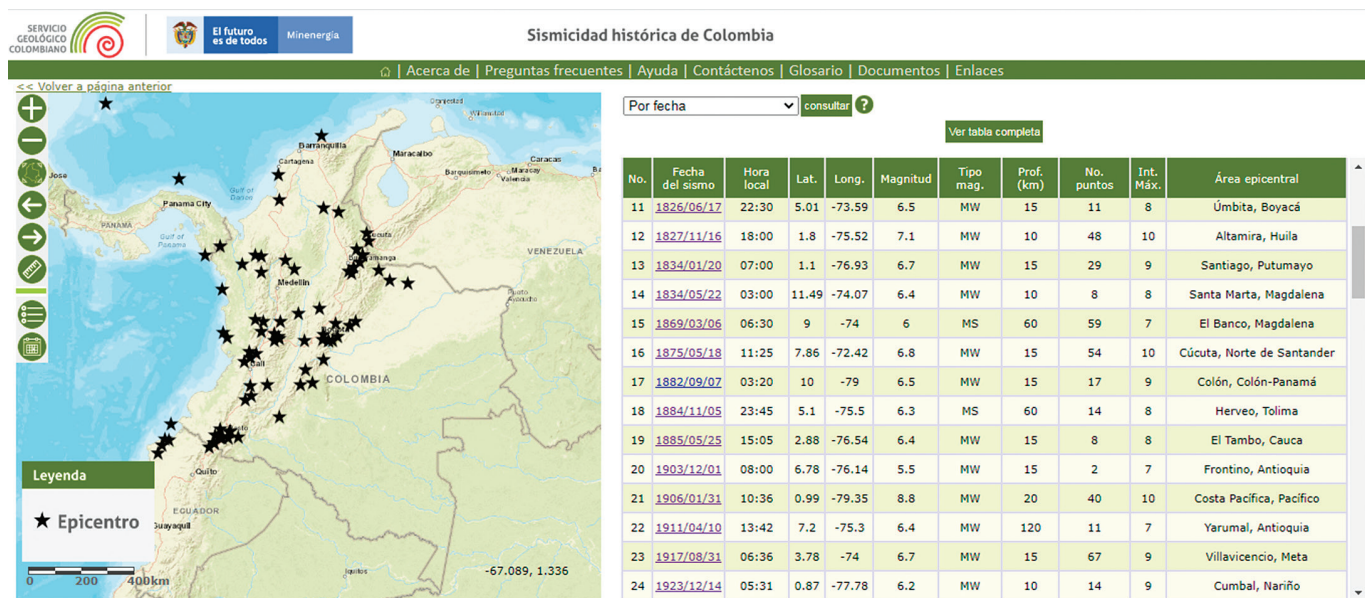


Figure 2. Input interface to the historical seismicity information system
 Source: SGC (2016), <http://sish.sgc.gov.co/visor/>

- a) By date is the default query when accessing the system. It simultaneously displays a map with the epicenters of the earthquakes, including tabular information in chronological order with the general parameters of each earthquake.
 - b) By site, a map is displayed with all the intensities evaluated for the 81 earthquakes, and the intensities evaluated for a department or a municipality, according to the EMS-98 intensity scale, are shown. When reviewing a municipality, a histogram is also generated that shows the intensities that have been reported at that site on a temporal scale.
 - c) By effects categorizes the impact of the earthquakes on people, infrastructure, nature, etc. According to the selected item, the consequences in fatalities, destruction of buildings, mass movements, tsunami, and other effects are identified.
 - d) By large earthquakes, is an query that identifies the most destructive earthquakes in Colombia throughout its history, that is, those that have been classified in intensity greater than or equal to 8 on the EMS-98 scale.
 - e) By quadrant identifies earthquakes based on the delimitation of a quadrant demarcated by coordinates.
- There is an additional query called “For false or doubtful earthquakes”, which presents a list of events recorded in various seismological catalogs and compilations, which are considered false or doubtful due to errors in the date or location or because they simply did not exist.
- To find the detailed information on each earthquake, you can select the hyperlink of the date; in this way, you can access the visualization of this information, with the possibility of downloading most of the content in.pdf and.xls formats, as follows:
- a) Summary: The seismological parameters of the earthquake are presented, as well as a summary of the most relevant effects and some observations that include information related to uncertainties in the seismological parameters, availability of historical documentation, and macroseismic evaluation, among others.
 - b) Documentation: In this section, previous studies of earthquakes, and the archives and libraries consulted are available. Also, documents are listed according to their typology and there is a genealogical tree, which is an image that presents primary documentation of the investigation in chronological order as well as the dependence of the secondary documents with the primary ones (Gisler et al., 2003).
 - c) Intensities: Maps with intensity data points evaluated by the SGC using the EMS-98 scale are presented in this section with a graph that shows the behavior of these intensity values, according to the distance to the hypocenter, a table with the intensities evaluated by multiple authors (including the SGC), the description of the effects occurred in all the sites classified by sensor and a graph that presents the number of sites that reported the same degree or interval of intensity for the earthquake of interest.
 - d) Audiovisual: Images, audio, infographic and videos related to the effects of the earthquake are shown.

4. MATERIALS AND METHODS

Historical seismicity studies, which have been carried out in the SGC, have allowed us to evaluate the effects and intensities of 81 significant earthquakes that occurred in the country from the 17th century to today, taking into account the adequate development of two components:

Table 3. Data specifications

Area	Earth Sciences
Specific subject area	Seismic hazard
Data type	Macroseismic intensity data and associated effects
How the data were acquired	Reports of historical seismicity studies (SGC group)
Data format	Primary and analyzed data
Parameters for data collection	Earthquakes that have caused significant effects in the Colombian territory
Description of data collection	<ul style="list-style-type: none"> - Rigorous search for information in historical archives and libraries - Collection of data on effects on people, objects, buildings and nature - Evaluation of intensity in the EMS-98 and MM scales
Location of the data source	Database and information system at the headquarters of the Servicio Geológico Colombiano, Bogotá, Colombia
Data accessibility	- Historical seismicity reports available on http://sish.sgc.gov.co/visor/

- a) Historical component: Documentary research in archives and libraries includes the initial review of historical and seismological compilations, the identification of the sources and records that have contributed to the compilations and, later, the review of contemporary sources of information about the event and the search for new documents to complement the information and improve the quality of the data. In some cases, surveys are also completed for the evaluation of intensities, which are addressed to the populations.

The most relevant studies on which the search for information has been based were those prepared by Ramírez (1975), Espinosa Baquero (2003 and 2012) and Salcedo and Gómez (2000), as well as the Catalog of Earthquakes for South America (Ceresis, 1985), which constitutes the most complete macroseismic study in South America and in which the intensities of the most significant events on the continent were evaluated and estimated.

The collected documents are scanned and organized according to their typology (book, newspaper, report, magazine, etc.) and, subsequently, a “transcription sheet” for each is prepared according to the practice established by Salcedo and Gómez (1998) in which basic bibliographic information of each source is recorded: author, title and date, as well as the literal transcription of the text that mentions the effects caused by the earthquake.

- b) Macroscopic component: includes the analysis and interpretation of the effects mentioned in the documents, taking into account the geographical context of the time, the typology of the construction, and the quality of the information, among others, to evaluate the intensities of the earthquake at each site from which the data were obtained. These effects are classified into the four sensors that usually handle the intensity scales: living beings, objects, buildings and the natural environment.

To evaluate the intensity, the methodology proposed by Grünthal (2009) was followed, when the *European Macroscopic Intensity Scale of 1998* (EMS-98) was developed, making it possible to include various construction typologies with an associated vulnerability and with the classification of the degree of damage, as well as the management of statistical values to minimize subjective interpretations and personal criterion that authors may give when assigning an intensity. In addition to the EMS-98 scale, the working

group has evaluated the intensities by using the Modified Mercalli scale, historically recognized worldwide.

The intensity values estimated at each site are classified with a criterion of the quality of the assignment as good, acceptable or insufficient since there are uncertainties inherent to the available information, the degree of detail obtained and the reliability of the source.

The results obtained are shown in a table and a map of intensity points. The historical seismicity group of the SGC decided to work with maps of intensity points, unlike most of the authors who had done macroseismic studies in the country and who developed isosist maps that join points of equal intensity value, which, unlike point maps, generalize information, mask relevant data for studies of local effects and prevent the heterogeneous behavior of the intensity distribution from being seen.

5. USE OF THE DATA

The intensity and effect data of earthquakes can be used for several purposes:

- » Complementing the seismic catalog: It is possible to increase the number of earthquakes in the catalogs, including pre-instrumental earthquakes that have occurred since the time of the Conquest, in the 16th century, when the recording of written information began. Seismic catalogs constitute a basic tool for the evaluation of seismic hazards.
- » Proposing macroseismic intensity attenuation models: Through mathematical and statistical processing and calibrations with recent earthquakes, it is possible to develop macroseismic intensity attenuation models that allow estimating and improving the evaluation of parameters such as magnitude (standardized at the Mw scale) and depth and location of historical earthquakes (e.g., Sarabia Gómez, 2016; Gómez et al., 2020, among others).
- » Improving the reliability of the solutions: An adequate record of historical seismicity and its integration with instrumental information constitutes an important tool for the characterization of seismic activity. A recent example, in which macroseismic data contributed to improving the seismological parameters of events in Colombia, is found in Di Giacomo and Sarabia Gómez (2021).
- » Expanding the knowledge of the potential of seismogenic sources: The estimation of the seismological parameters (date, location, magnitude) of the most destructive earth-

quakes is an indispensable element in the characterization of seismogenic sources, especially for the assignment of maximum magnitudes and information, which is fundamental in seismic hazard assessments.

- » Evaluating the seismic hazard: In addition to the contributions mentioned above, such as the expansion of the seismic catalog or seismotectonic characterization, knowledge of the frequency and recurrence of intense earthquakes and their effects is essential for seismic hazard assessments.
- » Developing maps of maximum observed intensity: These maps allow a rapid identification of the areas of the country that have been affected to a greater or lesser extent by earthquakes. A couple of examples of these maps for Colombia were prepared by Estrada and Ramírez (1977) and Sarabia Gómez (2015).
- » Studying local effects and seismic microzoning: Knowledge of the macroseismic intensity data and the detailed effects that historical earthquakes have caused in populations are essential for the development of seismic microzoning studies, as well as for identifying localities or sectors susceptible to presenting local effects.
- » Modeling damage scenarios: Using data of observed macroseismic intensity and the construction typologies in a locality, percentages of the degree of damage to the buildings are established, and in this way, earthquake damage scenarios are defined and serve to formulate response strategies.
- » Knowing the structural behavior of buildings: Knowledge of the behavior of buildings before a shock, taking into account their structure and materials used, are important variables in the determination of macroseismic intensities. This has been essential to raise seismic resistant building codes. Likewise, this information has been essential for the construction of the intensity scales that exist and to propose new scales that have a relationship more in line with the constructive reality of this region, since those currently used come from Europe and the United States.
- » Analyzing the impact of earthquakes: Reviewing the effects of the SISHC allows the preparation of reports related to the social, economic and environmental impact of earthquakes since there is quick access to data such as fatalities, missing persons, victims, damage to road infrastructure, impact on the provision of public services, mass movements, liquefaction, etc.

6. ACKNOWLEDGMENTS

Geographer Hernán Guillermo Cifuentes and physicist María Cristina Dimaté, who at the time was a professor in the Department of Geosciences at Universidad Nacional de Colombia, participated in the development of macroseismic studies and in the structuring of the first version of the Information System (SISHC).

Engineer Berenice Galán Cadena developed the data model for the first version of SISHC. Engineers William Guerrero and Marcela Rubio were in charge of programming and development of the spatial part. The development and implementation of the current version were carried out by systems engineer David Zornosa.

7. CONFLICT OF INTEREST

The authors declare that they have no economic interests or competing personal relationships that could have influenced the work reported in this document.

SUPPLEMENTARY DATA

Supplementary data for this article can be found online at <https://doi.org/10.32685/0120-1425/bol.geol.49.2.2022.638>

REFERENCES

- Ceresis. (1985). *Mapa de intensidades máximas en América del Sur*. (Vol. 12). Serie SISRA.
- Di Giacomo, D., & Sarabia Gómez, A. M. (2021). Use of macroseismic and instrumental data to reassess earthquake locations: Examples from pre-digital earthquakes in Colombia. *Journal of South American Earth Sciences*, 111, 103467. <https://doi.org/10.1016/J.JSAMES.2021.103467>
- Espinosa Baquero, A. (2003). *Historia Sísmica de Colombia, 1550-1830*. Academia Colombiana de Ciencias Exactas, Físicas y Naturales and Universidad del Quindío.
- Espinosa, A. (2012). *Enciclopedia de Desastres Naturales Históricas en Colombia*. Academia Colombiana de Ciencias Exactas, Físicas y Naturales and Universidad del Quindío.
- Estrada Uribe, G., & Ramírez, J. (1977). Mapa de riesgo sísmico. Instituto Geofísico Universidad Javeriana. Bogotá. Cita en: Asociación Colombiana de Ingeniería Sísmica (AIS)

- (1996). Estudio General de Amenaza Sísmica de Colombia. Asociación Colombiana de Ingeniería Sísmica, Universidad de los Andes, Ingeominas. Bogotá.
- Gisler, M., Fäh, D., & Schibler, R. (2003). Two significant earthquakes in the Rhine valley at the end of the 18th century: The events of December 6, 1795 and April 20, 1796. *Eclogae Geologicae Helvetiae*, 96, 357-366. <https://doi.org/10.1007/s00015-003-1095-0>
- Gómez Capera, A., Stucchi, M., Rodríguez, L., Arcila, M., Bufaliza, M., Choy, J., Minaya, E., Leyton, L., Pirchiner, M., Rendón, H., Sarabia, A., Tavera, H., & Yepes, H. (2020). Catálogo de terremotos de América del Sur homogéneo en Mw para el periodo pre-1964. *GEOS*, 40(1). <https://geos.cicese.mx/index.php/geos/article/view/58>
- Grünthal, G. (2009). *European macroseismic scale EMS-98. Notes of the European Center of Geodynamics and Seismology*, (vol. 15). 1, 100.
- Ramírez, J. E. (1975). *Historia de los terremotos en Colombia*. Instituto Geográfico Agustín Codazzi.
- Salcedo Hurtado, E. de J., & Gómez Capera, A. A. (1998). *Sismicidad histórica y reciente base de datos*. Ingeominas.
- Salcedo Hurtado, E. de J., & Gómez Capera, A. G. (2000). *Sismotectónica del territorio colombiano. Atlas macrosísmico de Colombia*. Ingeominas.
- Sarabia Gómez, A. M. (2015). *Mapa de intensidades máximas observadas para Colombia*. Servicio Geológico Colombiano. <https://recordcenter.sgc.gov.co/B6/21001100024689/documento/pdf/2105246891101000.pdf>
- Sarabia Gómez, A. M. (2016). *Relación de atenuación de la intensidad sísmica para sismos corticales en Colombia. Método Bakun & Wentworth*. Servicio Geológico Colombiano.
- Servicio Geológico Colombiano (SGC). (2016). Sistema de información de Sismicidad Histórica de Colombia. <http://sish.sgc.gov.co/visor/>
- Servicio Geológico Colombiano. (2022). Motor de Integración de información geocientífica (MIIG). <https://miig.sgc.gov.co/>



This work is distributed under the Creative Commons Attribution 4.0 License.

Received: May 6, 2022

Revision received: June 16, 2022

Accepted: June 21, 2022

Published online: October 28, 2022

Review article

Evolution of arc magmatic cycles from the Carboniferous to the Early Cretaceous in the western paleomargin of Gondwana, north of the Andes

Evolución de los ciclos magmáticos de arco desde el Carbonífero hasta el Cretácico Temprano, en la paleomargen occidental de Gondwana, norte de los Andes

Gabriel Rodríguez García¹, Ana María Correa Martínez¹, Juan Pablo Zapata¹, Diego Armando Ramírez¹, Carlos Andrés Sabrica¹

1. Servicio Geológico Colombiano, Special Geological Studies Group, Medellín, Colombia.

Corresponding author: Gabriel Rodríguez García, grodriguez@sgc.gov.co

ABSTRACT

This work presents a considerable volume of new and compiled data indicating that arc magmatism in the western paleomargin of Gondwana began in the Carboniferous and continued during the Permian and Early Triassic. Subsequently, the magmatism reactivated during the Early and Middle Jurassic due to the subduction of the Farallon Plate under the continental paleomargin. The arc pluton belts are distributed from the edge of the paleomargin toward the interior of the continent in the same orientation as the slab (west–east direction).

During the Carboniferous, between ca. 333 Ma and ca. 300 Ma, magmatism formed small calcic metaluminous gabbro and leucotonalite plutons of tholeiitic to calc-alkaline affinity on the western margin of Gondwana. Later, the second belt of arc plutons formed during the Permian/Triassic (between ca. 300 Ma and ca. 234 Ma) and are represented by metaluminous to peraluminous calc-alkaline to high-K calc-alkaline batholiths and stocks of heterogeneous composition (granites, granodiorites, diorites, quartz monzonites, and monzonites), which were intruded by dikes and minor granite bodies during the Middle Triassic.

Between ca. 214 Ma and ca. 186 Ma, peraluminous plutons of batholithic dimensions of monzogranitic to syenogranitic composition developed in the back-arc. Between ca. 197 Ma and ca. 186 Ma, back-arc magmatism occurred, while a new magmatic cycle began along the arc axis. At the end of the Jurassic, the magmatic arc cycle ended in the northwestern paleomargin of Gondwana (ca. 164 Ma). The intrusion ca. 159 Ma of porphyritic bodies of alkaline andesitic basalts toward the edge of the continental margin suggests the strangulation and collapse of the subduction zone in the mantle.

Citation: Rodríguez García, G., Correa Martínez, A. M., Zapata, J. P., Ramírez, D. A., & Sabrica, C. A. (2022). Evolution of arc magmatic cycles from the Carboniferous to the Early Cretaceous in the western paleomargin of Gondwana, north of the Andes. *Boletín Geológico*, 49(2), 15-43. <https://doi.org/10.32685/0120-1425/bol.geol.49.2.2022.663>

To the west, off the continental margin, a new arc magmatic cycle began over a different continental terrane ca. 171 Ma and extended to ca. 138 Ma, giving rise to a belt of calcic to calcic-alkaline plutons emplaced in the Ordovician metamorphic (Anaconda Terrane), Triassic (Tahamí Terrane), and Upper Jurassic (Tierradentro Orogen) rocks. The assemblage amalgamated to the western margin of Gondwana in this period.

Keywords: Colombia, arc magmatism, evolution of the Andes.

RESUMEN

Este trabajo presenta un volumen considerable de datos, nuevos y compilados, los cuales indican que el magmatismo de arco, en la paleomargen occidental de Gondwana, inició en el Carbonífero, continuó en el Pérmico y tuvo un evento menor a principios del Triásico. Posteriormente el magmatismo se reactivó durante el Jurásico Temprano y Medio debido a la subducción de la placa Farallones bajo la paleomargen continental de Gondwana. Los cinturones de plutones de arco se distribuyen desde el borde de la paleomargen hacia el interior del continente, en el mismo sentido del slab, es decir, en dirección oeste-este.

Durante el Carbonífero, entre ca. 333 Ma y ca. 300 Ma, inició un magmatismo que formó pequeños plutones de gabros y leucotonalitas toleíticas a calco-alcálicos, metaluminosos cálcicos, el cual se localizó en la margen occidental de Gondwana. Inmediatamente después se formó un segundo cinturón de plutones de arco durante el Pérmico (entre ca. 300 Ma y ca. 234 Ma), representado por batolitos y stocks de composición heterogénea (granitos, granodioritas, dioritas, cuarzomonzonitas y monzonitas), calco-alcálicos a calco-alcálicos de alto K, metaluminosos a peraluminosos, de granitoides cálcicos, calco-alcálicos y alcalino-cálcicos, los cuales fueron intruidos por diques y cuerpos menores de granitos durante el Triásico Medio.

Entre ca. 214 Ma y ca. 186 Ma se presentó magmatismo peraluminoso de composición monzogranítica a sienogranítica en el trasarco, y se formaron plutones de dimensiones batolíticas. Entre ca. 197 Ma y ca. 186 Ma, el magmatismo de trasarco ocurrió al tiempo que inició un nuevo ciclo magmático en el eje del arco. A finales del Jurásico finalizó el ciclo magmático de arco en la paleomargen noroccidental de Gondwana (ca. 164 Ma). La intrusión a ca. 159 Ma de cuerpos porfídicos de basaltos andesíticos alcalinos, hacia el borde de la margen continental, sugiere el estrangulamiento y el colapso de la zona de subducción en el manto.

Al occidente, por fuera de la margen continental, comenzó un nuevo ciclo magmático de arco sobre otra masa continental a ca. 171 Ma y se extendió hasta ca. 138 Ma, dando origen a un cinturón de plutones cálcicos a cálcico-alcálicos emplazado en rocas metamórficas del Ordovícico (terreno Anaconda), Triásico (terreno Tahamí) y Jurásico Superior (Orogéno de Tierradentro). El conjunto fue amalgamado a la margen occidental de Gondwana en este periodo.

Palabras clave: Colombia, magmatismo de arco, evolución de los Andes.

1. INTRODUCTION

Among the problems of the Carboniferous to Cretaceous magmatic interpretations of the northwestern paleomargin of South America are, until a few years ago, the lack of available U-Pb geochronology and whole-rock geochemistry data, the regional separation and grouping of the plutonic and volcanic bodies, and their spatial correlation. This uncertainty has resulted in the use of geological units that belong to different magmatic events in the interpretations.

Arc magmatism in the western paleomargin of Gondwana has been considered to have begun at the end of the Triassic and continued until the Lower Cretaceous due to the subduction of the Farallon Plate under the western margin of Gond-

wana (Álvarez, 1983; Bayona et al., 1994; Bustamante et al., 2016; Jaramillo and Escovar, 1980; Leal-Mejía, 2011; Leal-Mejía et al., 2019; Rodríguez et al., 2015f, 2018, 2020; Quandt et al., 2018; Quiceno et al., 2016; Spikings et al., 2015; Toussaint, 1995; Villagómez et al., 2015; Zapata et al., 2016; Zuluaga et al., 2015; Zuluaga and López, 2019). Under this framework, two models were postulated: 1) migration of arc magmatism in an east-west direction (Bayona et al., 2010; Bustamante et al., 2016; Leal-Mejía et al., 2019; López and Zuluaga, 2020; Quandt et al., 2018; Ramírez et al., 2020; Zuluaga and López, 2019) and 2) migration of magmatism in a west-east direction (taking into account the migration of the magmatic cycles of the Permian and the Early to Middle Jurassic) (Rodríguez et al., 2018; 2020a, 2020b).

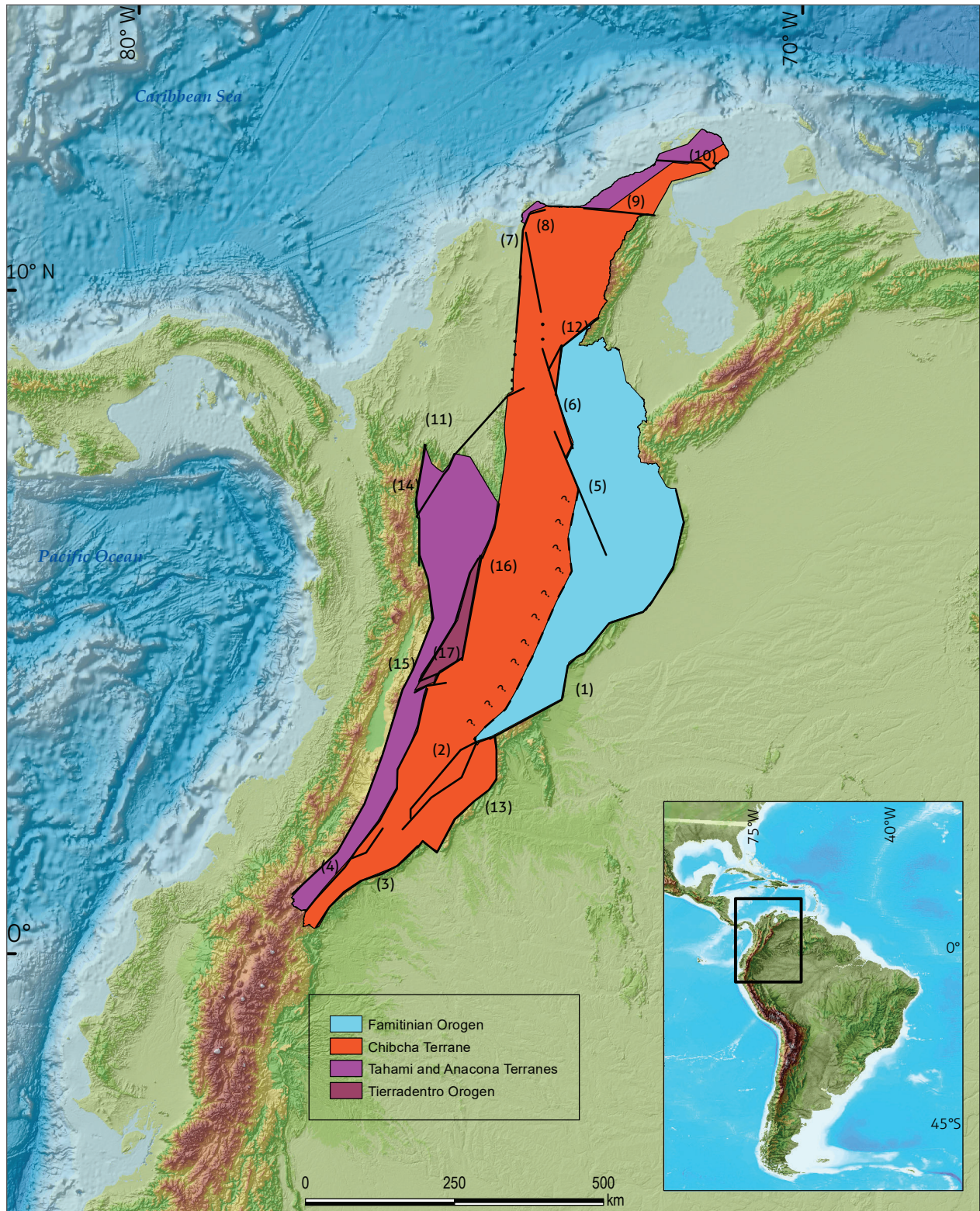


Figure 1. Terrains and orogens where the Carboniferous to Lower Cretaceous magmatic cycles were emplaced
 1. Eastern Fault System; 2. Algeciras Fault System; 3. Los Loros Fault System; 4. San Francisco - Yungillo Fault System; 5. Bucaramanga Fault; 6. Ocaña Fault; 7. Santa Marta Fault; 8. Orihueca Fault; 9. Oca Fault; 10. Cuisa Fault; 11. Espiritu Santo Fault; 12. Arenas Blancas Fault; 13. Caguán System Fault; 14. Romeral Fault System; 15. San Jerónimo Fault; 16. Palestina Fault; 17. Ibagué Fault.

In this work, nine U-Pb zircon ages are reported, whose importance lies in the discovery of three new units that were not previously described in the literature on the geology of Colombia and the improvement in the information of the three other units. In addition, this paper presents a considerable volume of published ages derived from the research conducted by the Servicio Geológico Colombiano. The information on the whole-rock geochemistry of numerous plutons is also supplemented. This research analyzes the magmatic cycles formed from the Carboniferous to the Lower Cretaceous, the zircons inherited from the initial cycles, the geochemical composition of each cycle, and the geotectonic position of the magmatic belts with respect to the paleomargin of Gondwana in northern South America. In addition, a correlation is drawn of the units constituting the belts that make up a magmatic cycle and the position they currently occupy in the Andes of Colombia.

This study seeks to clarify the magmatic evolution of the arcs between the Carboniferous and the Lower Cretaceous, showing the correlation of units that make up each cycle, and presenting the development model of the magmatic cycles in the continental paleomargin of northwestern South America.

2. GEOLOGICAL FRAMEWORK

The western margin of Gondwana in northern South America was formed up to the Carboniferous by the Guyana Shield (northern half of the Amazonian Craton), which is currently located east of Colombia and is represented by units with ages of 2.5-1.5 Ga (Priem et al., 1982; Restrepo-Pace and Cedié, 2019). The western part of this shield in Colombia is composed of granitoids and high-grade metamorphic rocks that are part of the Río Negro Belt (1.84-1.72 Ga) (Kroonenberg, 2019; Tassinari 1981; Tassinari and Macambira, 1999), which is intruded by anorogenic granitoids of 1.55 Ga, such as the Parguaza Rapakivi Granite, and locally covered by sandstones and meta-sandstones of Naqué, Pradera, and Tunuí (Kroonenberg, 2019).

The Andean margin currently rises to the west of the cratonic domain, and it is composed of a basement of high-grade metamorphic rocks (granulite to high amphibolite facies) along with some igneous bodies probably formed during the continental collision of Amazonia and Laurentia during the Grenville Orogeny (Cordani et al., 2010; Ibáñez-Mejía et al., 2011; Kroonenberg 1982; Kroonenberg, 2019). The units that make up the Andean margin are the Garzón Group, Mancagua and Guapotón gneisses, Las Minas migmatites, El Recreo gra-

nite, San Lucas gneiss, Los Mangos granulite, Buritaca gneiss, and Jojoncito gneiss (Cuadros, 2012; Cuadros et al., 2014; Ibáñez-Mejía et al., 2011, 2015; Jiménez Mejía et al., 2006; Kroonenberg and Diederix, 1982; Ordoñez-Carmona et al., 2002; Piraquive, 2017; Rodríguez, 1995a, b; Rodríguez et al., 2003; Tschanz et al., 1969; Tschanz et al., 1974; Velandia et al., 1996, 2001). These units present ages between 1.2 and 0.85 Ga (Ibáñez et al., 2011, 2015) and are denominated in some studies as the Chibcha Terrane (Figure 1) (Restrepo and Toussaint, 1989, 2020; Restrepo et al., 2009) or the Putumayo Orogen (Ibáñez et al., 2011, 2015). On this basement, arc magmatic belts were developed during the Carboniferous, Permian, and Early to Middle Jurassic, extending from northern (the upper Guajira and Sierra Nevada) to southern Colombia and into Ecuador (Figure 2).

Lower Paleozoic (Figure 1) and Ordovician rocks (Mantilla et al., 2016; Restrepo-Pace, 1995) are found between the Amazonian Craton and the Chibcha Terrane (in the Santander, Floresta, Quetame, and Mérida Andes massifs), extending in fragments from Chile to Venezuela along the western proto-margin of Gondwana (Otamendi et al., 2017; Ramos, 2008). This orogen is represented in Colombia by sedimentary and metasedimentary units of very-low-grade schists, migmatitic gneisses, paragneisses, and syntectonic and posttectonic granitoids (Mantilla et al., 2016; Rodríguez, 2022; Tazzo-Rangel et al., 2018; Van der Lelij et al., 2016), which reached the upper amphibolite and granulite facies at the top of the Famatinian Orogeny (~470 Ma) (Tazzo-Rangel et al., 2018; Zuluaga et al., 2017).

On this orogen, at the end of the Triassic and the beginning of the Jurassic (~214-184 Ma) (Rodríguez et al., 2017, 2019; Van der Lelij et al., 2016), magmatism that formed peraluminous, I- and S-type (López and Zuluaga, 2020; Rodríguez et al., 2017, 2019b, 2020; Zuluaga and López, 2019) batholithic bodies and stocks of predominantly monzogranitic to syenogranitic composition (Figure 2a) (Rodríguez et al., 2017, 2020a; Ward et al., 1973) developed in a more eastern position than the belts of the volcanic arcs of the Carboniferous (Leal Majía, 2011), Permian, and Lower to Middle Jurassic (Rodríguez et al., 2019, 2020a, 2020b) (Figure 2a and b).

3. DISTRIBUTION OF MAGMATIC BELTS

The arc magmatic belts that are discussed in this article are mostly emplaced in the Chibcha Terrain, the Famatinian Oro-

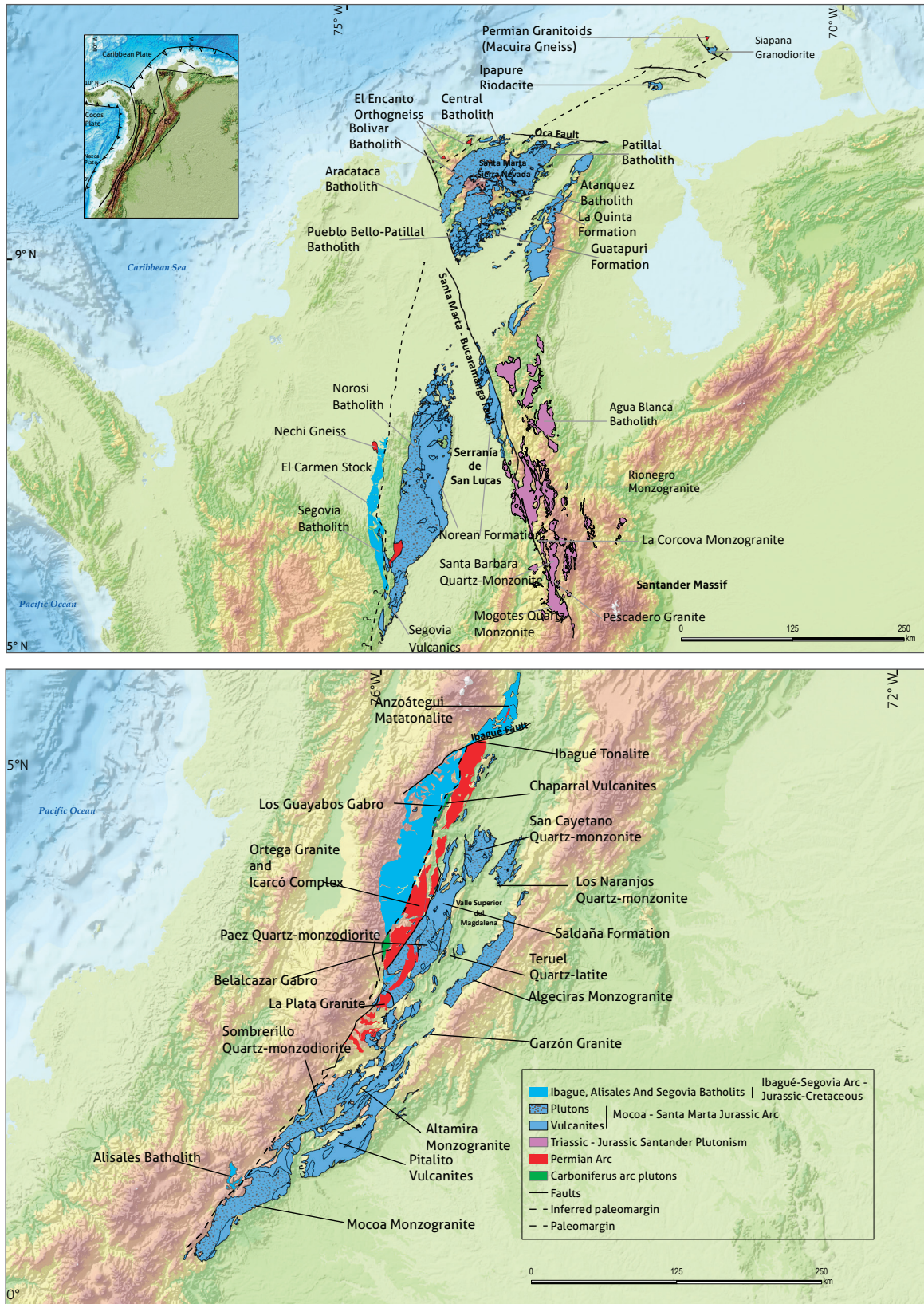


Figure 2. Distribution of the Carboniferous to Lower Cretaceous magmatic belts on the western margin of northern Gondwana in Colombia

gen, and to a lesser extent in the Tahamí and Anacona Terranes (Figure 1). These belts occupy part of the Central and Eastern cordilleras, the San Lucas range, the Sierra Nevada de Santa Marta, and La Guajira.

According to Restrepo and Toussaint (2020), the Chibcha Terrane mainly consists of a Grenvillian metamorphic basement (Stenian-Tonian) and Famatinian (Caledonian) low- to mid-grade metamorphic rocks. We consider the Andaqui Terrane of Restrepo and Toussaint (2020) part of the Chibcha Terrane, and we extracted the Famatinian Orogen (Santander, Floresta, and Quetame massifs). To the west, the limit of the Chibcha Terrane with the Tahamí and Anacona Terranes and the Tierradentro Orogen (which is described below), rather than the faults described by Restrepo and Toussaint (2020), corresponds to the undeformed pluton belts of the Carboniferous, Permian, and Early–Middle Jurassic continental margin arc magmatic cycles. These belts mark the limit of the western margin of Gondwana.

The Carboniferous rocks are distributed in a discontinuous belt of gabbros and tonalites, which currently crop out on the eastern slope of the Central Cordillera of Colombia. To the east of the Carboniferous rocks, also on the western margin of the Chibcha Terrane, a belt of batholiths and Permian stocks of varied composition (granites, granodiorites, diorites, quartz monzonites, and monzonites) was formed. Currently, the Permian plutons are dispersed along the western margin of the Chibcha Terrane, on the eastern slope of the Central Cordillera, in the San Lucas range, in the Sierra Nevada de Santa Marta, and in the La Macuira range. Some of the blocks to the north of the Ibagué fault are deformed and crop out next to metamorphic rocks of the Anacona and Tahamí Terranes identified by Restrepo and Toussaint (2020).

The batholiths and granitic stocks of the Santander massif, generated between the Late Triassic and Early Jurassic, crop out in the eastern part of the Famatinian Orogen in the eastern cordillera.

The belt of batholiths and stocks (monzodioritic, quartz monzodioritic and tonalitic) and volcanic and pyroclastic rocks formed between the Early Jurassic and the Middle Jurassic currently occupy a more eastern position than the Carboniferous and Permian plutons within the Chibcha Terrane, cropping out on both sides of the Upper Magdalena Valley, the Serranía de San Lucas, the Sierra Nevada de Santa Marta, the Serranía del Perijá, and in the Upper Guajira in the Serranía de Cosinas (Figure 1).

Of the belt of tonalitic to granodioritic batholiths and stocks formed from the Middle Jurassic to the Lower Cretaceous, some are in the suture, intruding the Anacona, Tahamí, and Chibcha Terranes. Others were emplaced within the Anacona and Tahamí Terranes, raising blocks of these two terrains that are conserved as roofs inside the plutons. The position of these plutons is more western than the belts of the Carboniferous, Permian, and Early to Middle Jurassic arcs. Currently, these plutons crop out in the axis and the eastern slope of the Central Cordillera and extend to the upper Guajira in the Serranía de La Macuira.

4. MATERIALS AND METHODS

For the development of this research, a regional sampling was made that included the Central Cordillera, upper Magdalena valley, Santander massif, Sierra Nevada de Santa Marta, Perijá range, and upper Guajira. The new data are integrated with results collected from previous works by the authors and others (Bustamante et al., 2010; Cuadros, 2012; Cuadros et al., 2014; González et al., 2015; Leal-Mejía, 2011; Quandt et al., 2018; Villamizar et al., 2021; Zapata et al., 2016, among others). The geochemical and U-Pb geochronology data were grouped according to the correlation of units of each magmatic cycle.

4.1. Whole-rock geochemical analyses

We compiled whole-rock geochemical analyses of the units that make up each magmatic belt, from the Carboniferous to the Lower Cretaceous, and collected new data in the unknown units (Belalcázar and Los Guayabos gabbros). The whole-rock geochemical analyses were performed in the Laboratory of Analytical Geochemistry of the Servicio Geológico Colombiano, Bogotá headquarters. The major oxides and minor elements were analyzed with a Panalytical AXIOS Mineral X-ray fluorescence spectrometer. The former were quantified from samples fused with lithium metaborate and tetraborate, while the latter were quantified in pressed samples. For the analysis of trace elements, a mass spectrometer with inductively coupled plasma, Perkin Elmer NEXION, was used.

The geochemical diagrams were obtained using the GCD-kit *software* of Janoušek et al. (2006).

4.2. Geochronology

The geochronological analyses of the units that make up each magmatic belt from the Carboniferous to the Lower Creta-

ceous were compiled, and in some undescribed units, new U–Pb analyses were performed by laser ablation inductively coupled plasma–mass spectrometry (LA–ICP–MS) in zircon.

The new analyses were performed on rock chips that were crushed, pulverized, and sieved following the separation procedures of Castaño et al. (2018) and analyzed via LA–ICP–MS according to the procedures described in Peña et al. (2018). The zircons were concentrated in the Chemical Laboratory of the Servicio Geológico Colombiano, Medellín, using hydrodynamic and magnetic separation, although some samples were concentrated in the field by panning. Then, the crystals were selected manually with the help of an Olympus binocular magnifying glass in the Petrography Laboratory, Medellín headquarters. Cathodoluminescence (LC) images were acquired from the zircon grain mounts.

The analyses were performed in Photon Machines ablation equipment with a 193 nm excimer laser coupled to an Element 2 mass spectrometer. The isotopes used for manual integration were ^{238}U , ^{206}Pb , and ^{204}Pb . Plešovice (Sláma et al., 2008), FC-1 (Coyner et al., 2004), 91500 (Wiedenbeck et al., 1995, 2004), and Mount Dromedary (Renne et al., 1998) were used as reference standards. The spots analyzed in the zircons were 20 microns in diameter. Data reduction was performed using the Iolite v2.5* program in IGOR Pro 6.3.6.4* (Hellstrom et al., 2008; Paton et al., 2010). The correction for common lead was performed according to the evolution model of Stacey and Kramers (1975). The results correspond to the mean of the data obtained after applying data discrimination to two standard deviations.

5. RESULTS

Figure 2 shows the current location of the magmatic belts defined by Rodríguez et al. (2019, 2020b), Leal et al. (2019), and

in the present work. The new ages obtained in this study are presented in Table 1. Supplementary Table TS1 summarizes the U–Pb data used to obtain the probability density plots of the magmatic cycles and presents 324 U–Pb ages in zircons obtained by different laboratories, mainly using LA–ICP–MS procedures, including the zircon ages of the nine rocks collected by the authors (Table 1) in regions without previous dating. Supplementary Table TS2 shows the chemical results, including the new analyses, which are used in the chemical classification diagrams of each magmatic cycle.

5.1. Geochronology

Los Guayabos and Belalcázar gabbros. Sample DAR-028 corresponds to a tonalite that outcrops near gabbro and gabbro breccia (composed of angular gabbro blocks of varied shapes and sizes surrounded by white leuco-tonalites). Sample WB-162 corresponds to a gabbro collected west of Belalcázar (Cauca). The zircons of sample DAR-028 are subhedral and euhedral prismatic, slightly pink, translucent, and *stubby*; some present inclusions, and most have fractured edges. In the CL image, the zircons have concentric zoning, in which the difference between the ages of the nucleus and the edges is approximately 10 Ma. The zircons of sample WB-162 are prismatic, colorless, and euhedral, with lengths between 100 and 200 μm and widths between 40 and 150 μm . In the CL images, it is possible to identify parallel banded linear textures in shades of light and dark gray (Figure 3).

For the calculation of the age of the DAR-028 sample, data with discordant values > 10% and precision errors > 5% were discarded. For the WB-162 sample, data with discordant values > 5% and precision errors > 3% were discarded. The average age for the DAR-028 sample was 317.2 ± 1.3 Ma ($n = 58$, MSWD = 2.4). The average age of the WB-162 sample was 325.9 ± 2.4 Ma ($n = 42$, MSWD = 3.3) (Figure 4). Both

Table 1. Carboniferous to Cretaceous U–Pb ages from rocks related to arc magmatic cycles

Sample			Rock	Unity	U–Pb Age (Ma)	MSWD
WB-162	1122000	791840	Gabbro	Belalcázar gabbro	325.9 ± 2.4	3.3
DAR-028	935484	843111	Tonalite	Los Guayabos gabbro	317.2 ± 1.3	2.4
AMC-0194	1735620	1026510	Mylonitic orthogneiss	El Encanto orthogneiss	276.2 ± 1.3	2.0
GOE-1106A	1842115	971410	Mylonitic gneiss	Macuira gneiss	278.5 ± 1.8	3.3
GOE-1106B	1842066	971421	Monzogranite	Macuira gneiss	288.7 ± 1.5	2.7
JPZ-376	1157889	817853	Granodiorite	Páez quartz monzodiorite	184.7 ± 0.9	3.8
GOE-1127	1161083	826740	Monzogranite	Páez quartz monzodiorite	187.4 ± 1.7	2.9
MIA-684	1827161	974762	Granodiorite	Siapana granodiorite	166.5 ± 1.5	2.6
GR-6808	1036215	1734551	Pl-Hbl mylonitic gneiss	Buritaca gneiss	151.3 ± 3.6	2.7

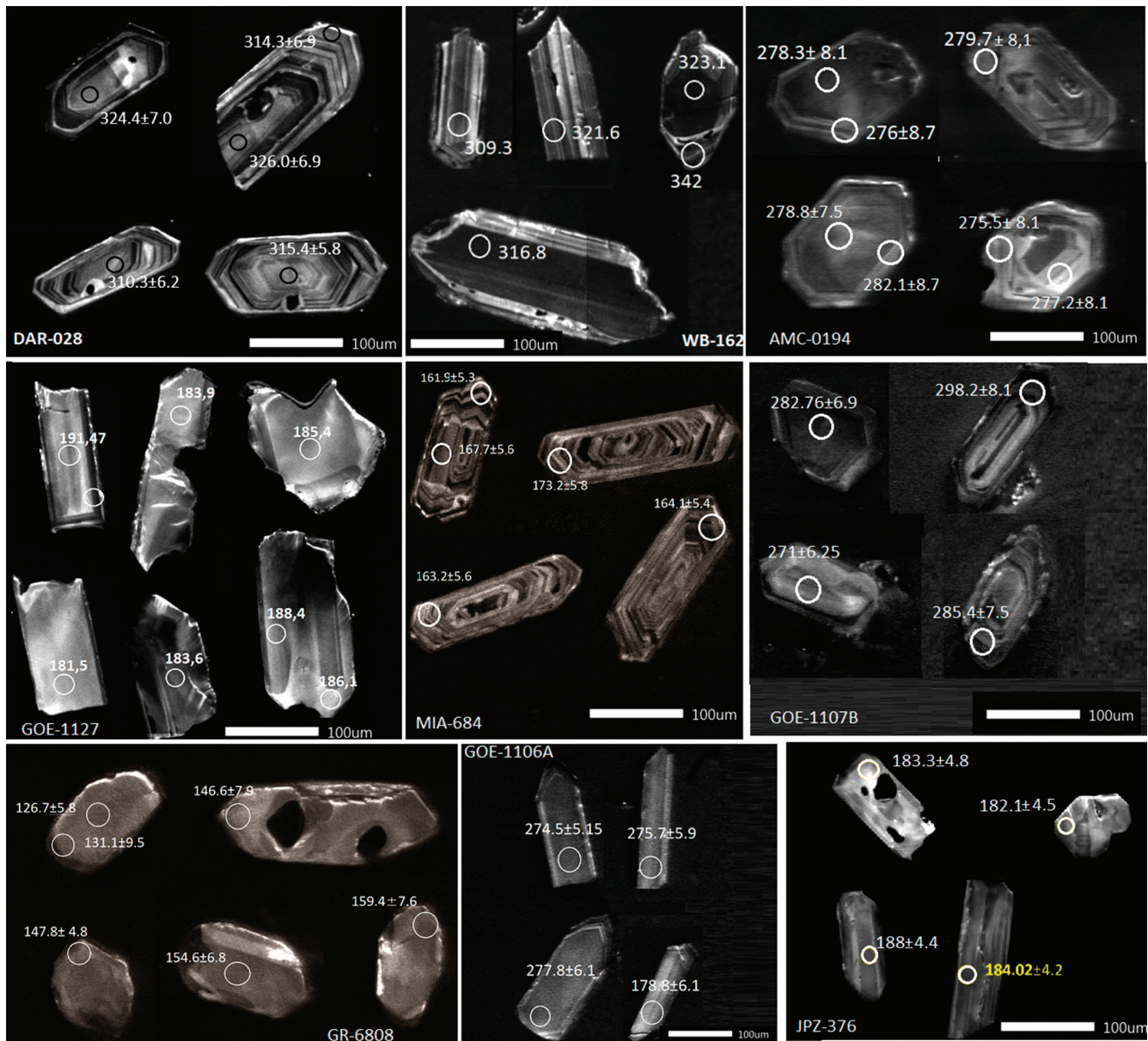


Figure 3. Representative cathodoluminescence images of zircon crystals of each dated sample

results are interpreted as crystallization ages with Th/U ratios between 0.2 and 1.7, typical of igneous zircons (Rubatto, 2002).

El Encanto orthogneiss and Permian ages in the Serranía de Macuira. Sample AMC-0194 corresponds to a plagioclase-quartz-amphibole-biotite-titanite mylonitic orthogneiss collected along the Buritaca-Guachaca road. The zircons are euhedral, colorless with a slight pale pink hue, generally without inclusions, with lengths between $80 \times 150 \mu\text{m}$ and $100 \times 200 \mu\text{m}$,

indicating *short stalky* shapes. In the CL images, the crystals are prismatic with homogeneous gray nuclei and edges with concentric zoning in different shades of gray (Figure 3).

For the calculation of age, data with discordant values $> 10\%$ and precision errors $> 5\%$ were discarded. The average age calculated for the AMC-0194 sample is $276.2 \pm 1.3 \text{ Ma}$ ($n = 101$, MSWD = 2.0), which is interpreted as the age of rock crystallization, in which Th/U ratios vary between 1 and 3.1, typical for igneous zircons (Rubatto, 2002).

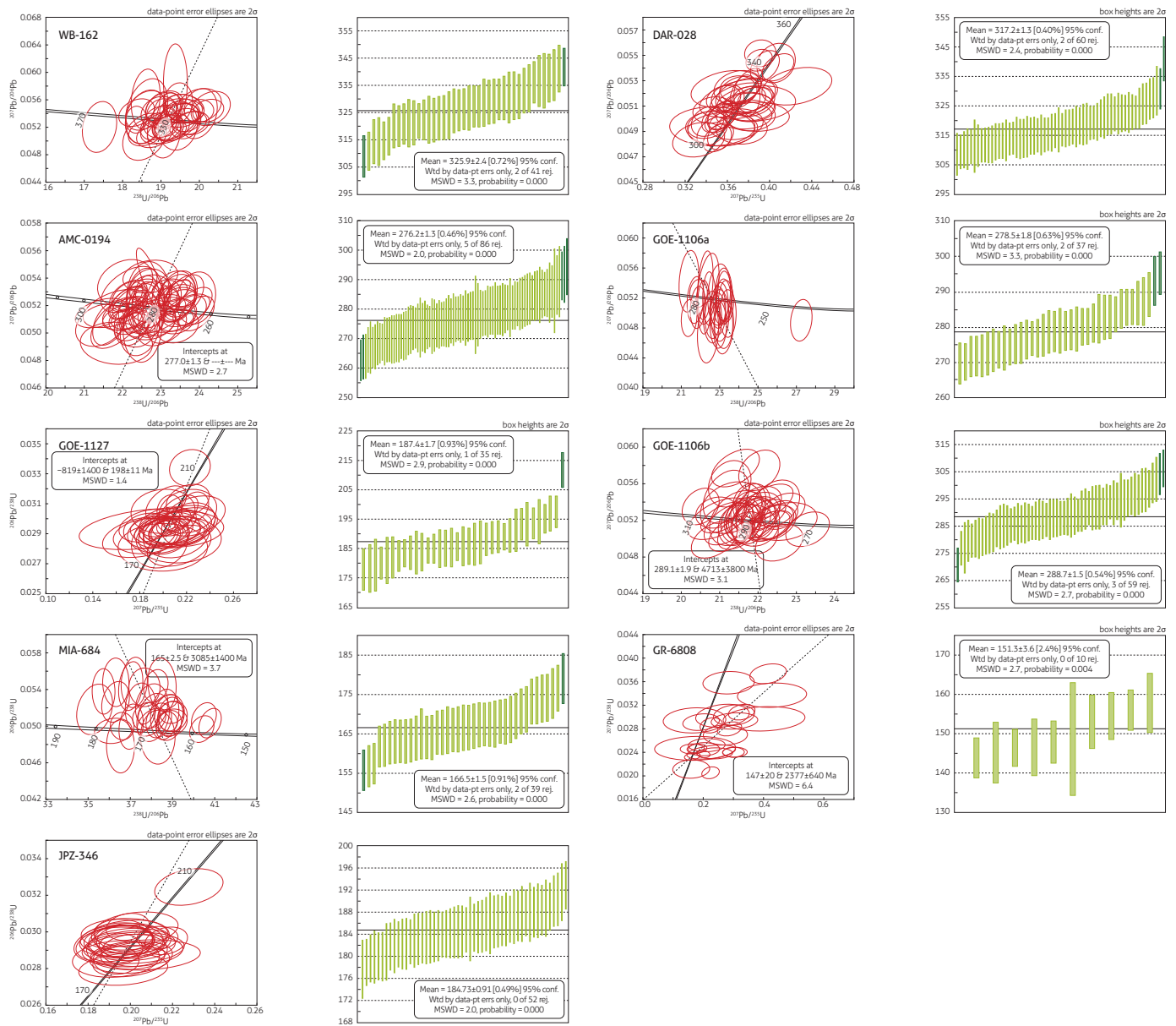


Figure 4. Wetherill and Tera-Wasserburg concordia diagrams and weighted mean age of the samples dated by the U-Pb method in zircon

In the Serranía de Macuira, two ages are calculated in rocks that are mapped as Macuira gneiss, corresponding to samples GOE-1106a and GOE-1106b, classified as a mylonitic granitoid and as a deformed monzogranite, respectively. The zircons of sample GOE-1106a are prismatic euhedral, stalky, and less frequently short euhedral crystals 80-120 μm in length. The zircons of sample GOE-1106b are colorless, stalky, and prismatic euhedral, with lengths of 80-120 μm . Some have inclusions, fractures, and surface oxides. In the CL images, the zircons of

sample GOE-1106a present homogeneous gray nuclei and thin edges with concentric or banded structures. The zircons of sample GOE-1106b present concentric structures in different shades of gray; some are microfractured and have few inherited xenocryst nuclei.

For the calculation of the ages of samples GOE-1106a and GOE-1106b, data with discordant values > 10% and precision errors > 5% were discarded. For the GOE-1106A sample, one concordant data point of 232.6 ± 5.1 Ma was discarded because

se it deviates from the main population with an average age of 278.5 ± 1.8 Ma ($n = 37$, MSWD = 3.3) (Figure 4). For the GOE-1106b sample, an average age of 288.7 ± 1.5 Ma ($n = 59$, MSWD = 2.7) was obtained (Figure 4). Both results are interpreted as crystallization ages and have Th/U ratios of 0.43 to 1.96 and 0.25 to 9.99, respectively.

Páez quartz monzodiorite. Sample JPZ-376 corresponds to a granodiorite that was collected in the Baché village of the municipality of Santa María (Huila), and sample GOE-1127 corresponds to a charnockite (mangerite) collected along the Planadas-Santa María road. The zircons of sample JPZ-376 are prismatic with euhedral shapes and sizes between 70 and 150 μm . In CL images, oscillatory zoning typical of igneous zircons, involute nuclei, and some with magmatic reabsorption edges are observed. In sample GOE-1127, the zircon crystals are prismatic euhedral with sizes > 100 μm , stalky to needle-shaped, generally fractured, and colorless. In the CL images, they present homogeneous nuclei with weak oscillatory zoning at the edges, some with a linear texture (Figure 2).

For the calculation of age, data with discordant values $> 10\%$ and precision errors $> 5\%$ were discarded. The average age calculated for the JPZ-346 sample was 184.7 ± 0.9 Ma ($n = 53$, MSWD = 3.8), with Th/U ratios between 0.55 and 1.27. The GOE-1127 sample yielded a weighted average age of 187.4 ± 1.7 Ma, with MSWD = 2.9 (Figure 4), and Th/U ratios between 0.99 and 1.70, corresponding to zircons formed in a magmatic chamber (Rubatto, 2002).

Siapana granodiorite. Sample MIA-684 is a granodiorite collected at El Tablazo-Siapana Hill in the Serranía de La Macuira.

The zircons are euhedral and stalky to columnar in shape; some are fractured, with few black inclusions. In the CL images, they present a concentric internal structure marked by changes in gray hue (Figure 3), typical of crystals generated in igneous environments.

For the calculation of the age of MIA-684, data with discordant values $> 10\%$ and precision errors $> 5\%$ were discarded. The average age calculated for the MIA-684 sample was 166.5 ± 1.5 Ma ($n = 39$, MSWD = 2.6) (Figure 4). The Th/U ratios varied between 0.11 and 0.77.

Buritaca gneiss. Sample GR-6808 was collected in the Buritaca gneiss unit on the road that borders the El Sol stream in the Sierra Nevada de Santa Marta and corresponds to plagioclase,

hornblende, and biotite mylonitic gneiss. The zircons are 50-100 μm , subhedral to euhedral, colorless, and stalky-short with oval to prismatic terminations.

In the CL images, the crystals present homogeneous color, incipient concentric and banded zoning, internal microfractures, and inclusions.

For the calculation of the age of GR-6808, data with discordant values $> 10\%$ and precision errors $> 10\%$ were discarded. In addition, two data points in a homogeneous zircon crystal of 126.7 ± 5.8 and 131.14 ± 9.5 Ma, one concordant and the other discordant, were discarded (Figures 3 and 4). The average age calculated for sample GR-6808, dating the crystal edges and nuclei, was 151.3 ± 3.6 Ma ($n = 10$, MSWD = 2.7), with Th/U ratios between 0.22 and 0.56, which are interpreted as zircons that formed in a magmatic chamber. A second population of inherited crystals yielded a weighted average age of 180.7 ± 6.0 Ma ($n = 10$, MSWD = 2.7), with a Th/U ratio between 0.11 and 0.37. The sample also presented inherited crystals with ages from the Triassic (202.99 ± 12.9 Ma and 228.8 ± 10.1 Ma, $n = 3$), Neoproterozoic (664.46 ± 4.8 Ma, 776.02 ± 47.8 Ma, 853.48 ± 50.8 Ma, 910.34 ± 42.5 Ma and 918.44 ± 45.6 Ma), and Mesoproterozoic (1037.92 ± 47.7 Ma).

6. DISCUSSION

6.1. Magmatic cycles, unit correlations, cycle composition, and spatial location

A magmatic cycle corresponds to the period of geological time that elapses during the initiation, development, and collapse of a continental margin arc, in which a belt of plutons and volcanic rocks is formed in a determined position and presents particular compositional characteristics. In this scenario, several magmatic cycles and pluton belts are generated from the same subduction zone.

The correlation of the plutons of each magmatic cycle is based on their location in relation to the paleomargin, their geochemical composition, and their crystallization age. The magmatic cycles are identified as peaks in the U-Pb probability density plots of the plutonic rocks (and, in some cases, the volcanic units). In addition, the general geochemical composition of the pluton belts that represent the magmatic cycle is shown.

6.2. Carboniferous (ca. 333 Ma to ca. 300 Ma)

The first products of continental margin arc magmatism in the western paleomargin of Gondwana occurred in the Carboni-

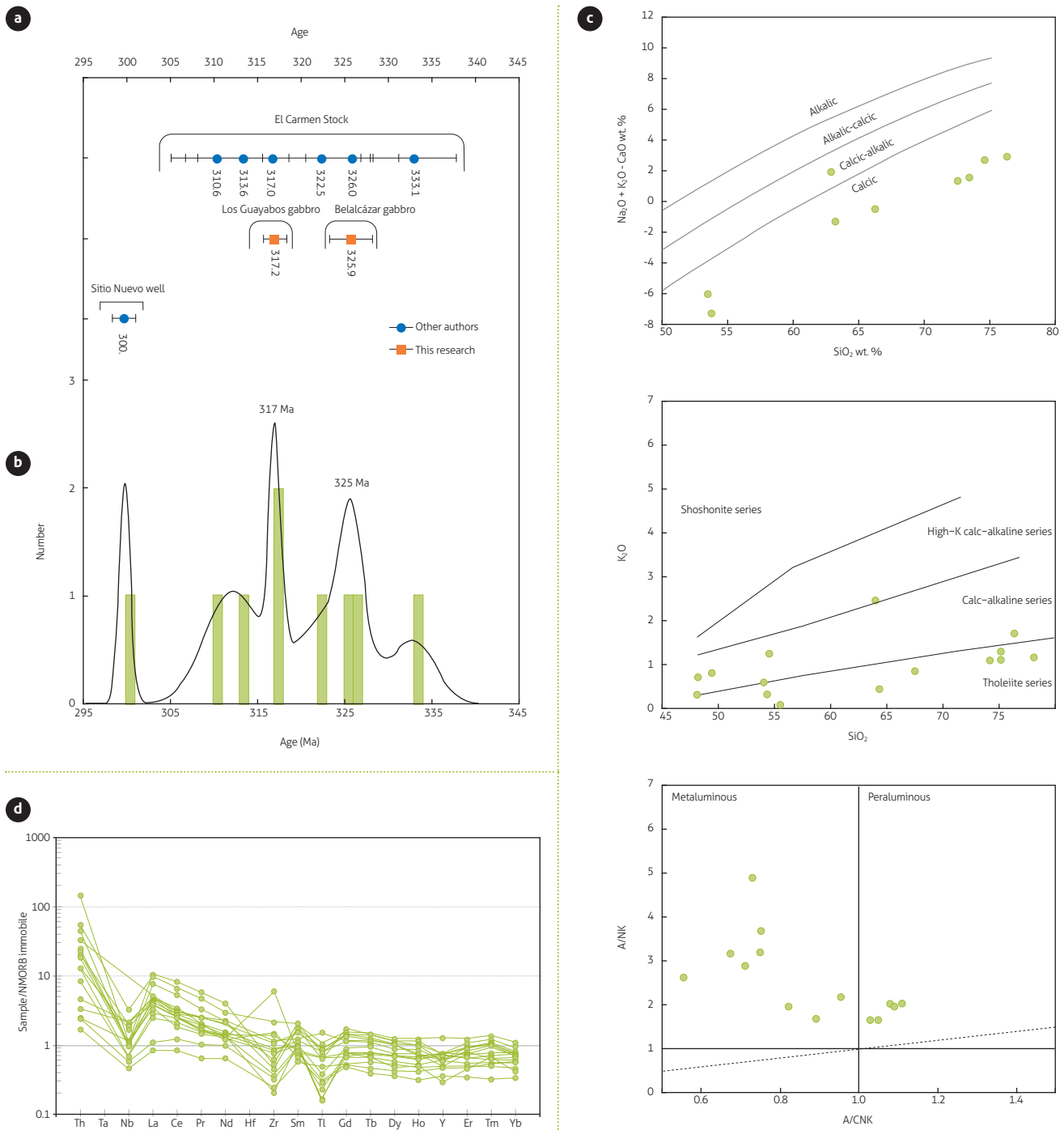


Figure 5. Age and composition of the plutons of the Carboniferous magmatic cycle

a) Correlation diagram of plutons of Carboniferous age; b) Diagram of probability density from the U-Pb ages of the plutons; c) Classification diagrams of carboniferous pluton samples; d) Diagram of immobile trace elements normalized to the normal mid-ocean ridge basalt (NMORB)

ferous from ca. 333 Ma to ca. 300 Ma (Leal Mejía, 2011; Leal Mejía et al., 2019; Rodríguez et al., 2019a). This magmatic record was recently discovered in the northern Andes, and thus

far, only the following bodies have been reported: the El Carmen stock (Leal Mejía, 2011) and Los Guayabos and Belalcázar gabbros (this work) in the Central Cordillera and a pyroxene

gabbro from the Sitio Nuevo-1 well in the lower Magdalena valley (Silva-Arias et al., 2016) (Figure 2).

The south to north geotectonic location of the Carboniferous plutons is as follows: the Belalcázar gabbro is located on the westernmost edge of the Gondwana paleomargin within the Neoproterozoic basement and is bound to the east by the Permian Ortega granite, and to the west, it is in faulted contact with the Upper Jurassic to Lower Cretaceous Ibagué batholith. The Los Guayabos gabbro outcrops farther north, in the same position related to the continental paleomargin. This unit is in faulted contact with Neoproterozoic metamorphic rocks and the Ibagué batholith to the west and in faulted contact with the Ibagué batholith and the Chaparral vulcanites to the east. The Chaparral vulcanites are from the Upper Jurassic and are located on the suture between the western margin of Gondwana and the metamorphic rocks previously described as Tierradentro gneisses and amphibolites. These latter rocks yielded Neoproterozoic maximum depositional ages in this sector and are older than the ages to the north of the Ibagué fault reported by Rodríguez et al. (2020a).

The El Carmen stock outcrops to the north of the Central Cordillera. This unit presents crystallization ages and compositions comparable to those of the Belalcázar and Los Guayabos gabbros. The El Carmen stock is located to the west of the Segovia batholith and is in faulted contact with the metamorphic rocks of the Cajamarca Complex (not yet dated in this sector) to the west of the Gondwana margin.

The ages of carboniferous magmatism vary between 333.1 ± 4.7 Ma and 300 ± 1.3 Ma and represent a magmatic cycle that lasted approximately 33 Ma, with two magmatic crystallization peaks ca. 325 Ma and ca. 317 Ma. The ages obtained for the Carboniferous plutons are shown in Figure 5a and Supplementary Table TS1.

The Carboniferous plutons are constituted by gabbros and I-type calcic leuco-tonalites (Figure 5b). The rocks are metaluminous and, to a lesser extent, peraluminous (in the most differentiated facies), presenting tholeiitic to calc-alkaline affinity (Figures 5c). The samples show Ba and Th enrichment, positive Pb anomalies, and negative Nb, Ti, and Zr anomalies (Figure 5d) related to magmas generated in subduction zones (Pearce, 2008), possibly in the first stages of continental margin arc magmatism.

The Carboniferous magmatic cycle is recorded in the zircons inherited in the Permian and Early Jurassic arc magmatic cycles (Figure 6), suggesting that these likely correspond to antecrysts or xenocrysts.

6.3. Permian to Triassic (ca. 300 Ma to ca. 234 Ma)

Following the Carboniferous magmatism, the second belt of continental arc plutons was emplaced on the Neoproterozoic basement of the western paleomargin of Gondwana during the Permian period (Figures 2 and 13). This cycle is represented by batholiths, stocks (La Plata and Ortega granites), igneous bodies with migmatitic structures (Icarcó Complex, parts of the La Plata Granite), and deformed mylonitic plutonic blocks (Nechí gneiss, El Encanto orthogneiss, and mylonites and deformed granites associated with the Macuira gneiss).

The latter rocks formed to the east of the continental margin of Gondwana; however, they are currently located to the west as deformed tectonic blocks. These rocks crop out along with rocks with Jurassic orogenic metamorphism and Triassic metamorphic blocks that are part of the collisional orogen (Tierradentro gneisses and amphibolites, the Cajamarca Complex, San Lorenzo schist, and La Macuira gneiss) (Blanco Quintero et al., 2014; Cardona et al., 2010; Piraquive, 2017; Rodríguez et al., 2020a; and this work).

The current location of each of the Permian plutons is to the east of the Carboniferous plutons (Figures 2 and 13). To the south, on the eastern flank of the Central Cordillera, the La Plata and Ortega granites and the Icarcó Complex are located within the western margin of Gondwana, in faulted contact to the east, and are intruded by plutons and vulcanites of the Early Jurassic (Mocoa-Santa Marta (AMSM) arc units; Rodríguez

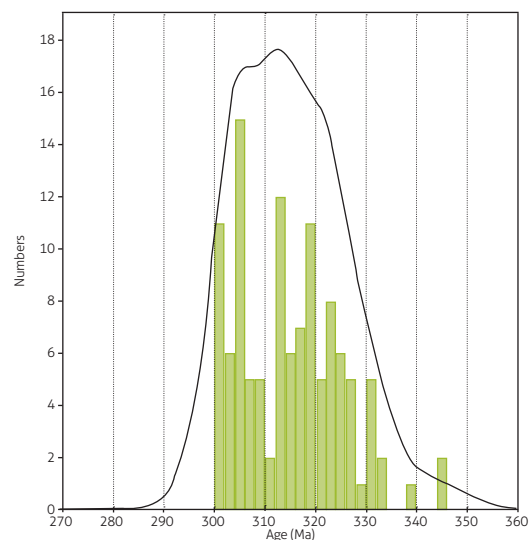


Figure 6. Probability density diagram based on inherited nuclei or zircons with Carboniferous ages obtained in the plutons of the Permian and Early to Middle Jurassic cycles

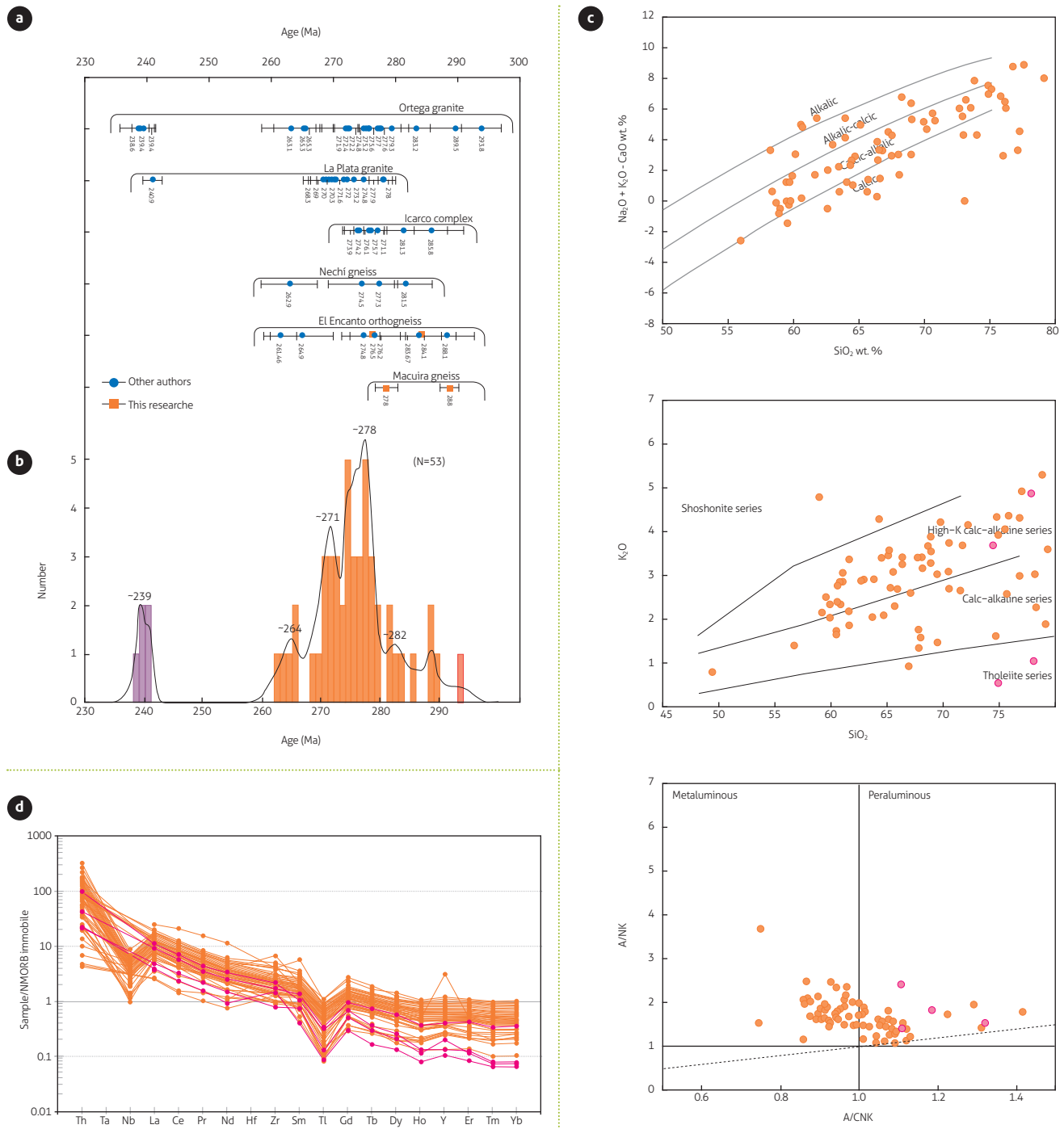


Figure 7. Age and composition of the plutons of the Permian and Triassic magmatic cycles
 a) Correlation diagram of plutons of Permian and Triassic age; b) Diagram of probability density from the U-Pb ages of the plutons; c) Classification diagrams of Permian pluton samples with Triassic dikes; d) Diagram of immobile trace elements normalized to the NMORB

et al., 2019, 2020b). The Ortega granite and the Icarco Complex, to the west, are in faulted contact with the Carboniferous Belalcázar gabbro and are intruded by the Late Jurassic to the

Early Cretaceous Ibagué batholith. In addition, they were intruded by porphyritic subvolcanic bodies of the same age as the Ibagué batholith (Upper Jurassic-Lower Cretaceous).

To the north of the Ibagué fault, a deformed block of a Permian pluton appears as a mylonitic orthogneiss associated with the Triassic and Upper Jurassic Tierradentro Gneisses and Amphibolites unit (Bustamante et al., 2017; Rodríguez et al., 2020a).

The Nechí gneiss outcrops in the Serranía de San Lucas and corresponds to a granitoid with local mylonitic structures located to the west of the Segovia batholith and within metamorphic rocks of the Central Cordillera (Cajamarca Complex).

In the Sierra Nevada de Santa Marta, several deformed blocks of arc granitoids crop out, grouped under the name of El Encanto orthogneiss (Cardona et al., 2010; Piraquive, 2017), located next to Triassic and Jurassic metamorphic rocks. Finally, in the Serranía de Macuira, mylonites of igneous protolith and deformed granitoids are associated with the Macuira gneiss outcrop (this work).

The ages obtained for the Permian plutons are summarized in Figure 7 and Supplementary Table TS1. The geochronological record of this magmatism shows dates between 293.8 ± 3.8 Ma and 262.9 ± 4.5 Ma (ca. 30 Ma magmatic cycle). When analyzing the behavior of the entire magmatic belt of the Permian arc, at least four main magmatic crystallization events are recognized that can be grouped into four intervals: from 297 to 283 Ma, the beginning of plutonism; from 282 to 264

Ma, the development of the arc, with the highest crystallization peak ca. 278 Ma; from 264 to 257 Ma, the decay of crystallization and the final phase of pluton formation, with a discrete crystallization peak ca. 264 Ma. Finally, pink granite dikes and smaller bodies during a late intrusion event between ca. 245 and ca. 234 Ma occur (cycle of ca. 11 Ma), which yielded a crystallization peak ca. 239 Ma (Figures 7 and 8).

The composition of the plutons of this belt is heterogeneous: granites, granodiorites, diorites, quartz monzonites, and monzonites; some of them are deformed and have mylonitic foliation (Nechí gneiss, El Encanto orthogneiss, and mylonites and granitoids associated with Macuira gneiss). These plutons are distributed in the calcic field (calc-alkaline and alkali-calcic granitoids), are calc-alkaline and high-K calc-alkaline, I-type, and vary from metaluminous to peraluminous, with negative Nb and Ti anomalies typical of rocks generated in an arc continental margin environment.

The plutons and deformed granitoid bodies correspond to granites, granodiorites, diorites, quartz monzonites, and monzonites, which are distributed in the fields of calcic (calc-alkaline and alkalic-calcic) granitoids and in the calc-alkaline and high-K calc-alkaline fields (Figure 7).

The Triassic arc granites analyzed in this work have no genetic relationship with the S-type Triassic gneisses of the Central Cordillera, which were formed by crustal fusion and are emplaced in another continental block (Vinasco et al., 2006). These outcrops crop out in a more western position than the Carboniferous and Permian arc pluton belts.

Carboniferous and Permian arc magmatism cycles are recorded in inherited zircons from plutonic and volcanic rocks of Early to Middle Jurassic arc magmatism (Ramírez et al., 2020; Rodríguez et al., 2020b.) and the Mocoa-Santa Marta arc (AMSM) (Rodríguez et al., 2020b) (Figure 8), suggesting that this last cycle was emplaced in the Carboniferous and Permian pluton belts.

The zircons obtained in plutons and volcanic units from the Early to Middle Jurassic cycle of the AMSM record the inheritances of the Carboniferous, Permian, and Triassic magmatic cycles, as shown in Figure 8.

6.4. Triassic to Early Jurassic (ca. 234 to ca. 197)

Between 234 Ma (the last record of magmatic crystallization in dikes and smaller granite bodies associated with the plutons of the Permian arc) and ca. 197 Ma (beginning of the AMSM magmatic cycle; Rodríguez et al., 2020b), the accumulation of

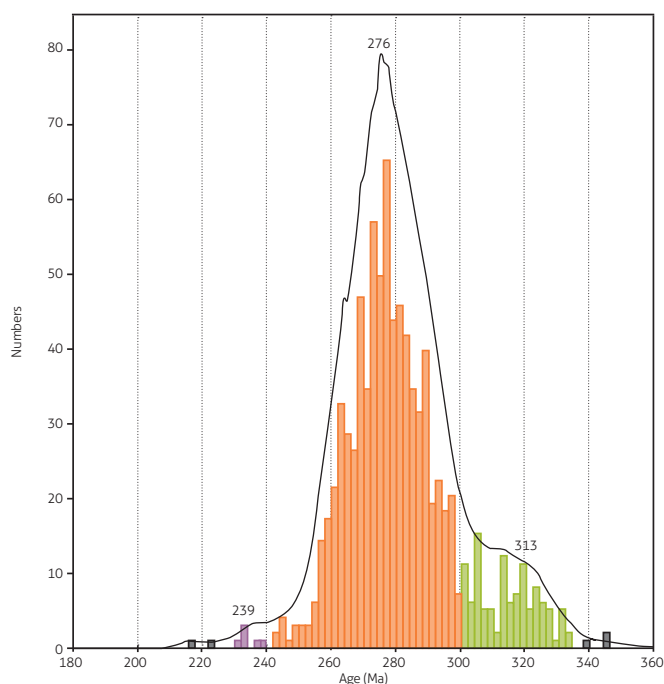


Figure 8. Probability density diagram for igneous ages obtained in inherited zircons in the plutons and volcanic rocks of the AMSM arc

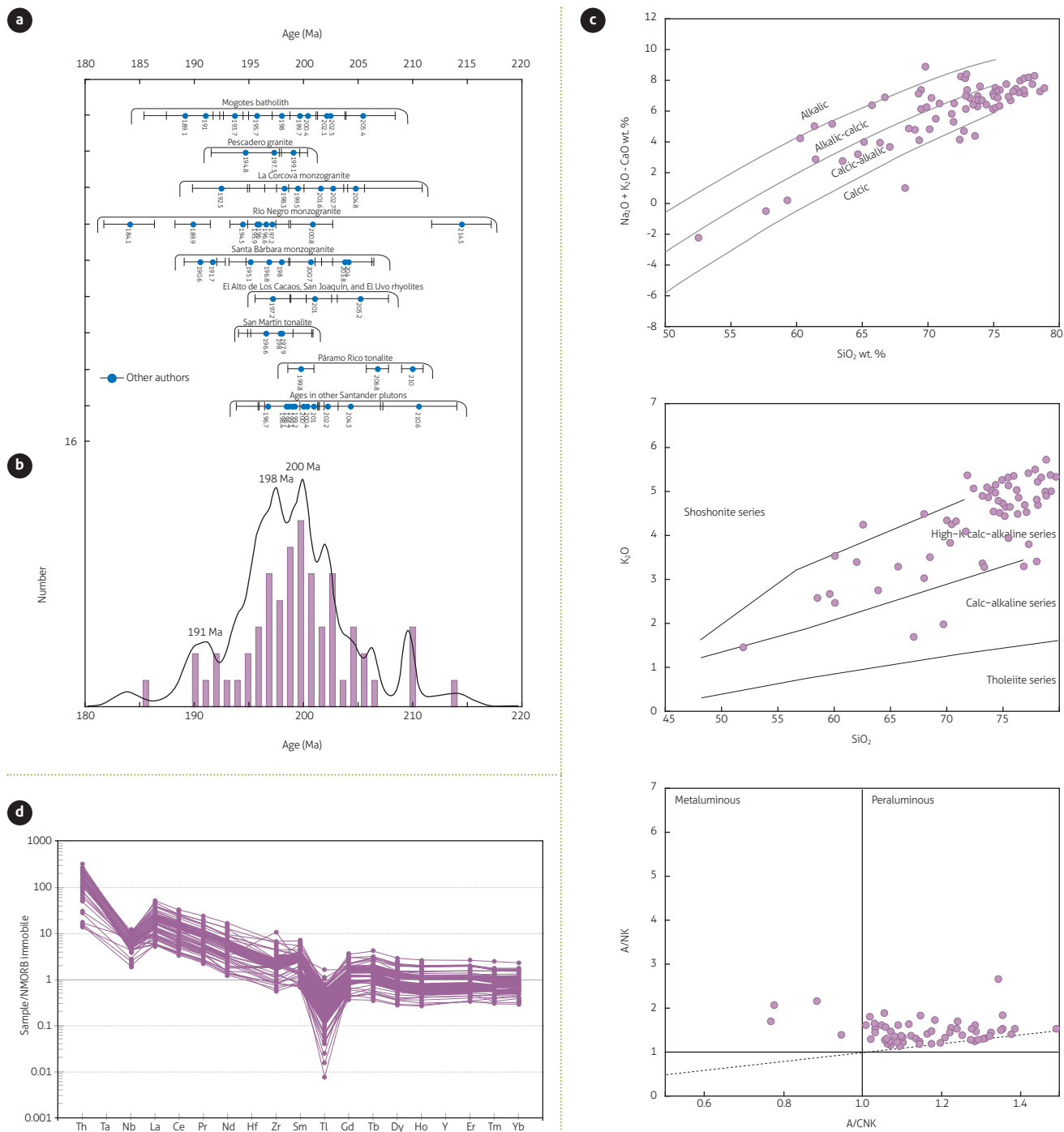


Figure 9. Age and composition of the plutons of the Triassic–Jurassic magmatic cycle of the Santander massif a) Correlation diagram of plutons of Triassic–Jurassic age; b) Diagram of probability density from the U–Pb ages of the plutons; c) Pluton sample classification diagrams; d) Diagram of immobile trace elements normalized to NMORB

conglomerates, sedimentary breccias and subordinate shales, siltstones, and arkoses of the Luisa Formation is recorded in the western paleomargin of Gondwana (Cediel et al., 1980,

1981; Núñez and Murillo, 1982). The conglomerates and breccias are constituted by granitoid, gneiss, and granulite clasts, likely eroded from the Carboniferous and Permian arc plutons

formed in the margin and from rocks of the Neoproterozoic basement. The Luisa Formation rests discordantly on intrusive rocks with Permian crystallization ages (Ortega granite) and corresponds to the sedimentary record of the uplift and erosion period of the continental margin.

After the deposition of the Luisa Formation, discordant dark gray limestones of the Payandé Formation and minor intercalations of sandstones and lutites were deposited (Chicalá Member; Gómez, 2003). The latter record upper Triassic marine fauna (Geyer, 1973) and are related to a marine transgression event in the continental margin. The Payandé Formation would have been covered by volcanic material during the magmatic cycle that began in the Early Jurassic and extended until the Middle Jurassic (Montefrío sedimentites, Saldaña, Noreán, La Quinta formations, Sierra Nevada volcanic complex, and La Teta and Ipapure rhyodacites).

While erosion, sedimentation, and marine transgression occurred on the extinct plutons of the Carboniferous and Permian arcs (deposition of the Luisa and Payandé Formations) in the western paleomargin of Gondwana, back-arc magmatism began ca. 214 Ma, lasting until ca. 184 Ma (ca. 30 Ma magmatic cycle) (Figure 9). This belt is located within the Famatinian Orogen of the Santander massif in an eastern position in the interior of Gondwana (Figures 2 and 13).

This magmatism was characterized by the formation of batholiths and stocks of monzogranite composition, with subordinate granodiorites, syenogranites, and tonalites, from multiple magmatic pulses (Mogotes batholith; La Corcova, Santa Bárbara, and Río Negro monzogranites; Pescadero granite; and El Alto de Los Cacaos, San Joaquín, and El Uvo rhyolites, among others).

From a geochemical point of view, the rocks of this magmatism plot within the calc-alkaline and subordinate alkali-calcic granitoid fields (Figure 9c) of the high-K calc-alkaline series (Figure 9c) and are peraluminous (Figure 9c) and highly differentiated (Figure 9c), presenting negative Nb and Ti anomalies in the diagram of immobile trace elements normalized to normal mid-ocean ridge basalt (NMORB) (Figure 9d).

The ages obtained for the plutons and subvolcanic bodies are summarized in Figure 9a and Supplementary Table TS1. Analyzing the behavior of the Triassic–Jurassic magmatism of Santander reveals that during the entire magmatic cycle, predominantly monzogranitic rocks were formed, and each of the plutons was formed during an extended period of crystallization from multiple magmatic pulses (Rodríguez et al., 2020a,

2021). The cycle started ca. 214 Ma, with a progressive increase in magmatism and with the highest crystallization peak between ca. 200 and 198 Ma, decreasing the crystallization progressively until the end of the cycle ca. 184 Ma (Figure 9a).

These granitoids were generated by the fusion of rocks of the Paleozoic metamorphic basement of the Famatinian Orogen (Leal et al., 2019; López and Zuluaga, 2020; Rodríguez et al., 2017; Van der Lelij et al., 2016; Zuluaga and López, 2019), as suggested by the abundance of inherited zircons from the basement in these plutons (Rodríguez et al., 2020a) and the isotopic data (Leal et al., 2019; Van der Lelij et al., 2019).

The origin of this magmatism has been related to oblique subduction processes during the fragmentation of Pangea (López and Zuluaga, 2020; Rodríguez et al., 2017; Van der Lelij et al., 2016; Zuluaga and López, 2019) or partial fusion of the Santander massif metamorphic basement, thermally induced by the ascent of the mantle as a consequence of an extensional process, during the fragmentation of Pangea without being directly associated with subduction (Leal-Mejía et al., 2019).

Crustal thickness calculations based on Profeta et al. (2015) for Triassic–Jurassic granitoids of the Santander massif yielded values of approximately 60 km. These data indicate that the crust was thickened and could have delaminated.

Therefore, this study proposes another process that would also explain the fusion of continental crust in the Santander massif, corresponding to the delamination of the thickened lower eclogitic crust. This mechanism, like that of asthenospheric decompression by thinning of the crust, allows the incursion of mantle heat and induces extensive fusion of the continental crust (Thompson and Connolly, 1995).

6.5. Early Jurassic–Middle Jurassic (ca. 197 to ca. 164)

On the western margin of Gondwana, the magmatic activity of the arc returned in the Early Jurassic, ca. 197 Ma and continued until ca. 164 (magmatic cycle of ca. 33 Ma, Figures 10 and 11), forming large volumes of volcanic and plutonic rocks emplaced on the Neoproterozoic basement (AMSM; Rodríguez et al., 2020b) currently located on the eastern flank of the Central Cordillera, Upper Magdalena Valley, Serranía de San Lucas, Sierra Nevada de Santa Marta, and Upper Guajira (Figure 2).

During this period, explosive volcanic and subordinate lava deposits occurred along the arc axis (Saldaña, Noreán, and La Quinta formations; Pitalito vulcanites; Sierra Nevada de Santa Marta volcanic complex; and Ipapure-La Teta Hill rhyodacite). The magmatic cycle began with the crystallization of plutons

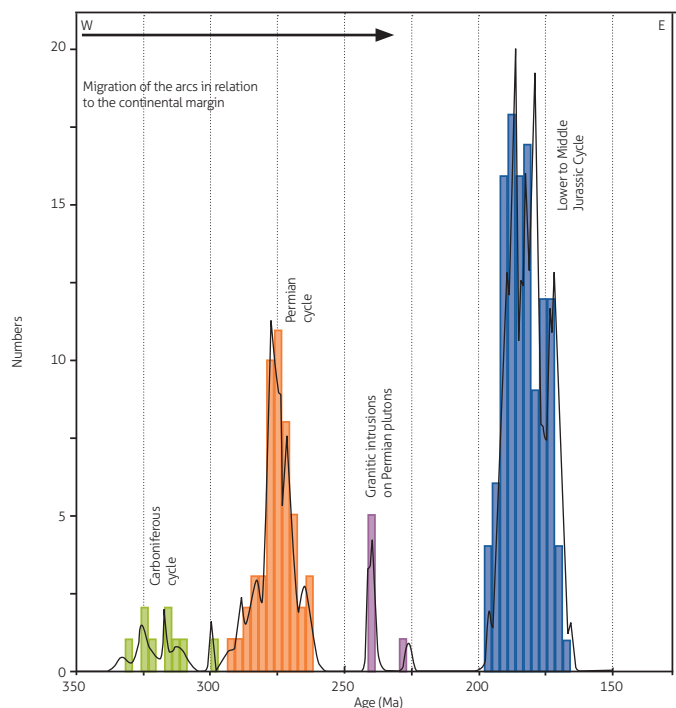


Figure 10. Magmatic arc cycles in the western margin of Gondwana between the Carboniferous and the Middle Jurassic

located to the east of the Carboniferous and Permian intrusive rocks (Sombrierillo quartz monzonite; Las Minas monzodiorite; El Astillero and Páez quartz monzodiorites; San Cayetano, Anchique, and Los Naranjos quartz monzonites; Dolores stock; Norosí granite; Guamocó granodiorite; Papayal monzonite; the Central batholith; and Ipapure granodiorite). This magmatism migrated to the east in the final stage of the arc cycle (Mocoa, Altamira, and Algeciras monzogranites; Garzón granite; Teruel quartz latite; and Pueblo Bello, Patillal, and Atánquez batholiths) (Figure 11).

The oldest Jurassic plutons of this cycle (located to the west) are metaluminous, and the youngest (located to the east) vary from metaluminous to peraluminous, indicating migration of magmatism in a west–east direction (Rodríguez et al., 2018, 2020b). The axis of the AMSM was located immediately to the east of the Carboniferous and Permian plutons, suggesting that the migration of the axis of the arcs between the Carboniferous and the Middle Jurassic occurred toward the interior of Gondwana in the same direction as the subduction of the Farallon Plate.

The first plutons of the AMSM, in southern Colombia, are located on the eastern flank of the Central Cordillera and Serranía de Las Minas. On their western edge, they intrude the Permian La Plata and Ortega granites, and toward the east, they intrude the Neoproterozoic basement of the Chibcha Terrane. To the north, in the Serranía de San Lucas, the plutons intrude the Neoproterozoic San Lucas gneiss, and in the Sierra Nevada de Santa Marta, they occupy the western flank, intruding the Neoproterozoic Los Mangos granulite and Buritaca gneiss.

The plutons of the AMSM are not deformed in the Serranía de San Lucas and the Sierra Nevada, as is the case with the granitoids of the Carboniferous and Permian arcs that were formed toward the edge in the western paleomargin of Gondwana.

When the AMSM migrated the plutonism toward the east, the pluton composition changed from tonalite and quartz monzonite to monzogranite (Rodríguez et al., 2018, 2020b). The later plutons crop out along the western flank of the Eastern Cordillera, upper Magdalena Valley, and eastern slope of the Sierra Nevada de Santa Marta, intruding the Neoproterozoic basement. These rocks partially cover or intrude the volcanic products of the same arc (Figure 2).

Between 197 and 184 Ma, coeval magmatism occurred in two different geotectonic positions in the interior of Gondwana: 1) the AMSM developed on the western flank of the Central Cordillera, Serranía de San Lucas, and the Sierra Nevada de Santa Marta; 2) back-arc magmatism developed in the Santander massif. Along the axis of the arc, I-type metaluminous plutonism and volcanism occurred, while in the back-arc, I- and S-type peraluminous plutonism, and probably volcanism, developed by crustal fusion in a radius of approximately 60 to 65 km, thickening the crust (calculated from La/Yb ratios) (Kay et al., 2014; Rodríguez et al., 2020a). In the back-arc, the magmatism ended ca. 184 Ma, while in the arc, it continued until ca. 164 Ma (Figures 9, 11, and 13).

The granitoids that constitute the AMSM cycle are calc-alkaline, with slight variations toward the alkali-calcic (Figure 11c); they belong to the high-K calc-alkaline series, and some are shoshonitic (Figure 11c). The oldest granitoids are metaluminous, and the youngest granitoids vary from metaluminous to peraluminous (Figure 11c), with negative Nb and Ti anomalies (Figure 11d).

The crystallization ages of the plutons of the AMSM vary between ca. 197 Ma and 164 Ma, with crystallization peaks at ca. 186 Ma, ca. 179 Ma, and ca. 170 Ma (Figure 11b).

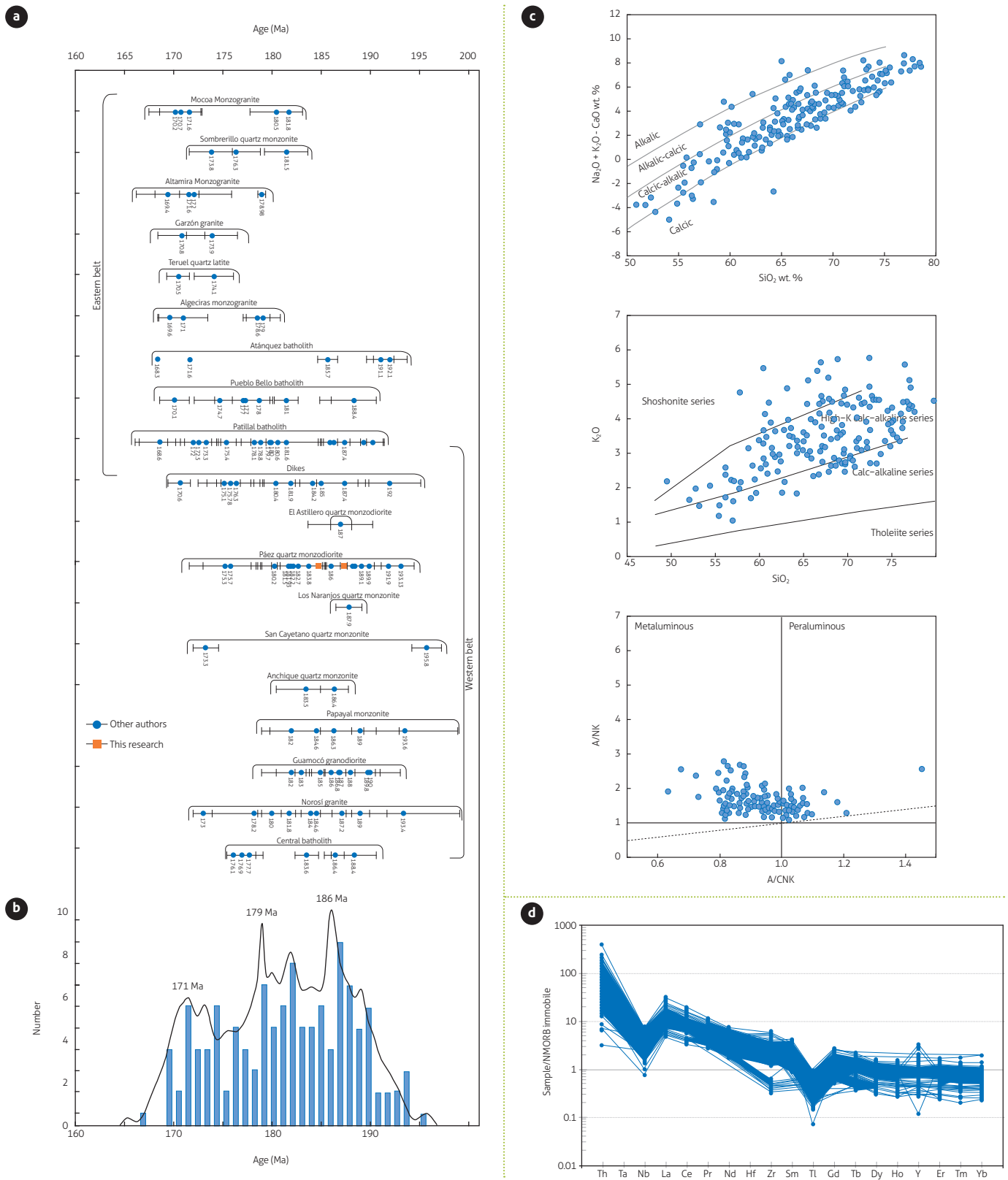


Figure 11. Age and composition of the plutons of the magmatic cycle of the lower to Middle Jurassic of the AMSM
a) Pluton correlation diagram; b) Diagram of probability density from the U-Pb ages of the plutons; c) Pluton sample classification diagrams; d) Diagram of immobile trace elements normalized to NMORB

6.6. Middle Jurassic to Lower Cretaceous (ca. 171 Ma and ca. 138 Ma)

Between ca. 171 Ma and ca. 138 Ma, several geological events occurred in the western paleomargin of Gondwana. Between 171 Ma and 164 Ma, magmatic activity occurred in two different geotectonic positions: 1) metaluminous and peraluminous monzogranite stocks and batholiths formed further into the interior of Gondwana on the western slope of the Eastern Cordillera and the eastern slope of the Sierra Nevada de Santa Marta during the final stages of the AMSM; 2) outside the western paleomargin of Gondwana, west of the Carboniferous, Permian, and Early to Middle Jurassic pluton belts, a new cycle of arc activity began in a basement composed of Ordovician and Triassic metamorphic rocks (Figures 2 and 13), traditionally called the Tahamí and Anaconda Terranes (Restrepo and Toussaint, 2020) or the Cajamarca Complex (Maya and González., 1995). This new arc magmatism located to the west of the previous magmatic arcs is called the Ibagué-Segovia arc (AIS) (Rodríguez et al., 2020a, 2020b).

A third magmatic event corresponds to the formation of alkaline porphyry minor bodies composed of basaltic andesites that crystallized ca. 159 Ma. These rocks are located on the eastern slope of the Central Cordillera, intruding the plutons and volcanic rocks of the AMSM on the continental edge near the paleomargin (Rodríguez, 2018) (Figure 13).

The new magmatic cycle of the AIS is constituted by the Alisales, Ibagué, and Segovia batholiths, the Anzoátegui metatonalite, the Ibagué tonalite, the Payandé stock, and further north, the Siapana granodiorite (Figures 2 and 13). Plutonism was accompanied by explosive volcanism (Chaparral vulcanites: this work; La Malena volcanics and Segovia vulcanites: González et al., 2015) and began its magmatic activity ca. 171 Ma, ending ca. 138 Ma (magmatic cycle of ca. 33 Ma), with crystallization peaks at ca. 166 Ma, ca. 158.5 Ma, ca. 154 Ma and ca. 145 Ma (Figure 12b).

The plutons that are part of this cycle are constituted by tonalites and granodiorites with minor variations to quartz diorites and monzogranites. These rocks crop out adjacent to andesitic and dacitic vulcanite units and andesitic porphyry hypabyssal bodies that were formed in the final stage of the magmatic cycle. The porphyry bodies intrude the pluton belts formed in the Carboniferous and Permian cycles south of Ibagué.

The magmatism of the AIS coincides with the end of the AMSM magmatic cycle, the formation of metamorphic rocks against the continental paleomargin of Gondwana during the

Late Jurassic, the amalgamation of new terranes at the margin, and the formation of subvolcanic bodies of alkaline basaltic andesites that are interpreted to be the result of the collapse and subsidence of the Farallon Plate in the mantle ca. 159 Ma (Rodríguez, 2018; Rodríguez et al., 2020b).

The magmatic cycle of the AIS extended before and after the collision of the Tahamí and Anaconda Terranes against the Chibcha Terrain on the western margin of Gondwana. Locally, some plutons were emplaced in the suture (e.g., Ibagué Batholith), while others occupied positions within the amalgamated terranes and in metamorphic rocks formed during the collisional orogeny (e.g., Segovia and Alisales batholiths), intruding Ordovician, Triassic, and Jurassic metamorphic rocks (e.g., Perla gneiss: Ordovician; Tierradentro gneisses and amphibolites: Triassic and Jurassic ages; La Cocha-Río Téllez Complex: Upper Jurassic metamorphic and crystallization ages).

Plutons such as the Ibagué batholith and some subvolcanic porphyries intruded the plutons located within the Carboniferous, Permian, and Early to Middle Jurassic (AMSM) continental margins. In this period, the Anzoátegui metatonalite was probably deformed, developing foliation parallel to the Jurassic metamorphic rocks, while the Ibagué batholith presents only local deformation (Rodríguez et al., 2022).

The granitoids of the AIS cycle are mainly calcic, with some samples plotting in the calc-alkaline and alkali-calcic fields (Figure 12b). These rocks belong to the calc-alkaline series, and some belong to the high-K calc-alkaline series (Figure 12c). The granitoids are metaluminous and vary to peraluminous (Figure 11d), presenting negative Nb and Ti anomalies (Figure 12e).

6.7. Evolution of the margin and composition and development of the collisional orogen between 168 Ma and 154 Ma

The interpretation of the continental paleomargin of Gondwana has varied with the advancement of geological knowledge and the acquisition of more geochronological data. The continental paleomargin is considered the western limit of the Chibcha Terrane, although it has been modified. The continental boundary of the Chibcha Terrane corresponds to the Neoproterozoic basement and the undeformed pluton belts of the Carboniferous, Permian, and Early to Middle Jurassic arc cycles, which were emplaced in this basement (Rodríguez et al., 2019a). On the western side, against the continental boundary, the metamorphic sequences of the Ordovician (Anaconda Terrane), Triassic (Tahamí Terrane), Late Jurassic (rocks with

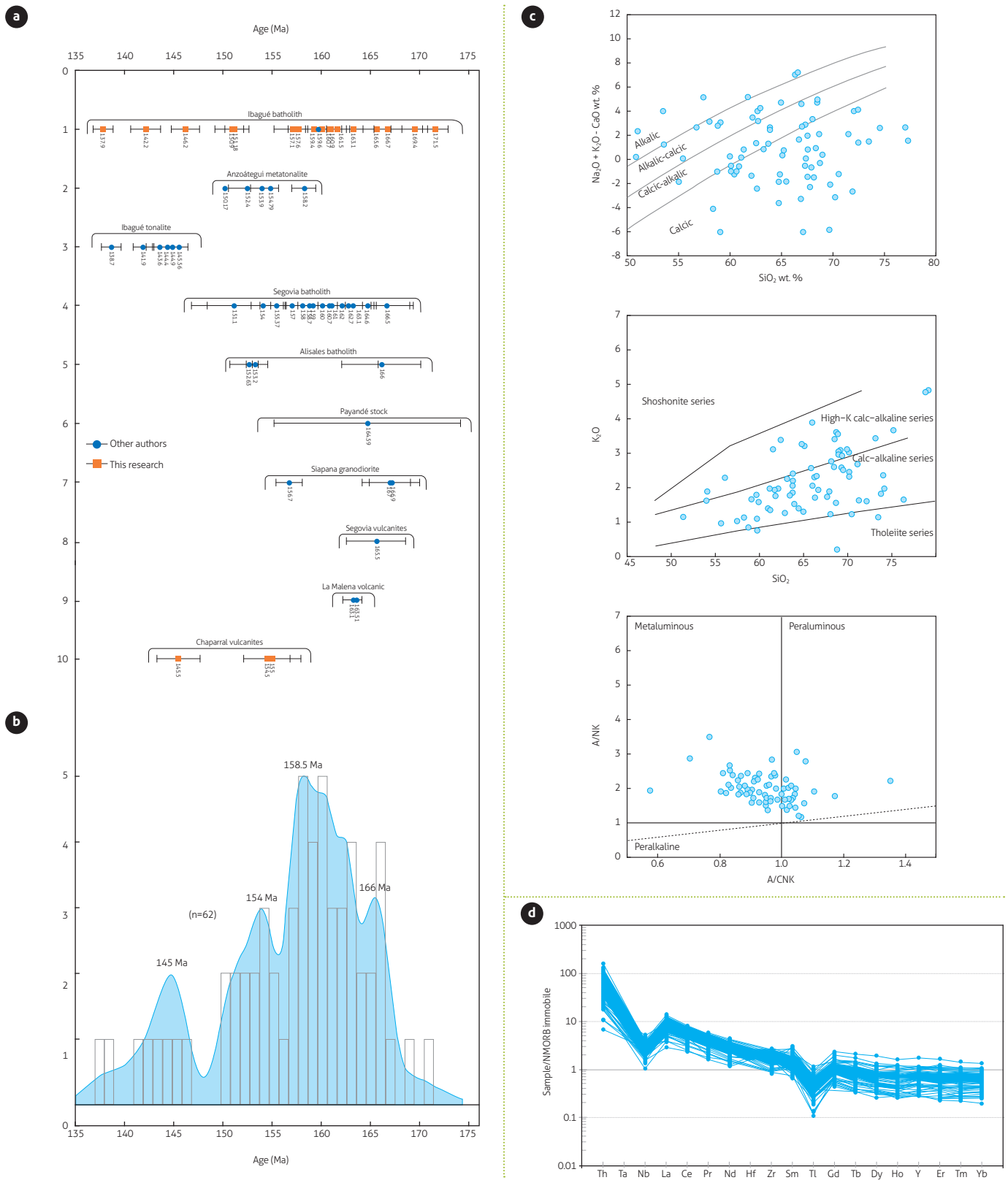


Figure 12. Age and composition of the plutons of the magmatic cycle from the Upper Jurassic to the Lower Cretaceous of the AIS
 a) Pluton correlation diagram; b) Diagram of probability density from the U-Pb ages of the plutons; c) Pluton sample classification diagrams; d) Diagram of immobile trace elements normalized to NMORB

overlapping orogenic metamorphism), and deformed blocks detached from both margins, and rocks of oceanic crust crop out, marking the suture.

The subduction of the Farallon Plate between ca. 330 Ma and ca. 164 Ma likely partially eroded the continental paleomargin (hanging block), affecting the plutons formed during the Carboniferous and Permian magmatic cycles. Currently, deformed blocks of granitoids of the Permian cycle are present north of the Ibagué fault in the Serranía de San Lucas, Sierra Nevada de Santa Marta, and Upper Guajira (Permian orthogneiss in the Tierradentro gneisses and amphibolites: Bustamante et al., 2017; Nechí gneiss: Rodríguez and Zapata, 2017; El Encanto orthogneiss: Cardona et al., 2010 and Piraquive, 2017; and granites and mylonites of Permian age in the Maquirá gneiss: this work), along with rocks with Triassic and/or Upper Jurassic metamorphism, interpreted as detached blocks that joined the amalgamated blocks during terrane collision. The erosion of the continental paleomargin, probably caused by subduction, was apparently lower south of the Ibagué fault, where the Carboniferous, Permian, and Early to Middle Jurassic pluton belts remain undeformed and inside the continental margin (Figure 2).

To the south of the Ibagué fault, the Ibagué batholith presents hanging roofs of the Ordovician metamorphic basement (La Perla gneiss) and the Triassic and Upper Jurassic Tierradentro gneisses and amphibolites, uplifted by the intrusion. In this sector, the Ibagué batholith and the Upper Jurassic subvolcanic bodies intrude the plutons of the Carboniferous, Permian, and Early to Middle Jurassic cycles on the eastern side of the suture.

Elsewhere in Colombia, the continental margin is limited on the western side by Upper Jurassic metamorphic rocks mixed tectonically with Triassic metamorphic rocks and Permian deformed plutonic blocks. This set of rocks is part of the collisional orogen located against the western paleomargin of Gondwana and was called the Tierradentro Terrane (Rodríguez et al., 2020a), but it is probably more accurate to consider it a collisional orogen that incorporates deformed blocks of both margins.

Orogenic metamorphism is present in units such as the Tierradentro gneisses and amphibolites (~167 to ~154 Ma; Rodríguez et al., 2017a, 2020a), the Cajamarca complex (~158 to ~147 Ma; Blanco-Quintero et al., 2014), La Cocha-Río Téllez complex (~163 Ma; Zapata et al., 2017), the metamorphic rocks of the Sierra Nevada de Santa Marta (Piraquive, 2017; this

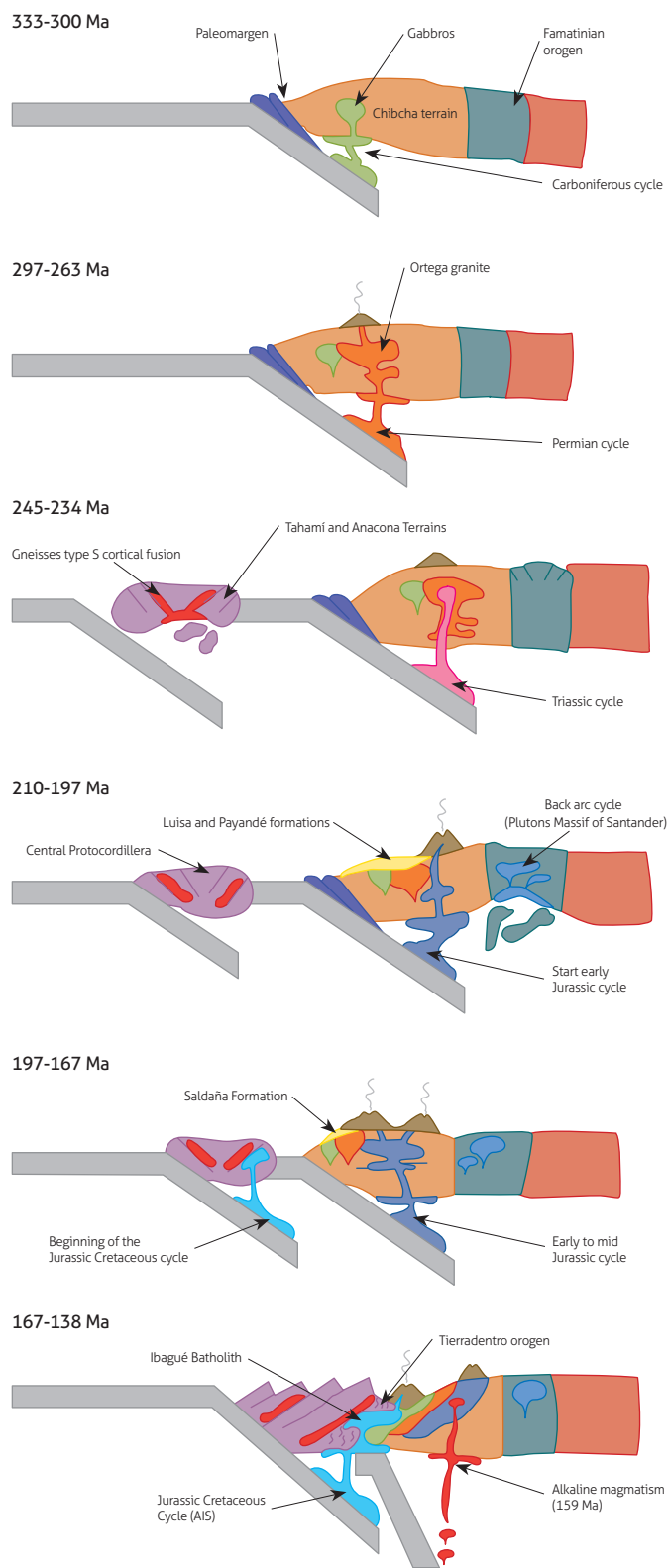


Figure 13. Tectonic reconstruction of the magmatic cycles between the Carboniferous and the Lower Cretaceous (330 to 138 Ma) in the northwestern paleomargin of Gondwana in Colombia

work), and most likely the Jarara and La Macuira ranges in the upper Guajira.

The rocks constituting the collisional orogen and the amalgamated blocks of the continental margin of Gondwana, immediately to the west of the continental paleomargin, vary in origin, age, and composition. These have been grouped into units and complexes (La Cocha - Río Tézlez and Cajamarca complexes, Tierradentro gneisses and amphibolites, Davis gneiss, San Lorenzo schist, among others) and include amphibolites formed from arc metabasites and NMORB oceanic crust (Rodríguez et al., 2020a), serpentine blocks, metasediments, paragneisses, marbles, Permian mylonitic orthogneiss blocks, and AIS pluton intrusions. Some of these plutons were probably deformed during the collisional orogeny (Anzoátegui metatonalite: Rodríguez et al., 2020a). The first NMORB oceanic crustal rocks appear on the western side of the continental paleomargin and correspond to amphibolites and ultramafic blocks. Thus, the suture between the Chibcha and Tahamí-Anaconda Terranes is a mixture of rocks of different origins, ages, and compositions.

Figure 13 summarizes the geotectonic evolution of the continental paleomargin of Gondwana between the Carboniferous and the Lower Cretaceous, following the known U-Pb geochronology data, the updated geology of the margin, and the whole-rock geochemistry of the magmatic cycles and metamorphic units located to the west of the paleomargin.

7. CONCLUSIONS

Each of the arc magmatic cycles that occurred in the western paleomargin of Gondwana between the Carboniferous and Middle Jurassic lasted approximately 30 to 35 Ma, except for the Triassic cycle, which lasted ca. 11 Ma.

The magmatic evolution between the Carboniferous and the Cretaceous shows a continuous compositional evolution between the continental margin arc cycles. In the Carboniferous, bodies of tholeiitic calcic gabbros and calc-alkaline tonalites predominate. In the Permian, calc-alkaline granites, granodiorites, diorites, quartz monzonites, and monzonites formed, with variations between the calcic and alkaline-calcic fields of the calc-alkaline to high-K calc-alkaline series. In the Early Jurassic, calc-alkaline quartz monzonites, quartz monzodiorites, monzodiorites, and tonalites of the high-K calc-alkaline series formed. At the end of the cycle, in the Middle Jurassic,

calc-alkaline and alkaline-calcic monzogranites and syenogranites of the high-K calc-alkaline series formed.

In the back-arc, the magmatic cycle lasted ca. 30 Ma, between ca. 214 Ma and ca. 186 Ma. The I- and S-type monzogranite and peraluminous syenogranite plutons formed during the entire cycle by crustal fusion. These rocks correspond to calc-alkaline to alkaline-calcic granites of the high-K calc-alkaline series.

At the end of the Jurassic, the intrusion of the AIS cycle began (ca. 171 Ma) outside the paleomargin in the Anaconda and Tahamí Terranes, lasting ca. 33 Ma until the early Cretaceous (ended ca. 138 Ma). At the same time, the collision of the Anaconda and Tahamí Terranes against the continental margin of Gondwana during the Late Jurassic (between ca. 167 Ma and ca. 154 Ma), and the collapse of the subduction zone that gave rise to the continental margin arc cycles of the Carboniferous, Permian, Triassic, and Early to Middle Jurassic occurred in the western margin of Gondwana. This latter collapse episode is marked by the intrusion of alkaline basaltic andesite bodies ca. 159 Ma.

The new zircon U-Pb age results presented in this study reveal two new Carboniferous gabbro bodies located on the eastern slope of the Central Cordillera. These new data improve the information and distribution of the Carboniferous magmatism of Colombia, previously included as part of the Ibagué batholith. In addition, in the upper Guajira, the first data of deformed granitoids of Permian age are obtained, extending the record of this magmatic cycle to northern Colombia.

SUPPLEMENTARY DATA

Supplementary data for this article can be found online at <https://doi.org/10.32685/0120-1425/bolgeol.49.2.2022.663>

REFERENCES

- Álvarez, J. (1983). Geología de la cordillera Central y el occidente colombiano y petroquímica de los intrusivos granitoides meso-cenozoicos. *Boletín Geológico*, 26(2), 1-175. <https://doi.org/10.32685/0120-1425/bolgeol.26.2.1983.53>
- Álvarez, M. J. (2013). *Petrología, geoquímica isotópica e metalogenia dos depósitos de ouro El Silencio e La Gran Colômbia, Distrito Mineiro Segovia-Remedios, Colômbia* [Master thesis]. Universidade de Brasília, Brasília.

- Arango, M. I., Rodríguez, G., Zapata, G., & Correa Martínez, A. M. (2020). Monzogranito de Rionegro. In *Catálogo de las unidades litoestratigráficas de Colombia: Macizo de Santander* (Vol. 1). Servicio Geológico Colombiano. <https://doi.org/10.32685/9789585279445-5-5>
- Arango, M. I., Rodríguez, G., Zapata, G., & Bermúdez, J. G. (2022a). Monzogranito de Mocoa. In *Catálogo de las unidades litoestratigráficas de Colombia: Valle Superior del Magdalena* (Vol. 2). Servicio Geológico Colombiano. <https://doi.org/10.32685/9789585313194.1>
- Arango, M. I., Rodríguez, G., Bermúdez, J. G., & Zapata, G. (2022b). Monzodiorita de Las Minas. In *Catálogo de las unidades litoestratigráficas de Colombia: Valle Superior del Magdalena* (Vol. 2). Servicio Geológico Colombiano. <https://doi.org/10.32685/9789585313194.4>
- Arango, M. I., Rodríguez, G., Bermúdez, J. G., & Zapata, G. (2022c). Cuarzomonzonita de Anchique. In *Catálogo de las unidades litoestratigráficas de Colombia: Valle Superior del Magdalena* (Vol. 2). Servicio Geológico Colombiano. <https://doi.org/10.32685/9789585313194.7>
- Arango, M. I., Rodríguez, G., Zapata, G., & Bermúdez, J. G. (2022d). Cuarzolatita de Teruel. In *Catálogo de las unidades litoestratigráficas de Colombia: Valle Superior del Magdalena* (Vol. 2). Servicio Geológico Colombiano. <https://doi.org/10.32685/9789585313194.9>
- Arango, M. I., Rodríguez, G., Zapata, G., & Bermúdez, J. G. (2022e). Monzogranito de Altamira. In *Catálogo de las unidades litoestratigráficas de Colombia: Valle Superior del Magdalena* (Vol. 2). Servicio Geológico Colombiano. <https://doi.org/10.32685/9789585313194.12>
- Bayona, G., García, D., & Mora, G. (1994). La Formación Saldaña: producto de la actividad de estratovolcanes continentales en un dominio de retroarco. In F. Etayo-Serna (ed.), *Estudios geológicos del Valle Superior del Magdalena*. Universidad Nacional de Colombia.
- Bayona, G., Jiménez, G., Silva, C., Cardona, A., Montes, C., Roncancio, J., & Cordani, U. (2010). Paleomagnetic data and K-Ar ages from Mesozoic units of the Santa Marta massif: A preliminary interpretation for block rotation and translations. *Journal of South American Earth Sciences*, 29(4), 817-831. <https://doi.org/10.1016/j.jsames.2009.10.005>
- Blanco-Quintero, I. F., García-Casco, A., Toro, L. M., Moreno, M., Ruiz, E. C., Vinasco, C. J., Cardona, A., Lázaro, C., & Morata, D. (2014). Late Jurassic terrane collision in the northwestern margin of Gondwana (Cajamarca complex, eastern flank of the Central Cordillera, Colombia). *International Geology Review*, 56(15), 1852-1872. <https://doi.org/10.1080/00206814.2014.963710>
- Bermúdez, J. G., Zapata, G., Rodríguez, G., & Arango, M. I. (2022a). Cuarzomonzonita de Sombrerillo. In *Catálogo de las unidades litoestratigráficas de Colombia: Valle Superior del Magdalena* (Vol. 2). Servicio Geológico Colombiano. <https://doi.org/10.32685/9789585313194.2>
- Bermúdez, J. G., Arango, M. I., Rodríguez, G., & Zapata, G. (2022b). Cuarzomonzonita de San Cayetano. In *Catálogo de las unidades litoestratigráficas de Colombia: Valle Superior del Magdalena* (Vol. 2). Servicio Geológico Colombiano. <https://doi.org/10.32685/9789585313194.8>
- Bustamante, C., Cardona, A., Bayona, G., Mora, A., Valencia, V., Gehrels, G., & Vervoort, J. (2010). U-Pb LA-ICP-MS geochronology and regional correlation of Middle Jurassic intrusive rocks from the Garzon Massif, upper Magdalena valley and Central Cordillera, southern Colombia. *Boletín de Geología*, 32(2), 93-109.
- Bustamante, C., Archanjo, C., Cardona, A., & Vervoort, J. (2016). Late Jurassic to Early Cretaceous plutonism in the Colombian Andes: a record of long-term arc maturity. *GSA Bulletin*, 128(11-12), 1762-1779. <https://doi.org/10.1130/B31307.1>
- Bustamante, C., Archanjo, C. J., Cardona, A., Bustamante, A., & Valencia, V. A. (2017). U-Pb ages and Hf isotopes in zircons from parautochthonous mesozoic terranes in the western margin of Pangea: implications for the terrane configurations in the northern Andes. *The Journal of Geology*, 125(5), 487-500. <https://doi.org/10.1086/693014>
- Cardona, A., Cordani, U., & MacDonald, W. D. (2006). Tectonic correlations of pre-Mesozoic crust from the northern termination of the Colombian Andes, Caribbean region. *Journal of South American Earth Sciences*, 21(4), 337-354. <https://doi.org/10.1016/j.jsames.2006.07.009>
- Cardona, A., Valencia, V., Garzón, A., Montes, C., Ojeda, G., Ruiz, J., & Weber, M. (2010). Permian to Triassic I to S-type magmatic switch in the northeast Sierra Nevada de Santa Marta and adjacent regions, Colombian Caribbean: Tectonic setting and implications within Pangea paleogeography. *Journal of South American Earth Sciences*, 29(4), 772-283. <https://doi.org/10.1016/j.jsames.2009.12.005>
- Castaño, J. M., Rodríguez, F., & García, C. A. (2018). Caracterización de parámetros en la concentración de circones para andesitas, monzogranitos, riolitas, cuarcitas y cuar-

- zomonzonitas. *Boletín Geológico*, (44), 25-38. <https://doi.org/10.32685/0120-1425/boletingeo.44.2018.6>
- Cediel, F., Mojica, J., & Macías, C. (1980). Definición estratigráfica del Triásico en Colombia, Suramérica. Formaciones Luisa, Payandé y Saldaña. *Newsletters on Stratigraphy*, 9(2), 73-104. <https://doi.org/10.1127/nos/9/1980/73>
- Cediel, F., Mojica, J., & Macías, C. (1981). Las Formaciones Luisa, Payandé, Saldaña sus columnas estratigráficas características. *Geología Norandina*, (3), 11-20.
- Cochrane, R. S. (2013). *U-Pb thermochronology, geochronology and geochemistry of NW South America: Rift to drift transition, active margin dynamics and implications for the volume balance of continents* [Ph.D. thesis]. University of Geneva, Switzerland. <https://doi.org/10.13097/archive-ouverte/unige:30029>
- Cordani, U. G., Fraga, L. M., Reis, N., Tassinari, C. C. G., & Brito-Neves, B. B. (2010). On the origin and tectonic significance of the intra-plate events of Grenvillian-type age in South America: a discussion. *Journal of South American Earth Sciences*, 29(1), 143-159. <https://doi.org/10.1016/j.jsames.2009.07.002>
- Correa-Martínez, A. M., Rodríguez, G., Arango, M. I., & Zapata-García, G. (2019). Petrografía, geoquímica y geo cronología U-Pb de las rocas volcánicas y piroclásticas de la Formación Noreán al NW del Macizo de Santander, Colombia. *Boletín de Geología*, 41(1), 29-54. <https://doi.org/10.18273/revbol.v41n1-2019002>
- Correa Martínez, A. M., Ramírez, D., Rodríguez, G., Zapata, J. P., Obando, G., Muñoz, J. A., Rayo, L. del P., & Ureña, C. I. (2020). *Batolito Central de la Sierra Nevada, Magdalena, La Guajira y Cesar*. Servicio Geológico Colombiano.
- Correa Martínez, A. M., Rodríguez, G., Arango, M. I., Zapata, G., & Bermúdez, J. G. (2020a). Batolito de Mogotes. In *Catálogo de las unidades litoestratigráficas de Colombia: Macizo de Santander* (Vol. 1). Servicio Geológico Colombiano. <https://doi.org/10.32685/9789585279445.1>
- Correa Martínez, A. M., Rodríguez, G., Bermúdez, J. G., Arango, M. I., & Zapata, G. (2020b). Riolitas del Alto Los Caos. In *Catálogo de las unidades litoestratigráficas de Colombia: Macizo de Santander* (Vol. 1). Servicio Geológico Colombiano. <https://doi.org/10.32685/9789585279445.9>
- Coyner, S. J., Kamenov, G. D., Mueller, P. A., Rao, V., & Foster, D. A. (2004). *FC-1: a zircon reference standard for the determination of Hf isotopic compositions via laser ablation ICP-MS*. American Geophysical Union, Fall Meeting. San Francisco, USA.
- Cuadros, F. A. (2012). *Caracterização geoquímica e geocronológica do embasamento mesoproterozóico da parte norte da serra de San Lucas (Colômbia)* [Master Thesis]. Universidade de Brasília.
- Cuadros, F. A., Botelho, N. F., Ordóñez-Carmona, O., & Matteini, M. (2014). Mesoproterozoic crust in the San Lucas Range (Colombia): An insight into the crustal evolution of the northern Andes. *Precambrian Research*, 245, 186-206. <https://doi.org/10.1016/j.precamres.2014.02.010>
- Frantz, J. C., Ordóñez, O., & Chemale, F. (2007). *Caracterización de ambientes geológicos con mineralizaciones de oro en los Andes colombianos* [Memories]. VIII Congreso Colombiano de Minería, Medellín.
- González, H., Maya, M., Tabares, L. F., Montoya, A., Palacio, A. F., Sánchez, C., Barajas, A., & Vélez, W. (2015a). Memoria explicativa: Plancha 118 San Francisco. Scale 1:100 000. Servicio Geológico Colombiano.
- González, H., Maya, M., García, J. F., Gómez, J. P., Palacio, A. F., & Vélez, W. (2015b). Memoria explicativa: Plancha 84 Los Canelos. Scale 1:100 000. Servicio Geológico Colombiano.
- González, H., Maya, M., García, J. F., Camacho, J. A., Gómez, J. P., Cardona, O. D., Palacio, A. F., & Vélez, W. (2015c). Memoria explicativa: Plancha 94 El Bagre. Scale 1:100 000. Servicio Geológico Colombiano.
- Hellstrom, J., Paton, C., Woodhead, J. D., & Hergt, J. M. (2008). *Iolite: software for spatially resolved LA-(quad and MC) ICP-MS analysis*. In P. Sylvester (Ed.), *Laser Ablation ICP-MS in the Earth Sciences: Current Practices and Outstanding Issues* (pp. 343-348). Mineralogical Association of Canada.
- Ibáñez-Mejía, M., Ruiz, J., Valencia, V. A., Cardona, A., Gehrels, G. E., & Mora, A. R. (2011). The Putumayo Orogen of Amazonia and its implications for Rodinia reconstructions: New U-Pb geochronological insights into the Proterozoic tectonic evolution of northwestern South America. *Precambrian Research*, 191(1-2), 58-77. <https://doi.org/10.1016/j.precamres.2011.09.005>
- Ibáñez-Mejía, M., Pullen, A., Arenstein, J., Gehrels, G., Valley, J., Ducea, M., Mora, A., Pecha, M., & Ruiz, J. (2015). Unraveling crustal growth and reworking processes in complex zircons from orogenic lower-crust: The Proterozoic Putumayo Orogen of Amazonia. *Precambrian Research*, 267, 285-310. <https://doi.org/10.1016/j.precamres.2015.06.014>
- Janoušek, V., Farrow, C. M., & Erban, V. (2006). Interpretation of whole-rock geochemical data in igneous geochemistry:

- introducing Geochemical Data Toolkit (GCDkit). *Journal of Petrology*, 47(6), 1255-1259. <https://doi.org/10.1093/ptrology/egl013>
- Jaramillo, L. E., & Escovar, R. (1980). *Cinturones de pórfidos cupríferos en las cordilleras colombianas*. Simposio sobre metalogénesis en Latinoamérica, México D.F.
- Jiménez-Mejía, D. M. (2003). *Metamorphic and Geochronological Characterization of the Proterozoic Rocks of the Garzón Massif - Southeast of the Colombian Andes* [Master thesis]. Universidade de Sao Paulo.
- Jiménez Mejía, D. M., Juliani, C., & Cordani, U. G. (2006). P-T-t conditions of high-grade metamorphic rocks of the Garzon Massif, Andean basement, SE Colombia. *Journal of South American Earth Science*, 21(4), 322-336. <https://doi.org/10.1016/j.jsames.2006.07.001>
- Kroonenberg, S., & Diederix, H. (1982). *Geology of south-central Huila, uppermost Magdalena Valley, Colombia. A preliminary note*. Guide Book 21 Annual Field Trip Colombian Society Petroleum Geologists and Geophysicists.
- Kroonenberg, S. B. (1982). A Grenvillian granulite belt in the Colombian Andes and its relation to the Guiana Shield. *Geologie en Mijnbouw*, 61(4), 325-333.
- Kroonenberg, S. B. (2019). The Proterozoic Basement of the Western Guiana Shield and the Northern Andes. In F. Cediél y R. P. Shaw (eds.), *Geology and Tectonics of Northwestern South America. Frontiers in Earth Sciences* (pp. 115-192). Springer. https://doi.org/10.1007/978-3-319-76132-9_3
- Leal-Mejía, H. (2011). *Phanerozoic gold metallogeny in the Colombian Andes: A tectono-magmatic approach* [Ph.D. Thesis]. Universitat de Barcelona.
- Leal-Mejía, H., Shaw, R., & Malgrejo, J. C. (2019). Spatial-Temporal Migration of Granitoid Magmatism and the Phanerozoic Tectono- Magmatic Evolution of the Colombian Andes. In F. Cediél y R. P. Shaw (eds.), *Geology and Tectonics of Northwestern South America. Frontiers in Earth Sciences* (pp. 253-410). Springer. https://doi.org/10.1007/978-3-319-76132-9_5
- López-Isaza, J. A., & Zuluaga, C. A. (2020). Late Triassic to Jurassic magmatism in Colombia: Implications for the evolution of the northern margin of South America. In J. Gómez & A. O. Pinilla-Pachón (eds.), *The Geology of Colombia* (pp. 77-116, Vol. 2). Servicio Geológico Colombiano. <https://doi.org/10.32685/pub.esp.36.2019.03>
- Mantilla Figueroa, L. C., García, C. A., & Valencia, V. (2016). Propuesta de escisión de la denominada 'Formación Silgará' (Macizo de Santander, Colombia), a partir de edades U-Pb en zircones detríticos. *Boletín de Geología*, 38(1), 33-47. <https://doi.org/10.18273/revbol.v38n1-2016002>
- Maya, M., & González, H. (1995). Unidades litodémicas en la cordillera Central de Colombia. *Boletín Geológico*, 35(2-3), 43-57. <https://doi.org/10.32685/0120-1425/bolgeol35.2-3.1995.316>
- Núñez, A., & Murillo, A. (1982). *Memoria explicativa: Geología y prospección geoquímica de las planchas 244 Ibagué y 263 Ortega* [Report 1879]. Ingeominas.
- Ordoñez-Carmona, O., Pimentel, M. M., & De Moraes, R. (2002). Granulitas de Los Mangos: un fragmento Grenvilliano en la parte SE de la Sierra Nevada de Santa Marta. *Revista de la Academia Colombiana de Ciencias Exactas, Físicas y Naturales*, (26), 169-179.
- Otamendi, J. E., Ducea M., Cristofolini, E. A., Tibaldi A. M., Camilletti, G. C., & Bergantz G. W. (2017). U-Pb ages and Hf isotope compositions of zircons in plutonic rocks from the central Famatinian arc, Argentina. *Journal of South American Earth Sciences*, 76, 412-426. <https://doi.org/10.1016/j.jsames.2017.04.005>
- Paton, C., Woodhead, J. D., Hellstrom, J. C., Hergt, J. M., Greig, A., & Maas, R. (2010). Improved laser ablation U-Pb zircon geochronology through robust downhole fractionation correction. *Geochemistry, Geophysics, Geosystems*, 11(3), 36. <https://doi.org/10.1029/2009GC002618>
- Pearce, J. A. (2008). Geochemical fingerprinting of oceanic basalts with applications to ophiolite classification and the search for Archean oceanic crust. *Lithos*, 100(1-4), 14-48. <https://doi.org/10.1016/j.lithos.2007.06.016>
- Peña-Urueña, M. L., Muñoz-Rocha, J. A., & Urueña, C. L. (2018). Laboratorio de Geocronología en el Servicio Geológico Colombiano: avances sobre datación U-Pb en circones mediante la técnica LA-ICP-MS. *Boletín Geológico*, (44), 39-56. <https://doi.org/10.32685/0120-1425/boletin-geo.44.2018.7>
- Piraquive, A. (2017). *Marco Estructural: deformaciones y exhumación de los Esquistos de Santa Marta, la acreción e historia de deformación de un terreno caribeño al norte de la Sierra Nevada de Santa Marta* [Ph.D. Thesis]. Universidad Nacional de Colombia.
- Profeta, L., Ducea, M. N., Chapman, J. B., Paterson, S. R., Gonzales, S. M. H., Kirsch, M., & DeCelles, P. G. (2015). Quantifying crustal thickness over time in magmatic arcs. *Scientific Reports*, 5. <https://doi.org/10.1038/srep17786>
- Priem, H. N., P. Andriessen, N. A., Boelrijk, H., De Boorder, E. H., Hebeda, E., Huguett, E., Verdumen, A., & Verschure,

- R. (1982). Precambrian Amazonas region of southeastern Colombia (western Guiana Shield). *Geologie en Mijnbouw*, 61(3), 229-242.
- Quandt, D., Trumbull R., Altenberger, W., Cardona, A., Romer, R., Bayona, G., Ducea, M., Valencia, V., Vásquez, M., Cortés, E., & Guzmán, G. (2018). The geochemistry and geochronology of Early Jurassic igneous rocks from the Sierra Nevada de Santa Marta, NW Colombia, and tectono-magmatic implications. *Journal of South American Earth Sciences*, 86, 216-230. <https://doi.org/10.1016/j.jsames.2018.06.019>
- Quiceno, J., Osorio-Ocampo, S., Vallejo, F., Salazar, A., Ossa, C. A., Giraldo, L., & Romero, L. (2016). Petrografía y geoquímica del Stock de Payandé y su posible relación con el magmatismo Jurásico al sur de Colombia. *Boletín de Geología*, 38(2), 39-53. <https://doi.org/10.18273/revbol.v38n2-2016002>
- Ramírez, D. A., Correa-Martínez, A. M., Zapata-Villada, J. P., & Rodríguez, G. (2020). Tectono-magmatic implications of the Jurassic volcanic and volcanoclastic record of the Santa Marta Massif (Colombia). *Journal of South American Earth Sciences*, 104. <https://doi.org/10.1016/j.jsames.2020.102866>
- Ramos, V. A. (2008). The basement of the Central Andes: the Arequipa and related terranes. *Annual Review on Earth and Planetary Sciences*, 36, 289-324.
- Renne, P. R., Swisher, C. C., Deino, A. L., Karner, D. B., Owens, T. L., & DePaolo, D. J. (1998). Intercalibration of standards, absolute ages and uncertainties in $^{40}\text{Ar}/^{39}\text{Ar}$ dating. *Chemical Geology*, 145(1-2), 117-152. [https://doi.org/10.1016/S0009-2541\(97\)00159-9](https://doi.org/10.1016/S0009-2541(97)00159-9)
- Restrepo-Pace, P. (1995). *Late Precambrian to Early Mesozoic Tectonic Evolution of the Colombian Andes based on new geochronological, geochemical and isotopic date* [Ph.D. Thesis]. The University of Arizona.
- Restrepo-Pace, P., & Cediél, F. (2019). Proterozoic Basement, Paleozoic Tectonics of NW South America, and Implications for Paleogeographic Reconstruction of the Americas. In F. Cediél y R. P. Shaw (eds.), *Geology and Tectonics of Northwestern South America, Frontiers in Earth Sciences* (pp. 97-112). Springer. https://doi.org/10.1007/978-3-319-76132-9_2
- Restrepo, J. J., & Toussaint, J. F. (1989). Terrenos alóctonos en los Andes colombianos: Explicación de algunas paradojas geológicas. In *Memorias V Congreso Colombiano de Geología* [Vol. I, pp. 92-107]. Sociedad Colombiana de Geología.
- Restrepo, J. J., Ordóñez-Carmona, O., Martens, U., & Correa, A. M. (2009). Terrenos, complejos y provincias en la cordillera Central colombiana. *Ingeniería, Investigación y Desarrollo*, 9(2), 49-56.
- Restrepo, J. J., & Toussaint, J. F. (2020). Tectonostratigraphic terranes in Colombia: An update. First part: Continental terranes. In J. Gómez y D. Mateus-Zabala (eds.), *The Geology of Colombia* (pp. 37-63, Volume 1). Servicio Geológico Colombiano. <https://doi.org/10.32685/pub.esp.35.2019.03>
- Restrepo, J. J., Martens, U., & Giraldo-Ramírez, W. E. (2020). The Anaconda Terrane: A small early Paleozoic peri-Gondwanan terrane in the Cauca-Romeral Fault System. In J. Gómez y D. Mateus-Zabala (eds.), *The Geology of Colombia* (pp. 149-165, Volume 1). Servicio Geológico Colombiano. <https://doi.org/10.32685/pub.esp.35.2019.08>
- Restrepo, J. J., Ordoñez-Carmona, O., Armstrong, R., & Pimentel, M. M. (2011). Triassic metamorphism in the northern part of the Tahamí Terrane of the Central cordillera of Colombia. *Journal of South American Earth Sciences*, 32(4), 497-507. <https://doi.org/10.1016/j.jsames.2011.04.009>
- Rodríguez, G. (1995a). Petrografía y microtexturas del Grupo Garzón y el Granito de Anatexis de El Recreo, macizo de Garzón, cordillera Oriental-Colombia. *Revista Ingeominas*, (5), 17-36.
- Rodríguez, G. (1995b). Petrografía del macizo de La Plata, departamento del Huila. *Revista Ingeominas*, (5), 5-16.
- Rodríguez, G., Zapata, G., Velásquez, M. E., Cossio, U., & Londoño, A. C. (2003). Geología de las planchas 367 Gigante, 368 San Vicente del Caguán, 389 Timaná, 390 Puerto Rico, 391 Lusitania (parte noroccidental) y 414 El Doncello, escala 1:100 000 [Explanatory memory]. Ingeominas.
- Rodríguez, G., Arango, M. I., Zapata, G., & Bermúdez, J. G. (2016). *Catálogo de unidades litoestratigráficas de Colombia, Formación Saldaña. Cordilleras Central y Oriental Tolima, Huila, Cauca y Putumayo*. Servicio Geológico Colombiano.
- Rodríguez-García, G., Obando, G., Correa-Martínez, A. M., Zapata, G., Correa, T., Obando, M., Rincón, A., & Zapata, J. P. (2017a). *Redefinición del bloque norte del Batolito de Ibagué con base en nuevos datos de petrografía, litogeoquímica y geocronología U-Pb*. XVI Congreso Colombiano de Geología, Santa Marta, Colombia.
- Rodríguez, G., Zapata, G., Correa-Martínez, A. M., y Arango, M. (2017b). *Caracterización del magmatismo triásico-jurásico del macizo de Santander*. Servicio Geológico Colombiano.

- Rodríguez, G., Arango, M. I., Zapata, G., & Bermúdez, J. G. (2018). Petrotectonic characteristics, geochemistry, and U-Pb geochronology of Jurassic plutons in the Upper Magdalena Valley-Colombia: implications on the evolution of magmatic arcs in the NW Andes. *Journal of South American Earth Sciences*, 81, 10-30. <https://doi.org/10.1016/j.jsames.2017.10.012>
- Rodríguez G., Correa Martínez, A. M., Zapata Villada, J. P., & Obando, G. (2019a). Fragments of a Permian arc on the western margin of the Neoproterozoic basement of Colombia. In *The Geology of Colombia* (Volumen 1, pp. 204-245). Servicio Geológico Colombiano.
- Rodríguez, G., Zapata Villada, J. P., Obando, G., Correa Martínez, A. M., Ramírez, D., Muñoz, J. A., Rayo, L. del P., & Ureña, C. L. (2019b). *Batolito de Atánquez Sierra Nevada de Santa Marta Cesar*. Servicio Geológico Colombiano.
- Rodríguez, G., & Obando, G. (2020). Volcanism of the La Quinta Formation in the Perijá mountain range. *Boletín Geológico*, (46), 51-94. <https://doi.org/10.32685/0120-1425/boletin-geo.46.2020.535>
- Rodríguez-García, G., Correa-Martínez, A. M., Zapata-García, G., Arango-Mejía, M. I., Obando-Erazo, G., Zapata-Villada, J. P., & Bermúdez, J. G. (2020a). Diverse Jurassic magmatic Arcs of the Colombian Andes: Constraints from petrography, geochronology and geochemistry. In J. Gómez y A. O. Pinilla-Pachón (eds.), *The Geology of Colombia* (pp. 77-99, Volume 2). Servicio Geológico Colombiano. <https://doi.org/10.32685/pub.esp.36.2019.04>
- Rodríguez-García, G., Zapata, J. P., Correa-Martínez, A. M., Ramírez, D. A., & Obando, G. (2020b). Aportes al conocimiento del plutonismo del arco Mocoa-Santa Marta durante el Jurásico temprano-medio, en la margen noroccidental de los Andes, Colombia. *Boletín de Geología*, 42(3), 15-50. <https://doi.org/10.18273/revbol.v42n3-2020001>
- Rodríguez, G., Correa Martínez, A. M., Zapata, G., & Arango, M. I. (2020c). Monzogranito de La Corcova. In *Catálogo de las unidades litoestratigráficas de Colombia: Macizo de Santander* (Vol. 1). Servicio Geológico Colombiano. <https://doi.org/10.32685/9789585279445.4>
- Rodríguez, G., Zapata, G., Arango, M. I., & Correa Martínez, A. M. (2020d). Monzogranito de Santa Bárbara. In *Catálogo de las unidades litoestratigráficas de Colombia: Macizo de Santander* (Vol. 1). Servicio Geológico Colombiano. <https://doi.org/10.32685/9789585279445.3>
- Rodríguez, G., Zapata, G., Correa Martínez, A. M., & Arango, M. I. (2020e). Tonalita de San Martín. In *Catálogo de las unidades litoestratigráficas de Colombia: Macizo de Santander* (Vol. 1). Servicio Geológico Colombiano. <https://doi.org/10.32685/9789585279445.6>
- Rodríguez, G., Arango, M. I., Correa Martínez, A. M., & Zapata, G. (2020f). Riolita de San Joaquín. In *Catálogo de las unidades litoestratigráficas de Colombia: Macizo de Santander* (Vol. 1). Servicio Geológico Colombiano. <https://doi.org/10.32685/9789585279445.8>
- Rodríguez, G., Zapata Villada J. P., Correa Martínez A. M., Ramírez, D., Obando, G., Muñoz, J. A., Rayo, L. del P., & Ureña, C. L. (2020g). *Batolito de Pueblo Bello Sierra Nevada de Santa Marta Cesar*. Servicio Geológico Colombiano.
- Rodríguez, G., Sabrica, C., Zapata, J. P., Ramírez, D., Correa-Martínez, A. M., Obando, G., & Muñoz, J. A. (2022a). *Catálogo de unidades estratigráficas de Colombia, Granito de Ortega, cordillera Central*. Servicio Geológico Colombiano.
- Rodríguez, G., Sabrica, C., Zapata, J. P., Ramírez, D., Correa-Martínez, A. M., Obando, G., & Muñoz, J. A. (2022b). *Catálogo de unidades estratigráficas de Colombia, Granito de La Plata - cordillera Central*. Servicio Geológico Colombiano.
- Rodríguez, G., Arango, M. I., Zapata, G., & Bermúdez, J. G. (2022c). Cuarzomonzodiorita del Astillero. In *Catálogo de las unidades litoestratigráficas de Colombia: Valle Superior del Magdalena* (Vol. 2). Servicio Geológico Colombiano. <https://doi.org/10.32685/9789585313194.5>
- Rodríguez, G., Arango, M. I., Bermúdez, J. G., & Zapata, G. (2022d). Cuarzomonzonita de Los Naranjos. In *Catálogo de las unidades litoestratigráficas de Colombia: Valle Superior del Magdalena* (Vol. 2). Servicio Geológico Colombiano. <https://doi.org/10.32685/9789585313194.6>
- Rodríguez, G., Zapata, G., Arango, M. I., & Bermúdez, J. G. (2022e). Monzogranito de Algeciras. In *Catálogo de las unidades litoestratigráficas de Colombia: Valle Superior del Magdalena* (Vol. 2). Servicio Geológico Colombiano. <https://doi.org/10.32685/9789585313194.10>
- Rodríguez, G., Arango, M. I., Zapata, G., & Bermúdez, J. G. (2022f). Granito de Garzón. In *Catálogo de las unidades litoestratigráficas de Colombia: Valle Superior del Magdalena* (Vol. 2). Servicio Geológico Colombiano. <https://doi.org/10.32685/9789585313194.11>
- Rodríguez Ruiz, M. A. (2016). *Geochemistry and petrological characterization of the Payandé stock (Central cordillera, Colombia): crystallization conditions, structural input and geodynamic implications* [Bachelor Thesis]. Universidad de los Andes.

- Rubatto, D. (2002). Zircon trace element geochemistry: Partitioning with garnet and the link between U-Pb ages and metamorphism. *Chemical Geology*, 184(1-2), 123-138. [https://doi.org/10.1016/S0009-2541\(01\)00355-2](https://doi.org/10.1016/S0009-2541(01)00355-2)
- Silva-Arias, A., Páez-Acuña, L. A., Rincón-Martínez, D., Tamara-Guevara, J. A., Gómez-Gutiérrez, P. D., López-Ramos, E., Restrepo-Acevedo, S. M., Mantilla-Figueroa, L. C., & Valencia, V. (2016). Basement characteristics in the Lower Magdalena Valley and the Sinú and San Jacinto fold belts: Evidence of a Late Cretaceous magmatic arc at the south of the Colombian Caribbean. *Ciencia, Tecnología y Futuro*, 6(4), 5. <https://doi.org/10.29047/01225383.01>
- Spikings, R., Cochrane, R., Villagomez, D., Van der Lelij, R., Vallejo, C., Winkler, W., & Beate, B. (2015). The geological history of northwestern South America: from Pangaea to the early collision of the Caribbean Large Igneous Province (290-75 Ma). *Gondwana Research*, 27, 95-139. <https://doi.org/10.1016/j.jgr.2014.06.004>
- Stacey, J. S., & Kramers, J. D. (1975). Approximation of Terrestrial Lead Isotope Evolution by a 2-Stage Model. *Earth and Planetary Science Letters*, 26(2), 207-221. [https://doi.org/10.1016/0012-821X\(75\)90088-6](https://doi.org/10.1016/0012-821X(75)90088-6)
- Streckeisen, A. (1976). Classification and nomenclature of plutonic rocks. *Geologische Rundschau*, 63(2), 773-786. <https://doi.org/10.1007/BF01820841>
- Streckeisen, A. (1978). IUGS Subcommittee on the Systematics of Igneous Rocks: Classification and nomenclature of volcanic rocks, lamprophyres, carbonatites and melilitic rocks; recommendation and suggestions. *Neues Jahrbuch für Mineralogie*, 134, 1-14.
- Tassinari, C. C. G. (1981). *Evolução geotectônica da Província rio Negro-Juruena na região amazônica* [Master Thesis]. Instituto de Geociências, Universidade de São Paulo.
- Tassinari, C. C. G., & Macambira, M. J. B. (1999). Geochronological provinces of the Amazonian Craton. *Episodes*, 22(3), 174-182. <https://doi.org/10.18814/epiiugs/1999/v22i3/004>
- Tazzo-Rangel, D., Weber, B., González-Guzmán, R., Valencia, V., Frei, D., Schaaf, P., & Solari, L. (2018). Multiple metamorphic events in the Palaeozoic Mérida Andes basement, Venezuela: insights from U-Pb geochronology and Hf-Nd isotope systematics. *International Geology Review*, 61(13), 1557-1593. <https://doi.org/10.1080/00206814.2018.1522520>
- Thompson, A. B., & Connolly, J. A. D. (1995). Melting of the Continental-Crust: Some Thermal and Petrological Constraints on Anatexis in Continental Collision Zones and Other Tectonic Settings. *Journal of Geophysical Research*, 100, 15565-15579. <https://doi.org/10.1029/95JB00191>
- Toussaint, J. F. (1995). *Evolución geológica de Colombia. Triásico-Jurásico*. Universidad Nacional de Colombia.
- Tschanz, C. M., Jimeno, A., & Cruz, J. (1969). *Geology of the Sierra Nevada de Santa Marta (Colombia). Preliminary Report*. Ministerio de Minas y Energía, Instituto Nacional de Investigaciones Geológicas y Mineras y US. Geological Survey.
- Tschanz C. M., Cruz, J., Mehnert, H. H., & Cebula, G. T. (1974). Geologic Evolution of the Sierra Nevada de Santa Marta Northeastern Colombia. *GSA Bulletin*, 85(2), 273-284. [https://doi.org/10.1130/0016-7606\(1974\)85<273:GEOTSN>2.0.CO;2](https://doi.org/10.1130/0016-7606(1974)85<273:GEOTSN>2.0.CO;2)
- Van der Lelij, R., Spikings, R., & Mora, A., (2016). Thermochronology and tectonics of the Mérida Andes and the Santander Massif, NW South America. *Lithos*, 248-251, 220-239. <https://doi.org/10.1016/j.lithos.2016.01.006>
- Van der Lelij, R., Spikings, R., Gerdes, A., Chiaradia, M., Venemann, T., & Mora, A. (2019). Multi-proxy isotopic tracing of magmatic sources and crustal recycling in the Palaeozoic to Early Jurassic active margin of North-Western Gondwana. *Gondwana Research*, 66, 227-245. <https://doi.org/10.1016/j.jgr.2018.09.007>
- Velandia, F., Ferreira, P., Rodríguez, G., & Núñez, A. (1996). Memoria explicativa levantamiento geológico de la Plancha 366 - Garzón. Ingeominas.
- Velandia, F., Núñez, A., & Marquínez, G. (2001). Mapa geológico departamento del Huila. Escala 1:300 000 [Explanatory memory]. Ingeominas.
- Villagómez, D., Spikings, R., Magna, T., Kammer, A., Winkler, W., & Beltrán, A. (2011). Geochronology, geochemistry and tectonic evolution of the Western and Central cordilleras of Colombia. *Lithos*, 125, 875-896. <https://doi.org/10.1016/j.lithos.2011.05.003>
- Villagómez, D., Martens U., & Pindell J. (2015). *Are Jurassic and some older blocks in the northern Andes in-situ or far-travelled? Potential correlations and new geochronological data from Colombia and Ecuador*. Symposium: Tectónica Jurásica en la parte noroccidental de Sur América y bloques adyacentes.
- Villamizar-Escalante, N., Bernet, M., Urueña-Suárez, C., Hernández-González, J. S., Terraza-Melo, R., Roncancio, J., Muñoz, J. A., Peña, M. L., Amaya, S., & Piraquive, A. (2021). Thermal history of the southern Central Cordille-

- ra and its exhumation record in the Cenozoic deposits of the Upper Magdalena Valley, Colombia. *Journal of South American Earth Sciences*, 107. <https://doi.org/10.1016/j.jsames.2020.103105>
- Ward, D. E., Goldsmith, R., Cruz B., J., & Restrepo A., H. (1973). Geología de los cuadrángulos H-12 Bucaramanga y H-13 Pamplona, departamento de Santander. *Boletín Geológico*, 21(1-3), 1-134. <https://doi.org/10.32685/0120-1425/bolgeol21.1-3.1973.383>
- Wiedenbeck, M., Allé, P., Corfu, F., Griffin, W. L., Meier, M., Oberli, F., von Quadt, A., Roddick, J. C., & Spiegel, W. (1995). Three natural zircon standards for U-Th-Pb, Lu-Hf, trace element and REE analyses. *Geostandards Newsletter*, 19(1), 1-23. <https://doi.org/10.1111/j.1751-908X.1995.tb00147.x>
- Zapata, S., Cardona, A., Jaramillo, C., Valencia, V., & Vervoort, J. (2016). U-Pb LA-ICP-MS geochronology and geochemistry of Jurassic volcanic and plutonic rocks from the Putumayo region (southern Colombia): tectonic setting and regional correlations. *Boletín de Geología*, 38(2). <https://doi.org/10.18273/revbol.v38n2-2016001>
- Zapata, G., Rodríguez, G., & Arango, M. I. (2017). Petrografía, geoquímica y geocronología de rocas metamórficas aflorantes en San Francisco Putumayo y la vía Palermo-San Luis asociadas a los complejos La Cocha-Río Téllez y Aleluya. *Boletín de Ciencias de la Tierra*, 41, 47-64.
- Zapata, G., Correa Martínez, A. M., Rodríguez, G., & Arango, M. I. (2020a). Granito de Pescadero. In *Catálogo de las unidades litoestratigráficas de Colombia: Macizo de Santander* (Vol. 1). Servicio Geológico Colombiano. <https://doi.org/10.32685/9789585279445.2>
- Zapata, G., Arango, M. I., Correa Martínez, A. M., & Rodríguez, G. (2020b). Riolitas El Uvo. In *Catálogo de las unidades litoestratigráficas de Colombia: Macizo de Santander* (Vol. 1). Servicio Geológico Colombiano. <https://doi.org/10.32685/9789585279445.7>
- Zapata, G., Rodríguez, G., Arango, M. I., & Bermúdez, J. G. (2022). Cuarzomonzodiorita de Páez. In *Catálogo de las unidades litoestratigráficas de Colombia: Valle Superior del Magdalena* (Vol. 2). Servicio Geológico Colombiano. <https://doi.org/10.32685/9789585313194.3>
- Zapata-Villada, J. P., Rodríguez, G., Correa-Martínez, A. M., Ramírez, D., & Obando, G. (2020). *Catálogo de unidades estratigráficas de Colombia, Batolito de Patillal*. Servicio Geológico Colombiano.
- Zapata-Villada, J. P., Rodríguez, G., Ramírez, D., Correa-Martínez, A. M., Obando, G., & Muñoz, J. A. (2022). *Catálogo de unidades litoestratigráficas de Colombia, Complejo Icarcó*. Servicio Geológico Colombiano.
- Zuluaga, C., Pinilla, A., & Mann, P. (2015). Jurassic silicic volcanism and associated continental-arc basin in Northwestern Colombia (southern boundary of the Caribbean plate). In C. Bartolini y P. Mann (eds.), *Petroleum geology and potential of the Colombian Caribbean margin, AAPG memoir* (pp 137-160). American Association of Petroleum Geologists.
- Zuluaga, C. A., Amaya, S., Urueña, C., & Bernet, M. (2017). Migmatization and low-pressure overprinting metamorphism as record of two pre-Cretaceous tectonic episodes in the Santander Massif of the Andean basement in northern Colombia (NW South America). *Lithos*, 274-275, 123-146. <https://doi.org/10.1016/j.lithos.2016.12.036>
- Zuluaga, C., & López, J. (2019). Ordovician Orogeny and Jurassic Low-Lying Orogen in the Santander Massif, Northern Andes (Colombia). In F. Cediél y R. P. Shaw (eds.), *Geology and Tectonics of Northwestern South America, Frontiers in Earth Sciences* (pp. 195-250). Springer. https://doi.org/10.1007/978-3-319-76132-9_4



Manantial en un fracturado y erodado.
Heliconia, Antioquia, Colombia.
Autora: @elsitadelnaturv.



This work is distributed under the Creative Commons Attribution 4.0 License.

Received: October 31, 2021

Revision received: August 15, 2022

Accepted: August 23, 2022

Published online: December 28, 2022

Research article

Potential and prospects for hydrogeological exploration according to lithostructural criteria in Antioquia department, Colombia

Potencial y perspectivas de exploración hidrogeológica según criterios litoestructurales en Antioquia, Colombia

Teresita Betancur¹, Cristina Martínez¹

¹. School of Engineering, Universidad de Antioquia, Medellín, Colombia.

Corresponding author: Teresita Betancur, teresita.betancur@udea.edu.co

ABSTRACT

In the department of Antioquia, in addition to the geological units with primary porosity, the tecto-structural characteristics of the hard rocks confer permeability properties to the metamorphic and igneous units that allow the flow and storage of groundwater. This work aims to synthesize useful information to identify potential areas to conduct new hydrogeological explorations in Antioquia.

The official geological map at 1:100 000 scale, adjusted to the geological map of Antioquia 1:400 000 scale, provided the basic input to separate the different types of rock and their structural affectations to identify permeability characteristics that were scored ranging from very low and very high. The concept of determining hydrogeological potential based on geological criteria is centered on the idea that the nature and distribution of aquifers and aquitards in a geological system are controlled by the lithology, stratigraphy, and structures of the deposits and geological formations.

The results of this study showed that the Medellín Dunite, slope deposits, Guineales Formation, Tertiary alluvial, Cerrito Formation, Sincelejo Group, Corpa Formation, terraces and recent alluviums, and Mesa Formation have very high aquifer potential (23.4% of the departmental area); 5% of the surface of the department has rocks with high aquifer potential; 35% has rocks with moderate aquifer potential; and the remaining 37% of the department has a lower aquifer potential.

Based on these findings, in terms of the groundwater potential in Antioquia, the area includes geological units with porosity and primary and secondary permeability. Thus, groundwater exploration in this department is urgently needed to provide hydrogeological knowledge to assist in the search for complementary sources of water supply for the population.

Keywords: groundwater, secondary permeability, hydrogeology in Antioquia.

RESUMEN

En el departamento de Antioquia, además de las unidades geológicas con porosidad primaria, la afectación tecteostructural presente en las rocas duras confiere a unidades metamórficas e ígneas propiedades de permeabilidad que permiten el flujo y almacenamiento de aguas subterráneas. Este trabajo tiene como objetivo sintetizar información útil para la identificación de potenciales zonas para la realización de nueva exploración hidrogeológica en Antioquia.

El ensamble de la cartografía geológica oficial, escala 1:100 000, ajustado al mapa geológico de Antioquia 1:400 000, suministró el insumo base para separar los distintos tipos de roca y la afectación estructural que sobre ellos se ha registrado, para así imprimirles características de permeabilidad que se calificaron con rangos entre muy bajo y muy alto. La determinación del potencial hidrogeológico, a partir de criterios geológicos, parte de la idea según la cual la naturaleza y distribución de acuíferos y acuitardos en un sistema geológico están controlados por la litología, estratigrafía y estructuras de los depósitos y las formaciones geológicas.

Como resultados, se encontró que la Dunita de Medellín, los depósitos de vertiente, la Formación Guineales, los aluviales del Terciario, la Formación Cerrito, el Grupo Sincelejo, la Formación Corpa, las terrazas y aluviones recientes, y la Formación Mesa tienen potencialidad acuífera muy alta (23,4 % del área departamental); el 5 % de la superficie del departamento tendría rocas con potencial acuífero alto, y el 35 %, medio; en el 37 % restante el potencial sería menor.

A partir de estos hallazgos se concluye que el potencial de aguas subterráneas en Antioquia abarca unidades geológicas con porosidad y permeabilidad primaria y secundaria; en este sentido, la exploración de aguas subterráneas en el departamento es una tarea urgente en pro del conocimiento hidrogeológico y la búsqueda de fuentes complementarias de abastecimiento para la población.

Palabras clave: aguas subterráneas, permeabilidad secundaria, hidrogeología en Antioquia.

1. INTRODUCTION

Aquifers are geological formations that allow the storage and circulation of water under conditions that meet the quality and quantity, from an economic perspective, to satisfy human needs (Betancur et al., 2020). However, the domain of the *hydrogeology* discipline transcends the field of aquifer formations and focuses on the water-rock relationship under geological (Verma et al., 2016; Hoque et al., 2017), hydrological, and ecosystem considerations (Brkió, 2019), including the interaction of groundwater with surface and marine waters, and considering recharge, transit, and discharge zones (De Vries and Simmers, 2002; Harlow and Hagedorn, 2018; Mussa et al., 2020).

A hydrogeological unit is a geological formation, part of a geological formation, or a group of geological formations with similar hydraulic properties. Among their characteristics, conductivity is the one that determines the importance degree of an aquifer, and then, references can be established to determine the potential of a unit as more or less productive. It should be clear that the conditioning of the economic viability of extracting water from a geological formation is mediated by the need or demand of the resource; thus, in terms of hydraulic conditions, no net limits can be established to qualify a formation as an aquifer or not. Classical hydrogeology recognizes the aquifer characteristics of formations with conductivities up

to the order of 10^{-4} m/day; thus, those that exceed 1 m/day are more favorable (Custodio and Llamas, 1996).

Determining hydrogeological potential based on geological criteria is based on the classical concept that the nature and distribution of aquifers and aquitards in a geological system are controlled by the lithology, stratigraphy, and structures of the deposits and geological formations. Lithology is the physical structure of these formations, including the mineral composition, the size, and the packing of the grains, the sediments, and the rocks that constitute the geological system, as well as the dynamic effects printed on them by tectonics. Stratigraphy describes the geometry and age relationships between various units. The structural characteristics, such as foliation, fractures, folds, and faults, are the conditions of the geological system produced by deformation on the rocks. In unconsolidated deposits, lithology and stratigraphy are the most important controls. Thus, knowledge of lithology, stratigraphy, and structures directly affects the understanding of aquifer and aquitard distributions (Freeze and Cherry, 1979).

Deposits and detrital sedimentary rocks, as well as volcanoclastic formations, are associated with their original porosity characteristics and, with them, permeability variables that are translated into hydraulic conductivity (Ren and Santamarina, 2018). Limestone formations usually develop karst structures (Kalhor et al., 2019). At the same time, crystalline intrusive

and metamorphic rocks are naturally moderate with very low permeability, given their compact texture; consequently, their aquifer potential is considered limited compared to that of porous formations (Briški et al., 2020).

Studies on aquifers in fractured environments have increased given the extent of hard rocks in the global geological context and the growing dependence on the water that circulates through them (Fiume et al., 2020). Hard rocks constitute the basement of all continents (Lachassange et al., 2021) and are particularly exposed on the surface of the great shields of Africa, India, North America, South America, Australia, and Europe.

Regarding the hydraulic conductivity (Qian et al., 2019) and the presence of fractures and cleats presented by several authors, notably (Srinivasa Rao et al., 2000), the differentiation and analysis of factors such as density, suitability, roughness (Scesi and Gattinoni 2007), and openness make it possible to define the aquifer conditions. Lachassange et al. (2021) show that dyke-type structures can also lead to the occurrence of routes for the movement of fluids such as water. The development of shear zones, a satellite effect common to faulting processes, represents another source of permeability qualities in hard rocks (Henriksen and Braathen, 2006).

On the surface, rocks are exposed to intense weathering processes, which affect their storage capacity and hydraulic conductivity. Lachassagne et al. (2021) suggest that hard rock aquifers develop mainly within the first 100 m below the soil surface on profiles that comprise an unconsolidated layer, generally of low permeability, followed by a layer on which a layer network of fractures that generate permeability has developed. Given this concept, the role of weathering is fundamental for the formation of aquifers in fractured environments.

Anand and Paine (2002) and Dewandel et al. (2006) showed that fractured aquifers, mainly in igneous and metamorphic rocks, are subject to weathering, especially chemical weathering, which leads to variable porosity and hydraulic conductivity. Based on hydraulic tests, according to the volumes of injected water, these authors estimated conductivities above 10^{-5} m/day. Rukavicková et al. (2021) studied the hydraulic conductivity of eight different granitoids in the Bohemian massif in the Czech Republic and found that in comparison to the other granitoids, the coarse-grained granitoids have microcracks with greater length and opening, connectivity, and hydraulic conductivity. In addition, they noted that for different types of granitoid rocks, the appearance of the fractures and the hydraulic conductivity of the rock matrix were similar.

The use of spatial modeling tools to determine the possible conditions that favor the presence of groundwater in hard rocks has been applied in several regions where there is a need for alternative sources of groundwater. Arnous (2016) combined geospatial analysis methods to define the possible presence of water in rock masses in Egypt, and Anbarasu et al. (2020) used spatial analysis tools to delimit areas of aquifer interest in India. In both cases, satellite image interpretation methods were used to determine the thickness of weathering profiles and lineament density.

Hydrogeological data in Colombia covers less than 15% of the national territory, although the data do identify more than 75% of the territory has favorable natural characteristics for developing aquifers (Vargas et al., 2013; Ideam, 2019). However, access to high-quality water continues to be a condition experienced in many regions, including more than 40% of the population in rural areas, and in many urban centers (DNP, 2021). This same scenario occurs in the department of Antioquia.

The regional context of the geology of Antioquia, including the geodynamic situation associated with its location in a zone of tectonic plate interaction, leads to the need to consider that, in addition to the geological units with primary porosity, the tecto-structural effect present in the hard rocks confers metamorphic and igneous formation permeability properties that allow the flow and storage of groundwater.

This study aims to synthesize, from the geological maps of the Servicio Geológico Colombiano (SGC) –scale 1: 100 000– and other official sources, useful information to identify potential aquifers for future hydrogeological exploration in Antioquia.

2. GEOLOGICAL FRAMEWORK

The department of Antioquia, located in the northern corner of Colombia, is a territory in which physiographic conditions are marked by a great variety of reliefs, from the coast in the Gulf of Urabá, the paramos of the Western and Central cordilleras, the depressions in the Valleys of Cauca and Magdalena, and the foothills of the coastal zone at the entrance to the Atlantic (Figure 1). The topographic conditions, the influence of the intertropical convergence zone, and the impact of air currents from the Pacific, Caribbean, and Amazonia determine its complex climatic conditions and variable humidity regimes (Arias et al., 2021).

The mosaic of covers and types of soil, together with the dense network of currents, move the runoff flows that conver-

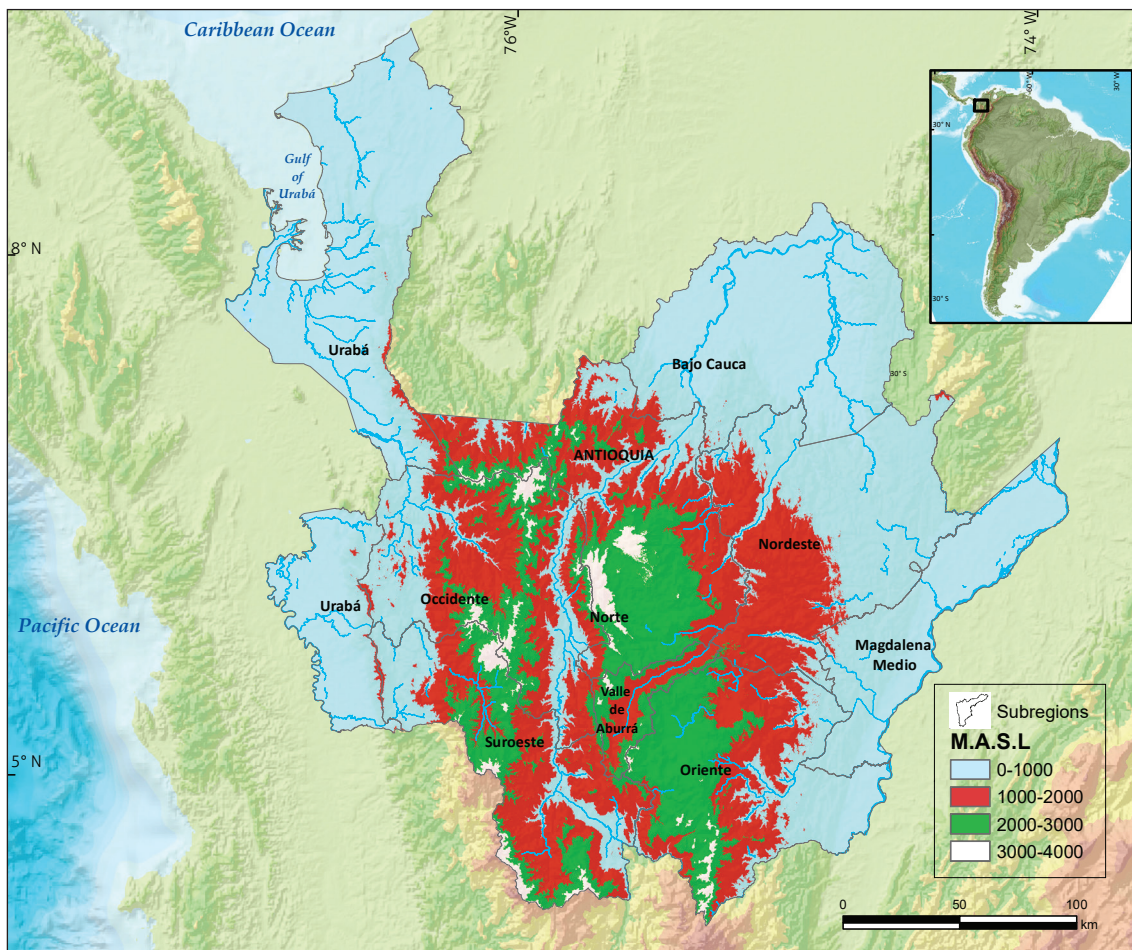


Figure 1. Study area
Source: Official DTM.

ge in the different hydrographic subzones (Vargas et al., 2013), and all the tributaries finally reach the Caribbean Sea.

The average annual precipitation in Antioquia is 2920 mm/year (Poveda, 2007), varying spatially between 1500 mm and 4000 mm/year (Mejía, 2008). The areas with lower rainfall are in the valley of the Cauca River, to the west of the department. The greatest rainfall amount occurs at the boundaries of the department of Chocó, at the southwestern end, in the vicinity of El Carmen de Bolívar, followed by the lower Cauca of Antioquia and the southeastern part in the Central Cordillera. The distribution of rainfall during the year is bimodal in most of the department; however, to the north, in the lower Cauca and the Gulf of Urabá, the regime is monomodal with a single dry season from December to March and a rainy season the remainder of the year. On average, evapotranspiration is 1170 mm/year (Poveda, 2007).

At the interannual time scale (several years, less than a decade), the climate of most of Earth is controlled by the El Niño Southern Oscillation (ENSO) phenomenon, which occurs because of the interaction between the circulation of winds and sea temperatures over the tropical Pacific. In Colombia, specifically in Antioquia, during El Niño, there is a drastic decrease in rainfall and river flows. During La Niña, the opposite processes occur, and there are storms, river floods, and other flooding events (Poveda et al., 2010).

For Antioquia, these characteristics evoke the image of a territory full of water: humidity in the atmosphere, rainfall over the entire geographical area, and drainage circulating in intricate channels on the surface. However, it should be noted that this territory experiences other complex events that occur naturally and through human action, such as deforestation and illegal mining, and climate change with a change in hydrologi-

cal systems. In addition, groundwater, whose occurrence will also depend on geological conditions, is also important.

In the department of Antioquia, there are metamorphic, igneous, and sedimentary rock units, whose ages have been assigned from the Proterozoic to the Recent (González, 2001).

The rocks of the Precambrian and Paleozoic periods were affected by several plutonic bodies until the Cretaceous period, a time in which, in addition to magmatic activity, the accumulation of sediments and products of oceanic volcanism to the west of the Central Cordillera occurred. These rocks were attached, by tectonic effects, to the continent in the Mesozoic period (González, 2001).

As observed on the different versions of the geological map of Antioquia (González et al., 1996; González, 2001), the Cauca River basin, the lower Cauca, and the Urabá region are characterized by the presence of sedimentary rocks originating during the Paleogene-Neogene period.

González (2001) and Restrepo and Toussaint (2020), among others, noted that the uplift of the mountain ranges extended until the Pliocene, a period during which the action of erosive processes gave rise to the formation of alluvial and lacustrine deposits, marine areas and watersheds; this activity continues today.

As implicit in the previous text, the structural impact on the rock units that frame the geology of Antioquia has determined the presence of faults and associated with them, fractures, joints, and shear zones that have modified the original structural patterns conferring to these hard formations secondary permeability conditions that favor the presence and flow of groundwater, from recharge to transit to discharge.

Colombia has been divided into 16 hydrogeological provinces, considering the sedimentary basins and tectonic units

that correspond to unique geological events whose physical limits are marked by regional megafractures documented in the geological studies of the country, especially those that describe the subdivision of land (Vargas et al., 2013). In the territory of Antioquia, the provinces Sinú, San Jacinto, Urabá, Valle Medio del Magdalena, and Valle Bajo del Magdalena are present.

The hydrogeological knowledge of Antioquia is limited to 7 aquifer systems that represent approximately 12% of the departmental territory (Ideam, 2019). However, the use of groundwater exceeds the boundaries of these systems and transcends the field of sedimentary rocks with primary porosity. In addition, access to drinking water in mainly rural areas, and in some several urban centers is low and reaches, on average, 28% of the population (Gobernación de Antioquia, 2018), a circumstance that forces people to seek alternative water supply sources to improve their standard of living.

Ecosystem considerations are beyond the scope of this work, but it is necessary to note that surface water-groundwater interactions largely determine ecosystem functionality. This is one more argument in favor of increasing knowledge of the lithostructural conditions that can determine the dynamics of groundwater.

3. MATERIALS AND METHODS

Considering the purposes of this study, the geological-structural evaluation focused on determining the porosity and permeability conditions that are relevant to promoting the storage and flow of groundwater, in terms of defining aquifer potential to identify relevant structural features for the subsequent delimitation of potential recharge zones. The characteristics of the deposits and clastic sedimentary rocks were considered, and

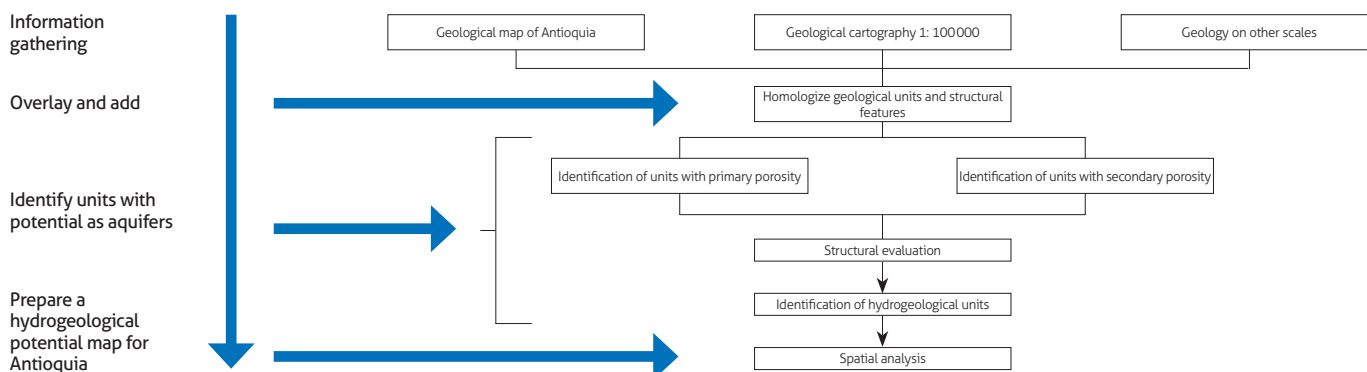


Figure 2. Methodological scheme

similarly, the conditions of the hydrogeological unit were determined for the hard rocks that have or have not been structurally affected and weathered. The approach for analyzing the information is illustrated in Figure 2.

The synthesis of Antioquia geological information was based on the review of the official geological map generated by the Servicio Geológico Colombiano (SGC) and on some field verification campaigns (Betancur and Martínez, 2021). A map at a scale of 1: 100 000 was used by González (2001), González et al. (1996); Kassem et al. (1979); Calle and González (1980, 1982); Bermúdez et al. (2012); Dávila et al. (2018a); Dávila et al. (2018b); Feininger (1970); Fonseca et al. (2011); Fonseca et al. (2012); Geotec (2003); Gómez et al. (2008); Gómez et al. (2009); Gómez et al. (2011); González (1992); Londoño and González (2002); González et al. (2015a); González et al. (2015b); González et al. (2015c); González et al. (2015d); González et al. (2015e); González (1980); Hall et al. (1970); Agustín Codazzi Geographical Institute (IGAC) and Geosciences, Mining and Chemical Research Institute (Ingeominas) (2005); Mejía et al. (1983 a and b); Rodríguez et al. (2013); Rodríguez et al. (2010); Rodríguez and Ulloa (1994); Rodríguez et al. (2005); Zapata et al. (2013); Zapata and Cossio (2001).

From this map, units were assembled, grouped, and confirmed, considering the interpretation and nomenclature recorded in the geological maps of Antioquia at a scale 1:400 000 (González, 2001) or in the most recent map product at 1:100 000. For the Bajo Cauca, details of the 1:25 000 map were included (Corantioquia and Universidad de Antioquia, 2014), and for the Aburrá Valley, the geological map at scale 1:10 000 was included (Metropolitan Area of the Aburrá Valley [AMVA], and Microzonation Consortium, 2007).

Clastic sedimentary rocks and deposits are geological units with primary porosity, while the presence of fractures, joints, shear, dissolution voids, and even weathering confer secondary porosity to the solid medium. No porosity characteristics are applied to an unaltered rock without structural affectation.

La Felice et al. (2014) characterized the fractures of the volcanic rocks on Mount Amiata in Italy, which are characterized by having a matrix that confers very low permeability; however, these rocks contain an aquifer of great importance. The authors deduced that within these rocks, the flow and storage of groundwater occur mainly through fractures, that is, faults and associated fracturing zones. The discontinuities and the intersections of the fractures are zones and potential sites of high permeability that favor the circulation and storage of ground-

water. This finding coincides with that described by Norton and Knapp (1997) and Faulkner et al. (2010), who state that in volcanic rocks, the flow of groundwater occurs mainly through discontinuities (fractures, shear zones, and faults).

Nikic et al. (2020) noted that ultramafic rocks generally have very low porosity, so they are classified as almost or completely waterless rocks. However, due to tectonic activity and exogenous processes over geological time, some ultramafic rocks exhibit a certain degree of secondary porosity due to fracturing. Thus, hydraulically interconnected fractures can form fractured aquifers, such as the one found in Gruda, on Mount Zlatibor, in western Serbia. These same authors stated that at a macroscale, the ultramafics of Gruda are rocks without porosity whose hydrogeological importance is not significant; however, at a medium scale (m), secondary porosity takes on some importance, and although it is not significant, this porosity allows some permeability and formation of a fractured aquifer. However, at a microscale (dm, cm), secondary fractures are significant from a hydrogeological perspective.

Cilona et al. (2016) performed a structural analysis on rock outcrops in a sandstone-shale sequence exposed along the Santa Susana Field Laboratory and its surroundings (California), and they studied the joints and faults of multiple scales that cross this area. In their study, they showed that the rock has a high frequency of hydraulically active fractures that consist of a combination of joints and strata divisions that slope 30° toward the northwest. This was determined from observations in vertical boreholes, which provided information on the parallel fractures of the formation but not on the subvertical characteristics. The authors state that the abundance of zones with shear fractures and zones of relatively small faults that cross these lithological units causes the strata of shale and siltstone that have very low primary permeability to exhibit strong vertical hydraulic connectivity.

In 1999, Karro and Lahermo noted that although intact igneous or metamorphic rocks are compact and do not contain groundwater, these rocks are almost always fissured and fractured to a variable degree and that the irregular appearance of fissures and fractures in the crystalline bedrock, their interconnection, and the size of their openings or the abundance of the filling material constitute a complex, heterogeneous, and anisotropic medium for the flow of groundwater. The same authors noted that groundwater is more mobile in the shallowest parts of bedrock and that its movement slows with increasing depth; in addition, the depth limit that would separate these two domains would be approximately 200 m.

The hydraulic conductivity (K) of open fractures and fractured rock zones can be high; however, it varies by orders of magnitude from 10^{-5} m/s to 10^{-12} m/s, depending on the tectonic properties of rock units, type of petrographic rock, and abundance of clayey fracture fillings (Karro and Lahermo, 1999). In the most favorable cases, the hydraulic conductivity of the upper part of fractured bedrock can equal the typical K values of the permeable stratified material ($<10^{-5}$ m/s).

Based on these considerations and the effects of weathering on the different types of rock, a scale was proposed to classify permeability values between the very high and very low ranges (Table 1).

Table 1. Criteria to rank the potential permeability according to structural characteristics

Structures	Permeability
Intense fracturing or dissolution (karstification)	Very high
Units with primary porosity and grain size greater than silt	High
Fractures, more joints and shears in the rock unit	Moderate
Presence of joints with uniform distribution in the geological unit	Low
Local jointing that does not incorporate the entire polygon of the geological unit	Very low
Structurally unaffected rocks	NA

Table 2 proposes a double-entry matrix to rank the hydrogeological potential of a geological unit, considering its conditions of porosity (horizontal reading) and permeability (vertical reading). To test the aquifer condition, hydrogeological exploration work that results in a conceptual hydrogeological model should be carried out, considering these prioritization criteria. For rock units without pores or permeability, the definition of potential does not apply.

Table 2. Possible aquifer potential according to porosity and permeability conditions

Porosity Permeability	Primary	Secondary by fracturing	Secondary by dissolution	No pores
Very high	Very high	Very high	Very high	Very low
High	Very high	Very high	Very high	Very low
Moderate	High	High	High	Very low
Low	Moderate	Low	Moderate	Very low
Very low	Low	Low	Low	Very low
Nonpermeable	Very low	Very low	Very low	Very low

4. RESULTS

According to the methodological order outlined above, the geological map of Antioquia, the structural conditions, and

the definition of aquifer potential according to litho-structural characteristics are described below.

4.1. Homologation of geological units: *Geological map of Antioquia*

During the map assembly process, four specific scenarios occurred:

- i) Between one plate and another, continuity and coincidence were recorded in the designation of the geological units. When this occurred, the polygons were merged, and the description and nomenclature were preserved.
- ii) Between two neighboring plates, discontinuities were recorded that led to discrepancies in the shape, extension, or characterization of units. In these circumstances, meticulous readings of the reports and, when available, field notebooks were used to compare rock types with the units arranged in the departmental geological map, and the new limits were digitized. Then, the name and description of the unit were assigned according to the geology of the departmental map of Antioquia.
- iii) There were gaps in the geological plates at a scale of 1:100 000 (Plate 103 was not available, and Plates 114, 115, and 104 did not overlap). Thus, these gaps were completed based on the geological mapping of 1:400 000 (Geotec, 2003; González et al., 1996).
- iv) There were some data with higher resolution scales, and thus, adjustments were applied to the areas of Bajo Cauca, Urabá, and Valle de Aburrá, including some units that had an extent was readable at 1:100 000.

Additionally, the major structural features, such as fault lines or lineaments, were coupled, and other structures were merged.

Considering the importance of knowing the geology in a hydrogeological context, first, we describe the units of hard rocks (metamorphic and igneous) were described, and then we describe the soft units (sedimentary rocks and unconsolidated deposits), also considering their age (Figure 3).

González (2001) presents an extensive description of metamorphism in Antioquia, and the evaluations are summarized here: the metamorphic rocks of the study area are located to the north of the department, on the western side, and on the axial part of the Central Cordillera. Some units have been assigned Precambrian ages, such as the Puente Peláez Mig-

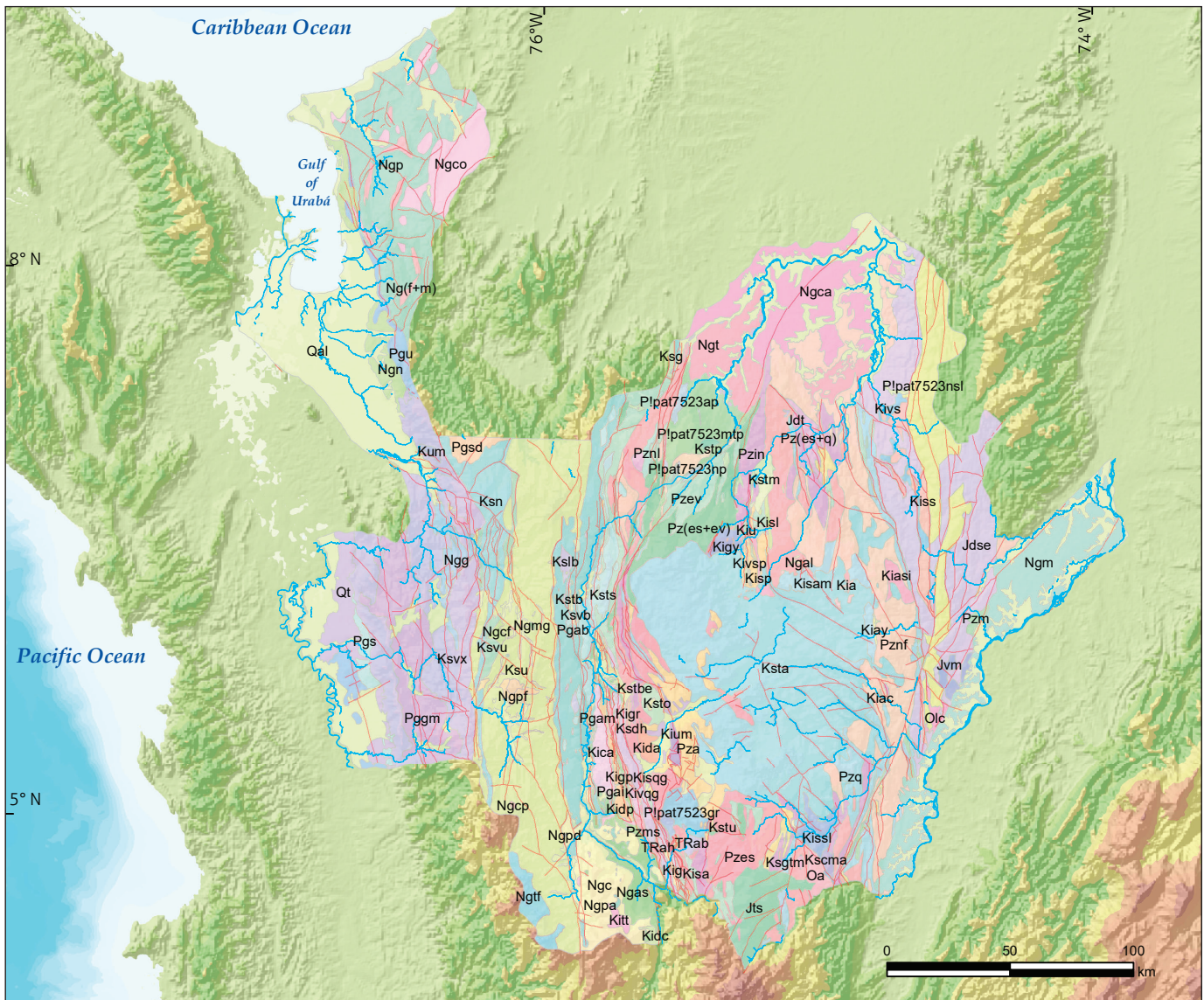


Figure 3. Geological map of Antioquia
 Geological legend can be read in González (2001) and referenced geological mapping bibliography.
 Source: adapted from González (2001).

matites (TRmPP-PEgr), the Puquí Complex (PEmt), and the San Lucas quartz-feldspatic (PEnsl). Those of Paleozoic age include the Cajamarca Complex (Pznf, Pznl, Pzes, Pzev, Pzq, and Pzm), the Valdivia Group, part of the Ayurá-Montebello Group, and the Cajamarca Group. During the Triassic and Jurassic periods, some migmatites were formed, including the Medellín Amphibolites (TraM) and gneissic bodies (TRgLC). Metamorphic rocks of Cretaceous age have been identified west of the Quebradagrande Complex, toward the Cauca River, and these rocks constitute a lithodemic unit called the Ar-

quía Complex (Kica). Tectonic activity in the Tertiary period determined the occurrence of very low metamorphism rocks (Pgsd).

Most likely, the igneous activity that marks the territory of Antioquia began during the Permian-Triassic event when the intrusion of some granitic stocks, such as those of Amagá Stock (Trga) and El Buey Stock (Trab), occurred (González, 2001; Mejía et al., 1983 a and b; Rodríguez et al., 2005). Igneous activity in the Central Cordillera extended until the Triassic with the intrusion of adamellitic stocks (Trah) on the

western flank of the Central Cordillera and continued, in a more intense way, during the Jurassic with the emplacement of the Segovia batholiths (Jdse) (González et al., 2015e) and Sonsón (Jts) (González, 1980), continuing until the end of the Cretaceous, with two well-defined magmatic cycles, one in the Early Cretaceous and another in the Late Cretaceous, corresponding to the great Antioquia Batholith (Ksta), located in the central part of the department (Gómez et al., 2011; Feininger et al., 1970). These intrusive cycles were manifested on both the eastern and western edges of the Central Cordillera. The basic plutonism affected both the axial part and the flanks of the Central Cordillera during the Lower Cretaceous: they have dioritic to gabbroid compositions; they are distinguished in Yarrumal, Pueblito, (Kidp), and Heliconia (Ksdh); in some cases, they are associated with serpentized ultrabasic rocks (Mejía et al., 1983 a and b).

The marine sedimentation of the Cretaceous was interrupted or followed by periods of intense basic volcanism of the ocean floor, such as that indicated in the Quebradagrande Complex (Kisqg) toward the western flank of the Central Cordillera in Campamento (Calle and González, 1980). The Cañasgordas Group with a basal unit, the Barroso Formation or Barroso Vulcanites (Ksvb), is the oldest lithological unit in the Cordillera Occidental and represents intense basic oceanic volcanism from the end of the Early Cretaceous to the Late Cretaceous (Mejía et al., 1983 a and b). Serpentized ultramafite bodies and gabbros associated with volcanic rocks could represent tectonically emplaced fragments of ophiolites during the Late Cretaceous (Ksvu, Kium) (Londoño and González, 2002; González and Salazar, 2002; Geotec, 2003).

On the Cordillera Occidental, syntectonic and post-tectonic plutons emerged, some with batholithic dimensions, such as the Farallones Pluton (Ngtf), which marked the continuation of the magmatic activity initiated in the Cretaceous. Related to the current valley of the Cauca River are subvolcanic intrusions, with predominant andesitic composition and porphyritic structure and ages between the late Miocene and the Pliocene (Ngpa, Ngpd) (Feininger, 1970; Calle and González, 1980).

Volcanic rocks of oceanic affinity are found in both the Central Cordillera and Cordillera Occidental; in the latter, they are normally interspersed with marine sediments. The boundary between the two mountain ranges is accompanied by ultramafics and gabbros in the Romeral fault system. According to their geographical and tectonic positions, the vulcanites of

the Quebradagrande Complex (Kivqg) and the Barroso Volcanic Member (Kivb) have been recorded in the study area (Mejía et al., 1983 a and b). Between the Mandé Batholith (Pggm) and the western flank of the Western Cordillera extends a body of volcanic rocks called the Santa Cecilia La Equis Complex (Ksvx) (Geotec, 2003).

On the sediments of the Amagá Formation, in contrast, the flows and pyroclastics of the Combia Formation (Ngc) were deposited, after which, a cycle of intense volcanic activity began that occurred until recently (Calle and González, 1980, 1982).

Cretaceous sedimentary rocks are associated with the two mountain ranges that cross the department (Central and Occidental). Some formations are exclusively sedimentary, while others are interspersed with basic volcanic rocks. According to their geographical or tectonic position and age, the following units were defined and described: San Pablo Formation (Kisp), La Soledad Formation (Kils), Abejorral Formation (Kisa), Quebradagrande Group (Kisqg), and Cañasgordas Group (Ksu.). Some of these lithological units are essentially sedimentary, but others show an intimate spatial relationship with basic volcanic rocks in an oceanic environment, both in the Western Cordillera and along tectonic systems in the Central Cordillera (Hall et al., 1970; González., 1980).

In the department, considering the differences in the sedimentological characteristics and accumulated environments of the different sedimentary and epiclastic sequences of the Cenozoic, these have been grouped for their description and characterization in basins according to their geographical location. One of these basins corresponds to the Amagá-La Pintada-Bolombolo basin, which is in the southern-central region of the department and is characterized by an intramontane basin of tectonic origin, where coal banks and mantles appear that are of economic importance and have been exploited for more than 80 years (González, 2001). Sedimentation in this basin during the Cenozoic was controlled by tectonism in the area along the Romeral Fault System. The Late Paleogene-Early Neogene sedimentation of the Cauca River basin is continental and constitutes the Amagá Formation (Ngsa, Pgia, Pgam), characterized by the presence of coal banks and layers (Calle and González, 1980).

Quaternary deposits are mainly alluvial (Qal, Qt) and increase their extent toward the flat areas of the department. Flow and colluvial deposits (Qf), due to their extension, are not always represented on the map, although they may be locally significant.

4.2. Structural conditions

The department of Antioquia is located near the union of the Nazca, Caribbean, and South American plates, which results in complex tectonics marked by subduction and faulting mechanisms. Of the successive deformations to which this territory has been subjected over time, the current tectonic conditions have only been valid in the late Neogene. That is, the Western and Central Cordilleras have acted approximately as a single tectonic block during the last episodes of the Andean orogeny (Restrepo and Toussaint, 2020).

The notion of segments or terrains indicates that northwestern Colombia, as part of the South American plate, was for-

med by a series of alloctene terranes (mosaic tectonic blocks limited by faults) accreted to an autochthonous block during different geological periods (González, 2001). According to Restrepo and Toussaint (2020), the Cordillera Central consists of the Tahamí terrain and part of the Chibcha terrain; the Western Cordillera is associated with the Calima terrain and part of the Cuna. The two mountain ranges are physiographically and geologically different.

The faults that are currently represented in Antioquia have a perpendicular arrangement: the first system is represented by the Palestina and Mulato faults to the east and Cauca-Romeral to the west with a direction between NNE-SSW and NE-

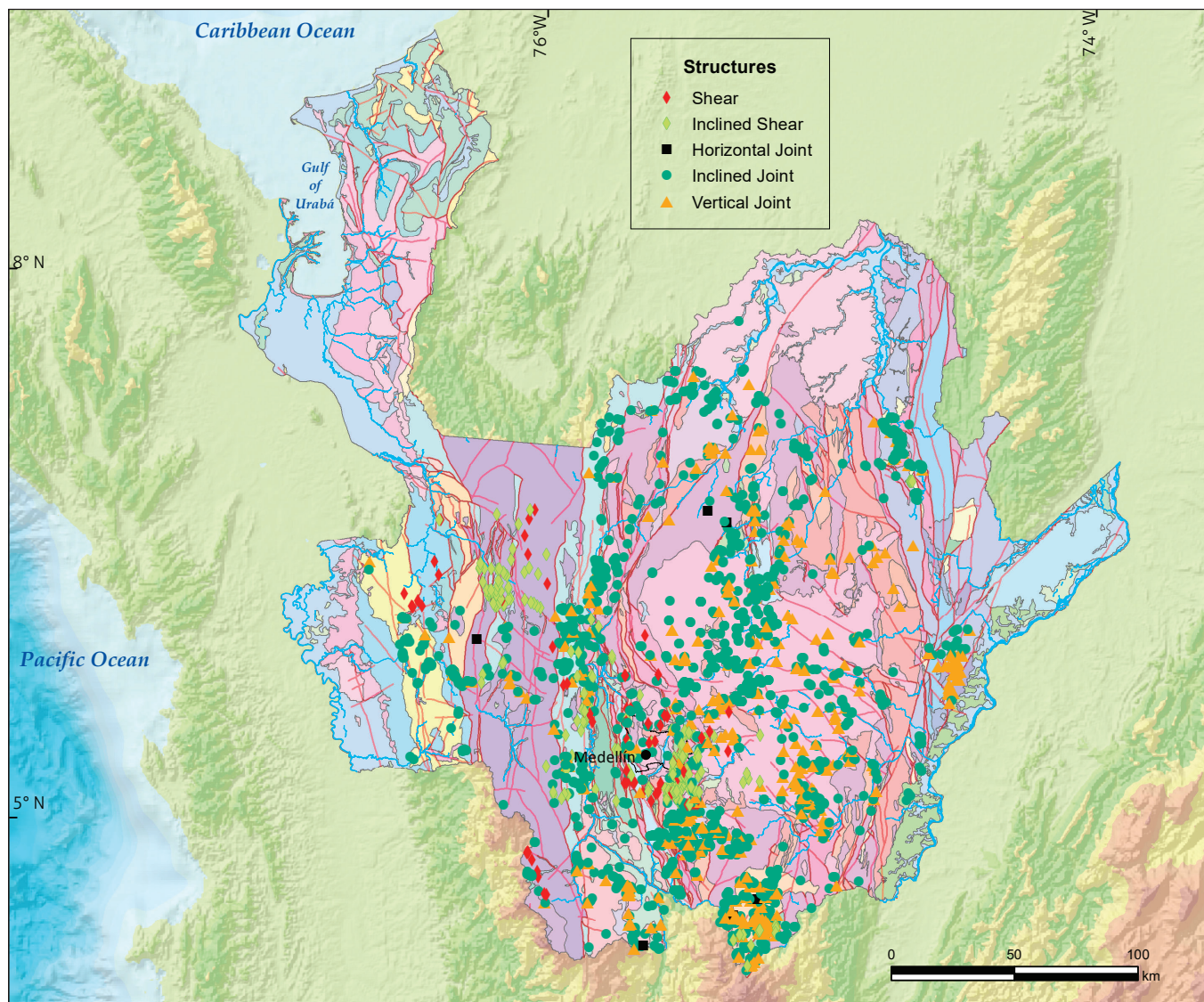


Figure 4. Structural features that determine secondary permeability
Source: Geology from González (2001) and studies carried out by environmental authorities.

SW. The second system has an approximate NW-SE to E-W direction and consists of the Monteloro, Nare, Nus, Caldera, Balseadero, and El Bizcocho faults and the alignments of the San Bartolomé and Arma Rivers (González, 2001). The most notorious fault systems in the Central Cordillera are Palestina, San Jerónimo, Espiritu Santo, and Romeral; those in the Western Cordillera are Sabanalarga, Cauca, Anzá, Peque, Urrao, Cañasgordas, Abriaquí, Tucurá, San Pedro, Murri, Murindó, and Atrato.

The remnants of this tectonic activity are marked at the lithological level by the occurrence of folds, fractures, joints, and shears that normally modify the initial permeability characteristics of the rocks. Figure 4 shows that the different hard rock units are marked by jointing effects and how the greater relative presence of vertical and inclined attitudes indicates factors that favor infiltration (first) and posterior lateral flow.

It should be noted that several of the igneous bodies and some metamorphic bodies derived from them have acidic to intermediate natures, in geochemical terms, and original granular textures, circumstances that at the time of weathering favored the development of profiles (for example, *grass*) like textures of permeable stratified media.

4.3. Aquifer potential according to litho-structures

Based on the identified permeability conditions, according to the presence and type of structural features and the primary or secondary porosity, the aquifer potential characteristics were identified for each rock unit present in the department of Antioquia (Figure 5 and Table 3.). According to the categories defined here, 23.4% of the departmental area has very high aquifer potential, 5% has high potential, 35% has moderate potential, and 34% has low potential.

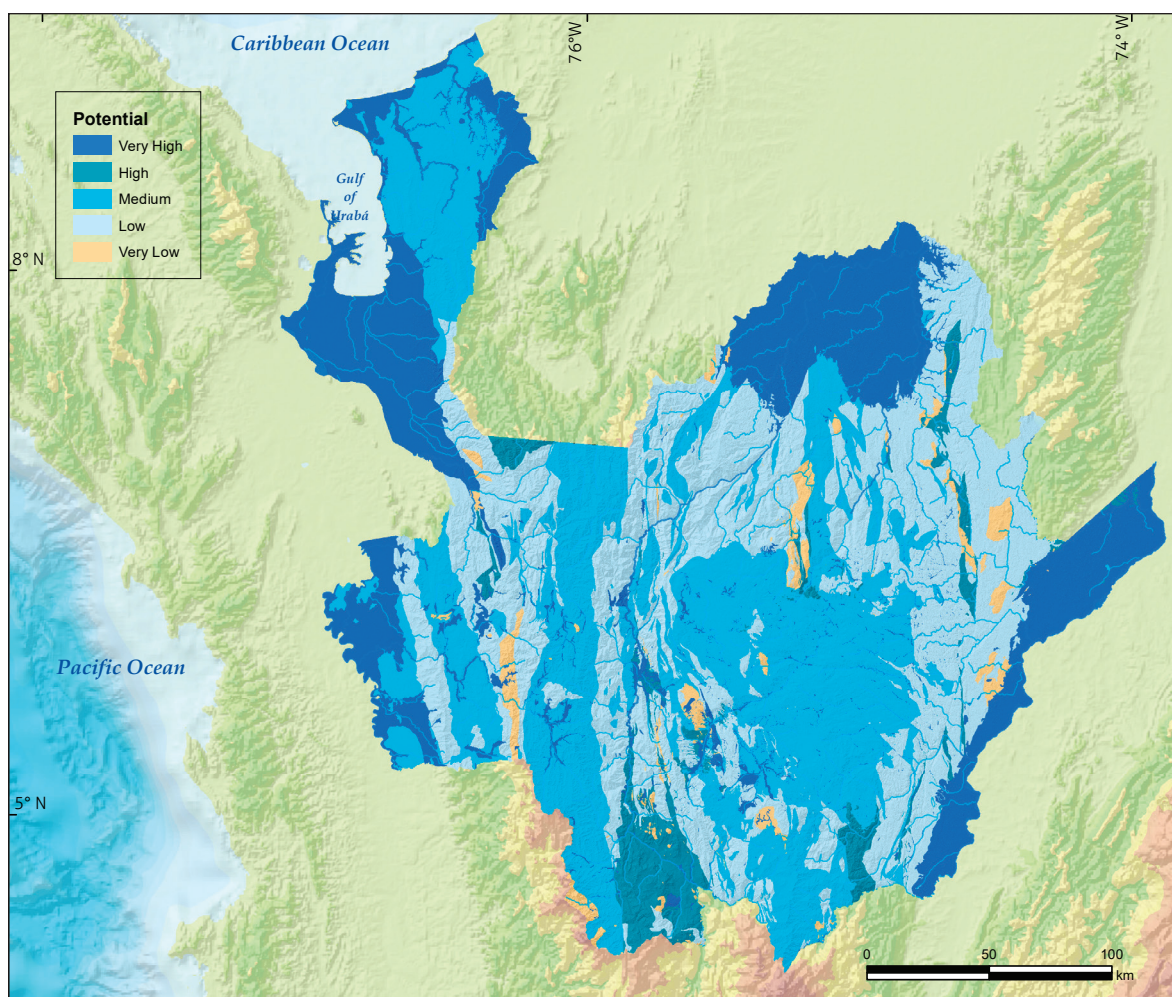


Figure 5. Groundwater potential in Antioquia department

Table 3. Hydrogeological potential by geological unit

Very high aquifer potential					
Kium	Medellín Dunite	Ngce	Cerrito Formation	Qt	Alluvial terraces
Q2v, Qd, Qfa, Qi	Slope deposits	NgQs	Sincelejo Group	Qal	Recent floods
Ngg	Guineales Formation	Ngco	Corpa Formation (T2)	Ngm	Mesa Formation
Tal	Tertiary alluvium	Qd	Sliding deposits	Q6	Slope deposits
High aquifer potential					
Oa	Aquitania metasediments	Ngc	Combia Formation – Volcanic Member	Kiss	Eastern Segovia Sedimentites
Pzm	Cajamarca Complex: Marbles	E1E2sc	Cruces Sedimentites	Ksam	Amalfi sediments
Pgai	Amagá Formation - Lower Member	N2Q	Vergel Sedimentites	Kissl	San Luis Sedimentites
Pgam	Amagá Formation - Middle Member	Kils	La Soledad Formation	Kisp	San Pablo Formation
Ngas	Amagá Formation - Upper Member	NFI	Debris flow deposits	N1rl	Real Group
Ngam	Amagá Formation	Qll	Anthropogenic Landfill	PGSD	Conglomerates
Moderate aquifer potential					
JKgms	Sajonia Mylonitic Gneiss	Ksta	Antioquia Batholith	Kisa	Abejorral Formation
TRmPP PEgr	Puente Peláez Migmatites El Retiro granulites and migmatites	Ksts	Sabanalarga Batholith	Kslb	Interstratified chert and fine clastic rocks
Pzes	Cajamarca Complex: Quartz-sericitic schists	Pggm	Mandé Batholith	Ksu	Cañasgordas Group Penderisco Formation - Urrao Member
N2qb	Quibdó Formation	Jts	Sonsón Batholith	N1 sv	Beibaviejo Sedimentites
Pgs	Salaquí Formation	Pgu	Uva Formation	Qto	Pyroclastic rocks
Q2fl, Q2 l: MEDIO	Lacustrine and fluviolacustrine deposits	Ng (pv + am) (T1)	Pavo Formations and Arenas Monas		
Low aquifer potential					
PEnl	San Lucas Feldspathic-quartz Puquí Complex:	Pza	Amphibolites	TRgLC	La Ceja Gneiss
PEnp, Peap, PEntp	Micaceous Gneiss Amphibolites (Peap) Metatonalite (PEntp) and Gneiss (PEnp)	Pzin	Gneiss Syntectonic Intrusive	Pn	Porphyroblastic Gneiss
Olc	La Cristalina Formation	Kica	Arquia Complex	Pnl	Augen Gneiss
Pzms	Sinifaná Metasediments	Pgnp	Palmitas Gneissic Granite	PzagC	Caldas Garnet amphibolite
Pzmf, Pznl	Cajamarca Complex: Feldspar-quartz and aluminum Gneisses	Pnc	Cataclastic Gneiss	TreAB	Baldias Amphibolic Schists
Pzev	Cajamarca Complex: Actinolite-chlorite schists	PzaM	Alto de Minas Amphibolites	TreC	Cajamarca Schists
Pzes + Pzev	Cajamarca Complex: Intercalated schists	Pzei	Amphibolites and Amphibolic schists	PzeC	Caldas Schists
Pzq: LOW	Cajamarca Complex: Quartzites	PraM	Medellín Amphibolites	Pcaa	Amphibolite lens
Pzmc	La Cruz Metasediments	fqd	Quartzodiorite	Pnia	Abejorral Intrusive Gneiss
Trga	Amagá Stock	Kigr	Romeral Gabbro	Kida	Altavista Stock
Trah	La Honda Stock	Kivqg	Quebradagrande Complex - Vulcanites	Kia: LOW	Adamelites
Work	El Buey Stock	Kivb	Barroso Formation- Vulcanites	Ksgtm	Tres Mundos Stock
Jdse	Segovia Batholith	Kivu	Uramita Volcanite	Kscma	Aquitania stock
Kidp	Pueblito Diorite	Kidc	Cambumbia Stock	Ksvx	Santa Cecilia - La Equis Complex
Kigy	Yarumal stock	Kitt	Támesis Stock	Pgab	Buriticá Andesites
Ngpf	Páramo de Frontino Stock	Ksvb	Cañasgordas Group - Barroso Formatiojn	KgSD	San Diego Stock
Ngcf	Cerro Frontino Stock	N1n4n5bb	El Boton Basalt	KcdE	Estancias Stock
Ngvpf	Paramo of Frontino Vulcanites.	Kcdu	Ursula Stock	KcdML	Medialuna Stock
Ksg	Gabbro	Pnim	Alto de Minas Gneissic Intrusive	J1gn	Norosí Granite
Kigc	Copacabana Gabbro	Kgn	Cataclastic Granite	Ku	Uré Basic Ultrabasic Complex Penderisco Formation
Pniv	Rio Verde Intrusive Gneiss	Kisqg	Quebradagrande Formation	Ksn	Nutibara Member
Traq	Quebrada Liborina Stock	Pnip	Pantaniello Intrusive Gneiss	Taa	Sandstones and clay stones

No aquifer potential					
Peam	Migmatites	Jvm	La Malena Volcanic Complex	Kivs	Segovia Vulcanites
Jml	La Iguaná Mylonite	Jdt	La Tina Stock	Ksdh	Heliconia Diorite
JkmbP	Picacho metabasites	Kiu	Ultramafics of Romeral	Kstmi	Quebrada Maní Batholith
Pbsd	Very low degree metamorphic rocks	Kum	Western Cordillera Ultramafics	Ksto: N/A	Ovejas Batholith
Kat	Felsic tonalite	Kstu	La Unión Dome	Ngtf	Farallones Batholith
Ngpd	Porphyritic hypo-abysal rocks	Ngmg	Morrogacho Stock	Ngpa, Ngpd	Porphyritic hypo-abysal rocks
	Dacitic porphyries				
E2PADP	Pantanos Porphyry	Nglh	La Horqueta Stock	Ngpa	Porphyritic augitic andesites
N1n4n5mn	Nudillales Monzonite	PRgb	San Isidro Granulites	Ngpa	Porphyritic Andesite
Kcdgm	Mistrato Pluton	Prga	San Isidro Granulites	K5K6-bp	Plutonic units associated with Barroso Formation
Tada	Dacitic porphyries	Kld	Diorite	JuR	Romeral Peridotite
Ksvu	La Horqueta Monzonite	Pca	Medellín Ultrabasic	J1gg	Guamocó Granodiorite
s	Skarn	J1nha	Norean Volcanic Complex	Kisls	El Sireno Lodolites
t	Ultramafics (talc)	K	Serpentinites		

In relation to the geological units that, because of this evaluation, have been called *formations with a very high hydrogeological potential*, it should be noted that to a large extent, they contain the aquifer systems evaluated and tested through hydrogeological exploration efforts. The Medellín Dunite (Kiu) is a pseudokarst formation, and important sinkhole systems have been identified through which the recharge and storage of groundwater is generated and manifested in permanent outcrops in the Santa Elena Plateau and the slopes of the Aburrá Valley; this area would thus constitute the Medellín Dunite aquifer (Universidad de Antioquia and AMVA, 2015, 2017), although notably, for some authors, this formation has the character of a recharge zone (Patiño et al., 2021); the Cerrito Formation (Ngce) and the Sincelejo Group (NgQs) host the aquifers of the lower Cauca (Corantioquia and Universidad de Antioquia, 2014). The Corpa Formation defines the presence of the confined aquifer, with a multilayer nature, of Urabá (Universidad de Antioquia and Corpourabá, 2016). Similarly, several of the aquifer systems identified in Antioquia include alluvial and watershed deposits within their units; this is the case for the middle Magdalena (Gotta Ingeniería and Corantioquia, 2018), western Antioquia (SHI SAS and Corantioquia, 2015), Valle de Aburrá (Ossa et al., 2021), and Valparaíso-La Pintada aquifers in southwestern Antioquia. (SHI SAS and Corantioquia, 2014). Therefore, these units are confirmed to have the characteristics of formations with very high aquifer potential.

The factor common to all the geological units categorized with high hydrogeological aquifer potentials is that their rocks have primary porosity, based on their detrital sedimentary genesis, with the presence of layers of sandy and conglomerate

textures. In addition, due to their structural involvement, these formations have developed (added) secondary porosity conditions, whose continuity and flow must be tested by hydrogeological exploration.

The units that have moderate aquifer potential include important bodies of igneous rock, some with a batholith dimension, others of a metamorphic nature, in which the presence of joints and the occurrence of powerful weathering profiles have been recorded.

5. DISCUSSION

Based on the level of knowledge about groundwater in Antioquia, it has an irregular spatial distribution and a limited representation. In the Eje Bananero de Urabá, the aquifer system has been studied continuously since 1994 (Universidad de Antioquia and Corpourabá, 2014). The hydrogeological system of the Aburrá Valley was evaluated for the first time in 2002 (Universidad de Antioquia and Integral, 2002), and then with the Metropolitan Area of the Aburrá Valley (AMVA), it has been monitored since 2010. In the subregions of the lower Cauca (Universidad de Antioquia and Corantioquia, 2014), Magdalena Medio (Gotta Ingeniería and Corantioquia, 2018), the western (SHI SAS and Corantioquia, 2015) and southwestern (SHI SAS and Corantioquia, 2014) subregions have generally complete hydrogeological information; for the eastern part of the department, attempts to evaluate the potential of groundwater have been carried out in the past.

After consulting and verifying in the field the socioeconomic conditions that account for access to and sources of water

supply for the population residing in the nine subregions of Antioquia, it was confirmed that access to groundwater resources goes far beyond what is in the official figures. The individual supplies from artisanal wells and that of many human conglomerates in rural areas since birth reveal a reality that has not been recorded in regional and national water assessments. Notably, springs are erroneously recorded as surface water sources in official records.

The results of the litho-structural characterization presented here clearly show that the groundwater potential in Antioquia is manifested through igneous and metamorphic formations that have acquired secondary permeability due to the tectonic effects printed on them by the geodynamics affecting northeastern Colombia in addition to the effect of weathering processes, which have reached depths that can reach several tens of meters. The potential of intermediate to acidic plutonic formations, in which the development of *gruss*-type textures defines permeability conditions close to those of granular sedimentary deposits, is striking. There are also several detrital sedimentary rock units that have not been explored.

The exploration of areas with very high and high hydrogeological potential can be undertaken using conventional techniques of hydrogeological research. The step toward researching and quantifying the volumes in hard rocks should be planned in terms of prioritizing and defining a methodological route that involves geophysical techniques, an evaluation of remote sensing information, hydrological quantification, a structural evaluation, geophysical tests, a hydraulic characterization, and geochemical and isotopic validation, among others.

It is important to highlight the importance of a thorough understanding of the hydrological dynamics in a territory in terms of ecosystem sustainability. In addition, if one considers that the largest reserves of fresh liquid water that exist on the planet are found underground, then any interference with the natural system implies a stress factor that can cause negative impacts.

6. CONCLUSIONS

Based on the evaluation of the textural and litho-structural characteristics of the rock units present in Antioquia, it was possible to delimit zones of very high, high, moderate, low, and very low hydrogeological potential. To make this determination, the porosity and permeability characteristics that enable the storage and flow of groundwater were analyzed from the genesis and evolution of the different units.

The geological units that showed a greater hydrogeological aquifer potential correspond to rocks with primary porosity whose genesis covers a wide time scale. However, the presence of moderate aquifer potential in the surface extension that covers 35% of Antioquia and is associated with saprolites derived from hard rocks previously affected by fracturing was significant.

Knowledge of the hydrogeological potential in a region is of crucial importance for identifying groundwater sources, as this knowledge helps in understanding regional hydrological dynamics and identifying factors to guide decision-making in relation to generating interventions that consider environmental sustainability criteria.

7. ACKNOWLEDGMENTS

This work compiled data on the hydrogeological characteristics of Antioquia obtained by entities such as the Universidad de Antioquia, Universidad Nacional de Colombia (Medellín), the Servicio Geológico Colombiano (formerly Ingeominas), Corporación de Desarrollo Sostenible de Urabá (Corpoura-ba), Corporación Autónoma Regional del Centro de Antioquia (Corantioquia), Área Metropolitana del Valle de Aburrá (AMVA), and the Corporación Autónoma Regional de las cuencas de Rionegro y Río Nare (Cornare). These data were able to be synthesized thanks to the sabbatical year commission given by the Universidad de Antioquia to the first author. This effort was supported by GIGA.

REFERENCES

- Anand, R. R., & Paine, M. (2002). Regolith geology of the Yilgarn Craton, Western Australia: Implications for exploration. *Australian Journal of Earth Sciences*, 49(1), 3-162. <https://doi.org/10.1046/j.1440-0952.2002.00912.x>
- Anbarasu, S., Brindha, K., & Elango, L. (2020). Multi-influencing factor method for delineation of groundwater potential zones using remote sensing and GIS techniques in the western part of Perambalur district, southern India. *Earth Science Informatics*, 13, 317-332. <https://doi.org/10.1007/s12145-019-00426-8>
- Área Metropolitana del Valle de Aburrá (AMVA), & Consorcio Microzonificación (Solingral S.A., Integral S.A., Intein-sa, Universidad EAFIT, Universidad Nacional de Colombia, sede Medellín). (2007). *Microzonificación sísmica detallada*

- de los municipios de Barbosa, Girardota, Copacabana, Sabaneta, La Estrella, Caldas y Envigado. <https://repositorio.gestiondelriesgo.gov.co/handle/20.500.11762/19862>
- Arias, P., Ortega, G., Villegas, L., & Martínez, A. (2021). Colombian climatology in CMIP5/CMIP6 models: Persistent biases and improvements. *Revista Facultad de Ingeniería, Universidad de Antioquia*, 100, 75-96.
- Arnous, M. O. (2016). Groundwater potentiality mapping of hard-rock terrain in arid regions using geospatial modelling: Example from Wadi Feiran basin, South Sinai, Egypt. *Hydrogeology Journal*, 24, 1375-1392. <https://doi.org/10.1007/s10040-016-1417-8>
- Bermúdez, J. G., Arango, M. I., Rodríguez, G., Zapata, G., & Ramírez, C. (2012). *Cartografía geológica de las planchas 72 Pueblo Nuevo y 82 Montelíbano, departamento de Córdoba. Escala 1:100 000*. Servicio Geológico Colombiano. <http://recordcenter.sgc.gov.co/B13/23008010024552/mapa/pdf/2105245521300004.pdf>
- Betancur, T., & Martínez, C. (2021). Acople de la cartografía geológica disponible para Antioquia a escala 1:100.000, base para la exploración hidrogeológica. In *Memorias XVIII Congreso Colombiano de Geología*. <https://sociadacolombianadegeologia.org/acople-de-la-cartografia-geologica-disponible-para-antioquia-a-escala-1100-000-base-para-la-exploracion-hidrogeologica/>
- Betancur, T., Duque, C., Martínez, C., García, D., Villegas, P., & Paredes, V. (2020). Delimitación de potenciales zonas de recarga. Caso de estudio: acuífero multicapa del eje bananero del Urabá antioqueño. *Revista Politécnica*, 16(32), 41-55.
- Briški, M., Stroj, A., Kosović, I., & Borović, S. (2020). Characterization of aquifers in metamorphic rocks by combined use of electrical resistivity tomography and monitoring of spring hydrodynamics. *Geosciences*, 10(4), 137. <https://doi.org/10.3390/geosciences10040137>
- Brkić, Z., Kuhata, M., Larva, O., & Gottetein, S. (2019). Groundwater and connected ecosystems: An overview of groundwater body status assessment in Croatia. *Environmental Sciences Europe*, 31, art. 75.
- Calle, B., & González, H. (1980). *Geología y geoquímica de la plancha 166 Jericó. Escala 1:100 000*. Servicio Geológico Colombiano. <http://recordcenter.sgc.gov.co/B4/13010010024374/mapa/pdf/0101243741300002.pdf>
- Calle, B., & González, H. (1982). *Geología y geoquímica de la plancha 186 Riosucio. Escala 1:100 000. Producto. Versión 1982 estandarizada en 2009*. Servicio Geológico Colombiano. <http://recordcenter.sgc.gov.co/B4/13010010024379/mapa/pdf/0101243791300002.pdf>
- Cilona, A., Aydin, A., Likerman, J., Parker, B., & Cherry, J. (2016). Structural and statistical characterization of joints and multi-scale faults in an alternating sandstone and shale turbidite sequence at the Santa Susana Field Laboratory: Implications for their effects on groundwater flow and contaminant transport. *Journal of Structural Geology*, 85, 95-114. <https://doi.org/10.1016/j.jsg.2016.02.003>
- Corporación Autónoma Regional del Centro de Antioquia (Corantioquia), & Universidad de Antioquia (2014). *Plan de manejo ambiental del sistema acuífero del Bajo Cauca antioqueño, segunda etapa*. https://www.corantioquia.gov.co/ciadoc/fauna/GA_CV_964_2013.pdf
- Custodio, E., & Llamas, M. R. (1996). *Hidrología subterránea*. Ediciones Omega.
- Dávila, C., Gil, C., Ibáñez, R., López, C., Orozco, L., Patiño, A., Pinilla, A., Quiñones, C., Román, J., Ramos, K., & Savanier, D. (2018a). *Anexo J. Mapa geológico de la plancha 92 Tierradentro. Escala 1:100 000*. Servicio Geológico Colombiano. https://recordcenter.sgc.gov.co/B23/678_19MemExPI92Tierradentro/Mapa/Pdf/AnexoJ_MapaGeolPI92.pdf
- Dávila, C., Gil, C., Ibáñez, R., López, C., Pinilla, A., Quiñones, C., Ramos, K., & Román, J. (2018b). *Anexo J. Mapa geológico de la plancha 91 Belencito. Escala 1:100 000*. Servicio Geológico Colombiano. Bogotá. https://recordcenter.sgc.gov.co/B23/677_19MemExPI91Belencito/Mapa/Pdf/AnexoJMapaGeolPI91.pdf
- De Vries, J. J., & Simmers, I. (2002). Groundwater recharge: An overview of processes and challenges. *Hydrogeology Journal*, 10, 5-17. <https://doi.org/10.1007/s10040-001-0171-7>
- Departamento Nacional de Planeación (DNP). (2021). Agua limpia y saneamiento. In *Objetivos de Desarrollo Sostenible*. <https://ods.dnp.gov.co/es/objetivos/agua-limpia-y-saneamiento>
- Dewandel, B., Lachassagne, P., Wyns, R., Marechal, J. C., & Krishnamurthy, N. S. (2006). A generalized 3-D geological and hydrogeological conceptual model of granite aquifers controlled by single or multiphase weathering. *Journal of Hydrology*, 330(1-2), 260-284. <https://doi.org/10.1016/j.jhydrol.2006.03.026>
- Faulkner, D. R., Jackson, C. A. L., Lunn, R. J., Schlische, R. W., Shipton, Z. K., Wibberly, C. A. J., & Withjack, M. D. (2010). A review of recent developments concerning the structure, mechanics and fluid flow properties of fault zones. *Jour-*

- Journal of Structural Geology*, 32(11), 1557-1575. <https://doi.org/10.1016/j.jsg.2010.06.009>
- Feininger, T., Barrero, D., Castro, N., Ramírez, O., Lozano, H., & Vesga, J. (1970). *Mapa geológico de Colombia, oriente de Antioquia. Cuadrángulo I-9 y parte de los cuadrángulos H-9, H-10, I-10, J-9 y J-10. Plancha 117 Amalfi, plancha 132 Yolombó, plancha 148 San Carlos, plancha 168 Argelia (Aquitania), plancha 188 La Dorada. Escala 1:100 000. Producto. Versión año 1970 estandarizada en 2010.* Servicio Geológico Colombiano. Bogotá. <http://recordcenter.sgc.gov.co/B4/13010010024246/mapa/pdf/0101242461300010.pdf>
- Fiume, B., João Fernandes, A., Bolognini Barbosa, M., Hirata, R., & Bertolo, R. (2020). Integrated application of geophysical loggings and fracture survey on rock exposures for identifying transmissive fractures in crystalline aquifer: Case study in the city of São Paulo. *Brazilian Journal of Geology*, 50(1), 1-17. <https://doi.org/10.1590/2317-4889202020190034>
- Fonseca, H. A., Fuquen, J. A., Mesa, L. D., Talero, C. A., Pérez, O. G., Porras, J. J., Gavidia, O. A., Pacheco, S. M., Pérez, J. F., Amaya, E., García, Y., & Enrique, F. (2011). *Cartografía geológica de la plancha 133 Puerto Berrío. Escala 1:100 000. Contrato 041/2010.* Servicio Geológico Colombiano. <http://recordcenter.sgc.gov.co/B13/23008010024508/mapa/pdf/2105245081300001.pdf>
- Fonseca, H. A., Fuquen, J. A., Mesa, L. D., Talero, C. A., Pérez, O. G., Porras, J. J., Gavidia, O. A., Pacheco, S. M., Amaya, E., García, Y., & Enrique, F. (2012). *Cartografía geológica de la plancha 108 Puerto Wilches. Escala 1:100 000. Contrato n.º 041/2010.* Servicio Geológico Colombiano. <http://recordcenter.sgc.gov.co/B13/23008010024507/mapa/pdf/2105245071300001.pdf>
- Freeze, R. A., & Cherry, J. A. (1979). *Groundwater*. Prentice Hall.
- Geotec Ltda. (2003). *Geología de los cinturones Sinú – San Jacinto – Planchas 50 Puerto Escondido, 51 Lorica, 59 Mulatos, 60 Canalete, 61 Montería, 69 Necoclí, 70 San Pedro de Urabá, 71 Planeta Rica, 79 Turbo, 80 Tierralta. Escala 1:100 000.* Servicio Geológico Colombiano. Bogotá. <http://recordcenter.sgc.gov.co/B4/13010010020013/mapa/pdf/0101200131300008.pdf>
- Gobernación de Antioquia. (2018). *Anuario estadístico de Antioquia*. <http://www.antioquiadatos.gov.co/index.php/anuario-estadistico-2018>
- Gómez, J. F., Albarracín, H., Sepúlveda, J., Sepúlveda L., Rodríguez, G., Salazar, G., Zapata, G., & Nivia, A. (2011). *Mapa geológico de la plancha 131 Santa Rosa de Osos. Escala 1:100 000.* Servicio Geológico Colombiano. Bogotá. <http://recordcenter.sgc.gov.co/B13/23008010024403/mapa/pdf/2105244031300001.pdf>
- Gómez, L. A., Fuquen, J. A., Quintero, C., Patiño, A., Beltrán, A., López, C., Lancheros, J. A., Renzoni, G., & Manrique, M. (2009). *Cartografía geológica y muestreo geoquímico escala 1:100 000 de la plancha 149 – Puerto Nare (Puerto Serriez). Contrato 398 de 2007. Producto. Versión 2009.* Servicio Geológico Colombiano. Bogotá. <http://recordcenter.sgc.gov.co/B12/23008010024352/mapa/pdf/2105243521300002.pdf>
- Gómez, L. A., Patiño, A., Renzoni, G., Beltrán, A., Quintero, C., & Manrique, M. (2008). *Cartografía geológica y muestreo geoquímico escala 1:100.000 de la plancha 119 – Barranca-bermeja Valle Medio del Magdalena. Contrato 398. Producto.* Servicio Geológico Colombiano. <http://recordcenter.sgc.gov.co/B12/23008010024350/mapa/pdf/2105243501300002.pdf>
- González, H. (1980). *Geología de la plancha 167 Sonsón y Plancha 187 Salamina. Escala 1:100 000. Versión 1980. Versión digital 2009.* Servicio Geológico Colombiano. Servicio Geológico Colombiano. Bogotá. <http://recordcenter.sgc.gov.co/B18/23008010028501/mapa/pdf/2105285011300005.pdf>
- González, H. (1992). *Mapa geológico de Colombia, plancha 106 Liberia. Escala 1:100 000. Producto. Versión 1992 estandarizado en 2009.* Servicio Geológico Colombiano. <http://recordcenter.sgc.gov.co/B4/13010010024236/mapa/pdf/0101242361300002.pdf>
- González, H. (2001). *Mapa geológico del departamento de Antioquia. Escala 1:400000.* Ingeominas. <https://miig.sgc.gov.co/Paginas/Resultados.aspx?k=130100101040020038000000000>
- González, H., & Salazar, G. (2002). *Geología de la Plancha 145 Urrao. Escala 1:100 000.* Servicio Geológico Colombiano. <http://recordcenter.sgc.gov.co/B4/13010010024480/mapa/pdf/0101244801300004.pdf>
- González, H., Cossio, U., Maya, M., Vásquez, E., & Holguín, M. (1996). *Mapa geológico del departamento de Antioquia. Escala 1:400 000. Mapa. Versión 1996.* Ingeominas. <https://recordcenter.sgc.gov.co/B4/13010040020038/mapa/pdf/0101200381300002.pdf>
- González, H., Maya, M., Cardona, O. D., Arias, E., N., Castañeda, D. M., Ruiz, C. F., Montero, J. E., Camacho, J. A., Palacio, A. F., Gómez, J. P., Vélez, W., & Álzate, G. A. (2015b). *Mapa geológico de la plancha 94 El Bagre. Escala 1:100 000.* Servicio Geológico Colombiano. <http://recordcenter.sgc.gov.co/B18/23008010028502/mapa/pdf/2105285021300007.pdf>

- González, H., Maya, M., García J., Gómez, J. P., Palacio A. F., Ruiz, C. F., Camacho, J., Montero, J. E., Grimaldo, J., & Álzate, G. A. (2015a). *Mapa geológico de la plancha 84 Los Canelos. Escala 1:100 000*. Servicio Geológico Colombiano. <http://recordcenter.sgc.gov.co/B18/23008010028501/mapa/pdf/2105285011300005.pdf>
- González, H., Maya, M., García, J., Gómez, J. P., Palacio, A. F., Ruiz, C. F., Montero, J. E., Camacho, J., Grimaldo, J., Vélez, W., & Álzate, G. A. (2015c). *Mapa geológico de la plancha 95 Buenavista. Escala 1:100 000*. Servicio Geológico Colombiano. <http://recordcenter.sgc.gov.co/B18/23008010028503/mapa/pdf/2105285031300005.pdf>
- González, H., Maya, M., Tabares, L. F., Montoya, A., Palacio, A. F., Sánchez, C., Barajas, A., & Vélez, W. (2015e). *Elaboración de la cartografía geológica de un conjunto de planchas. Escala 1:100 000, ubicadas en cuatro bloques del territorio nacional, identificados por el Servicio Geológico Colombiano. Plancha 118 San Francisco. Versión 2015*. Servicio Geológico Colombiano. <http://recordcenter.sgc.gov.co/B19/23008010028505/mapa/pdf/2105285051300007.pdf>
- González, H., Maya, M., Tabares, L., Montoya, A., Arias, E. N., Osorio, J. H., Pérez, O., Buriticá, L. F., Vélez, W., & Álzate, G. A. (2015d). *Mapa geológico de la plancha 107 Cerro Azul. Escala 1:100 000*. Servicio Geológico Colombiano. <http://recordcenter.sgc.gov.co/B19/23008010028504/mapa/pdf/2105285041300005.pdf>
- Gotta Ingeniería S. A. S., & Corporación Autónoma Regional del Centro de Antioquia (Corantioquia). (2018). *Formulación del plan de manejo ambiental del Sistema Acuífero del Magdalena Medio Antioqueño*. https://www.corantioquia.gov.co/ciadoc/AGUA/AIRNR_110_CNT1706_46_2017_00FASE%20APRESTAMIENTO.pdf
- Hall, R., Álvarez, J., Rico, H., & Vásquez, H. (1970). *Mapa geológico de Colombia. Cuadrángulo H-7 Ituango: plancha 104 Ituango - plancha 115 Toledo. Cuadrángulo H-8 Yarumal: plancha 105 Valdivia - plancha 116 Yarumal. Escala 1:100 000. Producto. Versión 1970 y 1975 estandarizado y digitalizado en 2010*. Servicio Geológico Colombiano. <http://recordcenter.sgc.gov.co/B4/13010010024235/mapa/pdf/0101242351300002.pdf>
- Harlow, J., & Hagedorn, B. (2018). SWB modeling of groundwater recharge on Catalina Island, California, during a Period of Severe Drought. *Water*, 11(1), art. 58. <https://doi.org/10.3390/w11010058>
- Henriksen, H., & Braathen, A. (2006). Effects of fracture lineaments and in-situ rock stresses on groundwater flow in hard rocks: A case study from Sunnfjord, western Norway. *Hydrogeology Journal*, 14, 444-461. <https://doi.org/10.1007/s10040-005-0444-7>
- Hoque, M., Burgess, W. G., & Ahmed, K. M. (2017). Integration of aquifer geology, groundwater flow and arsenic distribution in deltaic aquifers - A unifying concept. *Hydrological Processes*, 31(11), 2095-2109. <https://doi.org/10.1002/hyp.11181>
- Instituto de Hidrología, Meteorología y Estudios Ambientales (Ideam). (2019). *Estudio nacional del agua, 2018*. http://documentacion.ideam.gov.co/openbiblio/bvirtual/023858/ENA_2018.pdf
- Instituto Geográfico Agustín Codazzi (IGAC) e Instituto de Investigaciones en Geociencias, Minería y Química (Ingeominas). (2005). *Investigación Integral del Andén Pacífico Colombiano - Cartografía Geología, Geomorfología, Suelos y Amenazas de las planchas 58, 59, 68, 69, 79, 79BIS, 89, 89BIS, 90, 100, 101, 102, 112, 112BIS, 113, 127, 128, 143, 144, 163, 164, 165, 183, 184, 185, 202, 203, 204, 221, 222, 240, 241, 259, 260, 278, 279, 298, 299, 318, 319, 320, 339, 340, 341, 361, 361BIS, 362, 363, 383, 384, 385, 386, 407, 408, 409, 427, 427BIS, 428, 447 y 447BIS. Escala 1:100 000*. Servicio Geológico Colombiano. <http://recordcenter.sgc.gov.co/B4/13010010024479/mapa/pdf/0101244791300009.pdf>
- Kalhor, K., Ghasemizadeh, R., Rajic, L., & Alshwabkeh, A. (2019). Assessment of groundwater quality and remediation in karst aquifers: A review. *Groundwater for Sustainable Development*, 8, 104-121. <https://doi.org/10.1016/j.gsd.2018.10.004>
- Karro, E., & Lahermo, P. (1999). Occurrence and chemical characteristics of groundwater in Precambrian bedrock in Finland. *Geological Survey of Finland*, 27, 85-96.
- Kassem, B. T., Álvarez, A. J., & Arango C. J. (1979). *Mapa geológico del departamento de Antioquia. Escala 1:500 000. Mapa. Versión 1979*. Ingeominas. <https://recordcenter.sgc.gov.co/B4/13010040020038/mapa/pdf/0101200381300003.pdf>
- La Felice, S., Montanari, D., Battaglia, S., Bertini, G., & Gianelli, G. (2014). Fracture permeability and water-rock interaction in a shallow volcanic groundwater reservoir and the concern of its interaction with the deep geothermal reservoir of Mt. Amiata, Italy. *Journal of Volcanology and Geothermal Research*, 284, 95-105. <https://doi.org/10.1016/j.jvolgeores.2014.07.017>

- Lachassagne, P., Dewandel, B., & Wyns, R. (2021). Review: Hydrogeology of weathered crystalline/hard-rock aquifers—guidelines for the operational survey, and management of their groundwater resources. *Hydrogeology Journal*, 29, 2561-2594. <https://doi.org/10.1007/s10040-021-02339-7>
- Londoño, A. C., & González, H. (2002). *Geología de la plancha 129 Cañasgordas. Escala 1:100 000*. Servicio Geológico Colombiano. <http://recordcenter.sgc.gov.co/B4/13010010024480/mapa/pdf/0101244801300002.pdf>
- Mejía, M., Álvarez, E., González, H., & Grosse, E. (1983). *Geología de la plancha 130. Santa Fe de Antioquia. Escala 1:100 000*. Servicio Geológico Colombiano. <http://recordcenter.sgc.gov.co/B4/13010010001950/mapa/pdf/0101019501300002.pdf>
- Mejía, M., Álvarez, E., González, H., & Grosse, E. (1983). *Geología de la plancha 146. Medellín occidental. Escala 1:100000*. Servicio Geológico Colombiano. Bogotá. <https://recordcenter.sgc.gov.co/B4/13010010001950/mapa/pdf/0101019501300006.pdf>
- Mejía, O. (2006). *Algunos elementos sobre el recurso hídrico en la jurisdicción de Corantioquia*. Corantioquia. https://www.corantioquia.gov.co/ciadoc/AGUA/AIRNR_AGUA_473CD_2005_V1.pdf
- Mussa, K. R., Mjemah, I. C., & Machunda, R. L. (2020). Open-source software application for hydrogeological delineation of potential groundwater recharge zones in the Singida semi-arid, fractured aquifer, Central Tanzania. *Hydrology*, 7(2), art. 28. <https://doi.org/10.3390/hydrology7020028>
- Nikić, Z., Pušić, M., Papić, P., & Marić, N. (2020). Hydrodynamic model of hydrogeologic fracture system in Gruda ultramafic rocks, western Serbia. *Journal of Hydrology*, 580, 124268. <https://doi.org/10.1016/j.jhydrol.2019.124268>
- Norton, D., & Knapp, K. (1997). Transport phenomena in hydrothermal systems: The nature of porosity. *American Journal of Science*, 277(8), 913-936. <https://doi.org/10.2475/ajs.277.8.913>
- Ossa, J., Campillo, A. K., Omar, C., & Betancur, T. (2021). Representación espacial de zonas de recarga del agua subterránea a partir de mapas isotópicos de precipitación. Caso de estudio: Valle de Aburrá, Colombia. *Boletín Geológico y Minero de España*, 132(1-2), 65-75. <https://doi.org/10.21701/bolgeomin.132.1-2.007>
- Patiño-Rojas, S. M., Jaramillo, M., Espinosa-Espinosa, C. A., & Arias-López, M. F. (2021). Preferential groundwater flow directions in a pseudokarst system in Colombia, South America. *Journal of South American Earth Sciences*, 112, Part. 1. <https://doi.org/10.1016/j.jsames.2021.103572>
- Poveda, G. (2007). El clima de Antioquia. In M. Hermelin (ed.) *Geografía de Antioquia: Geografía histórica, física, humana y económica*. Universidad EAFIT. <https://repository.eafit.edu.co/handle/10784/17431?show=full>
- Poveda, G., Álvarez, D. M., & Rueda, O. A. (2010). Hydro-climatic variability over the Andes of Colombia associated with ENSO: A review of climatic processes and their impact on one of the Earth's most important biodiversity hotspots. *Climate Dynamics*, 36, 2233-2249. <https://doi.org/10.1007/s00382-010-0931-y>
- Qian, X., Wang, Y., Zhang, Y., Senebottalath, V., Zhang, A., & He, H. (2019). Petrogenesis of Permian-Triassic felsic igneous rocks along the Truong Son zone in northern Laos and their Paleotethyan assembly. *Lithos*, 328-329, 101-114. <https://doi.org/10.1016/j.lithos.2019.01.006>
- Ren, X. W., & Santamarina, J. C. (2018). The hydraulic conductivity of sediments: A pore size perspective. *Engineering Geology*, 233, 48-54. <https://doi.org/10.1016/j.enggeo.2017.11.022>
- Restrepo, J. J., & Toussaint, J. F. (2020). Tectonostratigraphic terranes in Colombia: An update. First part: Continental terranes. In J. Gómez, & D. Mateus-Zabala (eds.), *The geology of Colombia. Volume 1. Proterozoic – Paleozoic* (pp. 37-63). Servicio Geológico Colombiano. <https://doi.org/10.32685/pub.esp.35.2019.03>
- Rodríguez, E. E., & Ulloa, C. Rodríguez, G., Zapata, G., Gómez, J. F. (2013). E. (1994). *Geología de la plancha 169 Puerto Boyacá. Escala 1:100 000*. Servicio Geológico Colombiano. <http://recordcenter.sgc.gov.co/B4/13010010012149/mapa/pdf/0101121491300002.pdf>
- Rodríguez, G., Sierra, M. I., Zapata, G., Correa, T., Peláez, J., & Nivia, Á. (2010). *Geología de las planchas 58 Sapzurro (Capurganá), 68 Acandí y 79 Bis Unguía (Cerro Tagarí). Escala 1:100 000*. Servicio Geológico Colombiano. <http://recordcenter.sgc.gov.co/B12/23008010024303/mapa/pdf/2105243031300025.pdf>
- Rodríguez, G., Zapata, G., & Gómez, J. F. (2013). *Geología de la plancha 114 Dabeiba. Escala 1:100 000*. Servicio Geológico Colombiano. <http://recordcenter.sgc.gov.co/B14/23008010024725/mapa/pdf/2105247251300001.pdf>
- Rodríguez, G., Zapata, G., González, H., & Cossio, U. (2005). *Geología de la plancha 147, Medellín Oriental*.

- Departamento de Antioquia. Escala 1:100 000. Servicio Geológico Colombiano. <http://recordcenter.sgc.gov.co/B12/23008010002745/mapa/pdf/2105027451300002.pdf>
- Rukavičková, L., Holeček, J., Holečková, P., Najser, J., Gvoždík, L., & Pačes, T. (2021). Comparison of hydraulic conductivity of rock matrix and fractured blocks of granitic rocks. *International Journal of Rock Mechanics and Mining Sciences*, 144, 104743. <https://doi.org/10.1016/j.ijrmms.2021.104743>
- Scesi, L., & Gattinoni, P. (2007). Roughness control on hydraulic conductivity in fractured rocks. *Hydrogeology Journal*, 15(2), 201-211. <https://doi.org/10.1007/s10040-006-0076-6>
- SHI S. A. S., & Corporación Autónoma Regional del Centro de Antioquia (Corantioquia). (2015). *Diagnóstico para la formulación del plan de manejo ambiental del Sistema Acuífero del Occidente Antioqueño en la Territorial Hevéxicos de Corantioquia - Contrato 14-09-241*. https://www.corantioquia.gov.co/ciadoc/AGUA/AIRNR_CN_1608_77_2016_PMAA_OCCIDENTE_APRESTAMIENTO.pdf
- SHI S. A. S., & Corporación Autónoma Regional del Centro de Antioquia (Corantioquia). (2014). *Evaluación hidrogeológica en los municipios de La Pintada y Valparaíso jurisdicción de la Dirección Territorial Cartama de Corantioquia*. https://www.corantioquia.gov.co/ciadoc/AGUA/GA_CN_9909_2013.pdf
- Srinivasa Rao, Y., Reddy, T. V. K., & Nayudu, P. T. (2000). Groundwater targeting in a hard-rock terrain using fracture-pattern modeling, Niva River basin, Andra Pradesh, India. *Hydrogeology Journal*, 8, 494-502. <https://doi.org/10.1007/s100400000090>
- Universidad de Antioquia, & Área Metropolitana del Valle de Aburrá (AMVA). *Plan de manejo ambiental de acuíferos del Valle de Aburrá*. <https://www.metropol.gov.co/ambiental/recurso-hidrico/Paginas/PMAA.aspx>
- Universidad de Antioquia, & Corporación para el Desarrollo Sostenible del Urabá (Corpourabá). (2016). *Plan de manejo ambiental de acuífero Sistema Hidrogeológico Golfo de Urabá*. <http://repositorio.corpouraba.gov.co:8082/xmlui/handle/123456789/87>
- Universidad de Antioquia, & Corporación para el Desarrollo Sostenible del Urabá (Corpourabá). (2014). *Convenio Interadministrativo de Cooperación 136 de 2013 Universidad de Antioquia-Corporación para el Desarrollo Sostenible del Urabá*.
- Universidad de Antioquia, & Integral. (2002). *Estudio de zonas de recarga y acuíferos del Valle de Aburrá*. https://www.corantioquia.gov.co/ciadoc/agua/airnr_cn_2420_2000.pdf
- Vargas, O., Campillo, A., García, M., & Rodríguez, O. (2013). *Las aguas subterráneas en Colombia, una visión integral*. Instituto de Hidrología, Meteorología y Estudios Ambientales (Ideam).
- Verma, O., Khosla, A., Goin, F. J., & Kaur J. (2016). Historical biogeography of the Late Cretaceous vertebrates of India: Comparison of geophysical and paleontological data. *New Mexico Museum of Natural History and Science Bulletin*, 71, 317-330.
- Zapata, G., & Cossio, U. (2001). *Mapa fotogeológico con control de campo de la plancha 93 Cáceres. Escala 1:100 000*. Servicio Geológico Colombiano. Bogotá. <http://recordcenter.sgc.gov.co/B4/13010010002309/mapa/pdf/0101023091300002.pdf>
- Zapata, G., Bermúdez, J. G., Rodríguez, G., & Arango, M.I. (2013). *Cartografía geológica de la plancha 83 Nechí - Departamento de Antioquia. Escala 1:100 000*. Servicio Geológico Colombiano. <http://recordcenter.sgc.gov.co/B14/23008010024595/mapa/pdf/2105245951300001.pdf>



Manantial en saproilito del Batolito Antioqueño.
Vía Santa Rosa - San Pedro, Antioquia, Colombia.
Autora: Teresita Betancur V.



This work is distributed under the Creative Commons Attribution 4.0 License.

Received: October 31, 2021

Revision received: September 20, 2022

Accepted: October 21, 2022

Published online: December 28, 2022

Research article

Geomechanical characterization of samples in the pilot zone of Bogotá, Colombia, to determine its potential as aggregates for construction

Caracterización geomecánica de muestras en la zona piloto de Bogotá, Colombia, para determinar el potencial como agregados para la construcción

Juan Ricardo Troncoso Rivera¹, Nelly Páez Fonseca¹, Óscar René Másmela Rodríguez¹, Leonardo Fuentes Aldana¹ and Roberto Terraza Melo¹

¹. Servicio Geológico Colombiano, Bogotá, Colombia.

Corresponding author: Juan Ricardo Troncoso, jtroncoso@sgc.gov.co

ABSTRACT

The purpose of this project is to evaluate and determine potential areas for the exploitation of a mineral resource, considering that materials suitable for construction are a strategic line for the development of the country. In this sense, the pilot zone of Bogotá defined by a radius of 200 km around Bogotá was evaluated, in which lithostratigraphic units with potential for stone aggregates in areas free of mining licenses were studied through geotechnical testing of samples. A total of 198 samples were collected, which underwent the process of size reduction or crushing. Subsequently, granulometry tests were conducted to classify the samples by size, and finally, wear tests (hardness) and sand equivalent tests (cleanliness) were carried out. Once the tests were performed, the results were interpreted to define the potential use of this material as coarse aggregates (sizes in the range of 75 to 4.75 mm) and fine aggregates (sizes in the range of 4.75 to 0.075 mm), according to the *General Construction Specifications* of the National Highway Institute of Colombia (Invías). In terms of hardness and cleanliness, 60% of the samples collected in the pilot zone of Bogotá can be used to produce aggregates. A total of 118 potential sites for the exploitation of coarse aggregates and 19 potential sites for the exploitation of fine aggregates were defined.

Keywords: Bogotá pilot zone, hardness, cleanliness, construction materials, geomechanical tests.

RESUMEN

Este proyecto tiene como propósito evaluar y determinar zonas potenciales para la explotación de este tipo de recurso mineral, considerando que los materiales aptos para la construcción son un renglón estratégico para el desarrollo del país. En ese sentido, se evaluó la zona piloto de Bogotá definida por un radio de 200 km alrededor de Bogotá, en la cual se estudiaron las unidades litoestratigráficas con potencial para agregados pétreos en áreas libres de licenciamiento minero, mediante muestreos para ensayos geotécnicos. Se recolectaron 198 muestras, a las cuales se les realizó el proceso de reducción de tamaño o trituración; posteriormente se ejecutó el ensayo de granulometría para clasificar las muestras por tamaños, y finalmente se realizó el ensayo de desgaste (dureza) y ensayo de equivalente de arena (limpieza). Una vez realizados los ensayos, se interpretaron los resultados para definir el uso potencial como agregados gruesos (tamaños en el rango de 75 a 4,75 mm) y agregados finos (tamaños en el rango de 4,75 a 0,075 mm), de acuerdo con las Especificaciones generales de construcción del Instituto Nacional de Vías de Colombia (Invías). En términos de dureza y limpieza, el 60 % de las muestras recolectadas en la zona piloto de Bogotá se puede usar para la producción de agregados. Se definieron 118 sitios potenciales para explotación de agregados gruesos y 19 sitios potenciales para explotación de agregados finos.

Palabras clave: Zona piloto de Bogotá, dureza, limpieza, materiales de construcción, ensayos geomecánicos.

1. INTRODUCTION

The objective of this project is to evaluate and determine potential areas of exploitation of construction materials, which constitute a strategic line for the development of the country. This project follows the methodology of Fuentes et al. (2020) for the prospecting of construction materials in Colombia. The geomechanical characterization of the samples taken in the field in the framework of the construction materials project is presented below.

A total of 198 representative samples, each weighing 80 kg, were processed to carry out the geomechanical characterization through crushing, size classification, and wear performance and sand equivalent testing.

The characterization of the materials was performed with the following tests: density indices, wear on the Los Angeles machine, micro-Deval, sulfate fastness, shape indices (elongation and flattening), fractured faces, durability-sag, sand equivalent, methylene blue and alkali-silica reaction (Montero et al., 2009). The project included the performance of wear and sand equivalent tests, which were the most important analyses in terms of distinguishing coarse aggregate and fine aggregate.

Initially, granulometric analysis testing of the coarse and fine aggregates was conducted (Standard INV E-213, Invías, 2013), to classify the crushed material of a sample into varied sizes or sieves to determine the portion of gravels, sands, and fines, as well as to obtain the fractions of certain sieve sizes for the execution of other tests.

The second test corresponds to the wear or the determination of the resistance to the degradation of the coarse aggregates using the Los Angeles machine (Standard INV E-218 and

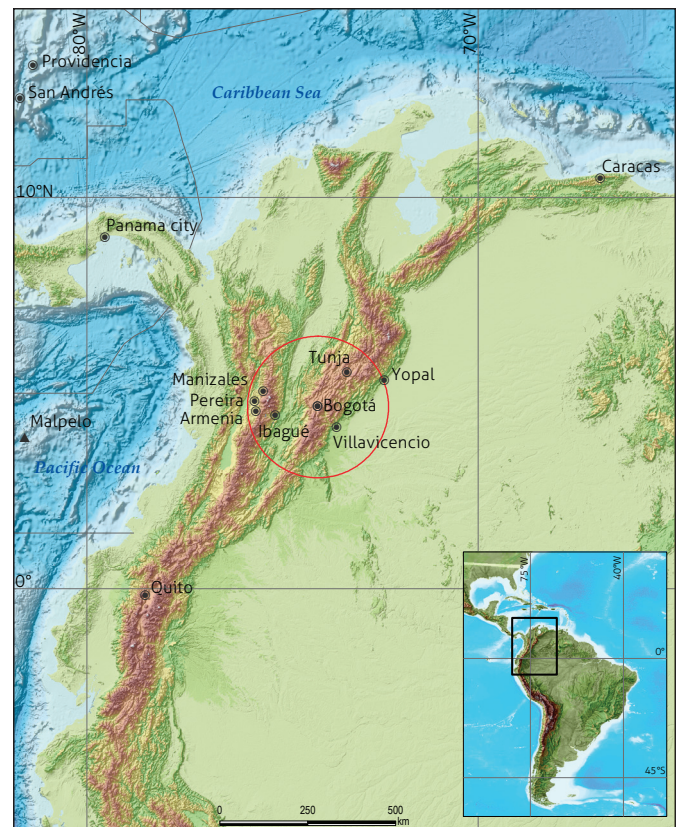


Figure 1. Geographical location of the pilot zone of Bogotá

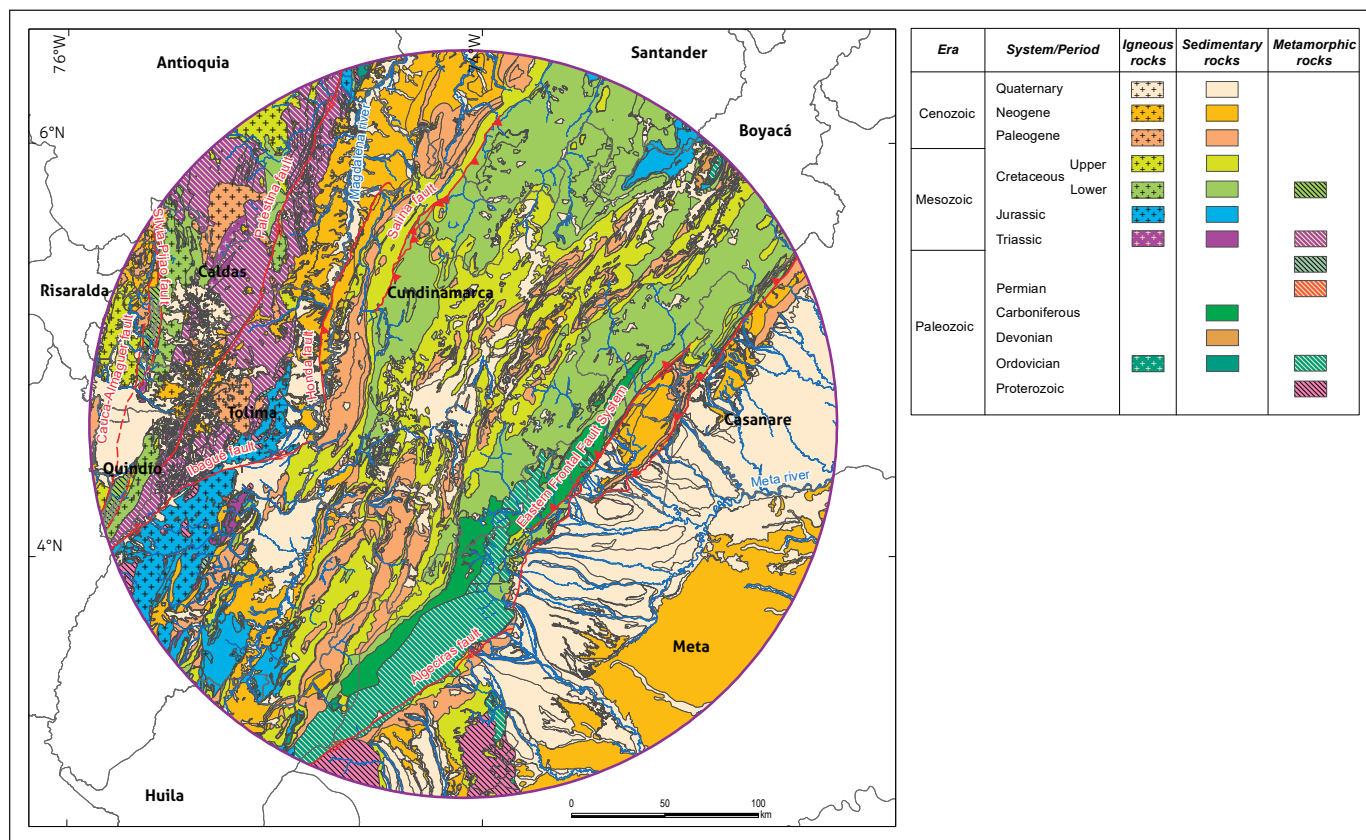


Figure 2. Chronostratigraphic geological map of the pilot zone of Bogotá
Source: taken and modified from Gómez et al. (2015).

E-219, Invías 2013), in which the loss of resistance of a material under an abrasive load and continuous movement is classified. The type A granulometry was defined, which represents the granulometries of granular materials, asphalt mixtures, and hydraulic concrete, established in the *General Construction Specifications* of the National Highway Institute of Colombia (Invías).

The last test was carried out on samples of fine aggregate, the product of secondary crushing: the sand equivalent test (INV E-133, Invías, 2013). This test represents the percentage of the fine silty sand portion in relation to the fine clay portion, which has a harmful nature, because the minerals present can generate volumetric changes or accelerated weathering of the remaining granular material and thus affect the quality and stability of the work where it is used.

2. GEOLOGICAL SETTING

2.1. Location of the study area

The study area is called *the pilot zone of Bogotá*, defined by a radius of 200 km around the city, which has the highest demand for construction materials in Colombia. This zone includes part of the departments of Cundinamarca, Tolima, Boyacá, Santander, Meta, Casanare, Antioquia, Quindío, Risaralda, Caldas, and Huila (Figure 1).

2.2. Regional geology

The pilot zone of Bogotá contains rocks from the Eastern Cordillera, Central Cordillera, Middle and Upper Magdalena Valley, and Eastern Plains, with Precambrian, Paleozoic, Mesozoic, and Cenozoic ages, which correspond to igneous, metamorphic, and sedimentary rocks (Figure 2).

Structurally, in the southeastern sector, a system of faults of the Eastern Cordillera and the Algeciras fault is present; in the western part, the Cauca-Almaguer, Silvia-Pijao, Ibagué, Honda, Palestina and La Salina faults are present.

3. METHOD

Geomechanical characterization begins with the process of size reduction or crushing of the collected samples to carry out laboratory tests and measure the properties of hardness (wear test) and cleanliness (sand equivalent test) depending on the type of rock.

Once these tests were performed, the results were interpreted to define the potential use of this material as coarse aggregates (sizes in the range of 75 to 4.75 mm) and fine aggregates (sizes in the range of 4.75 to 0.075 mm), according to the *General Construction Specifications of Inviás*.

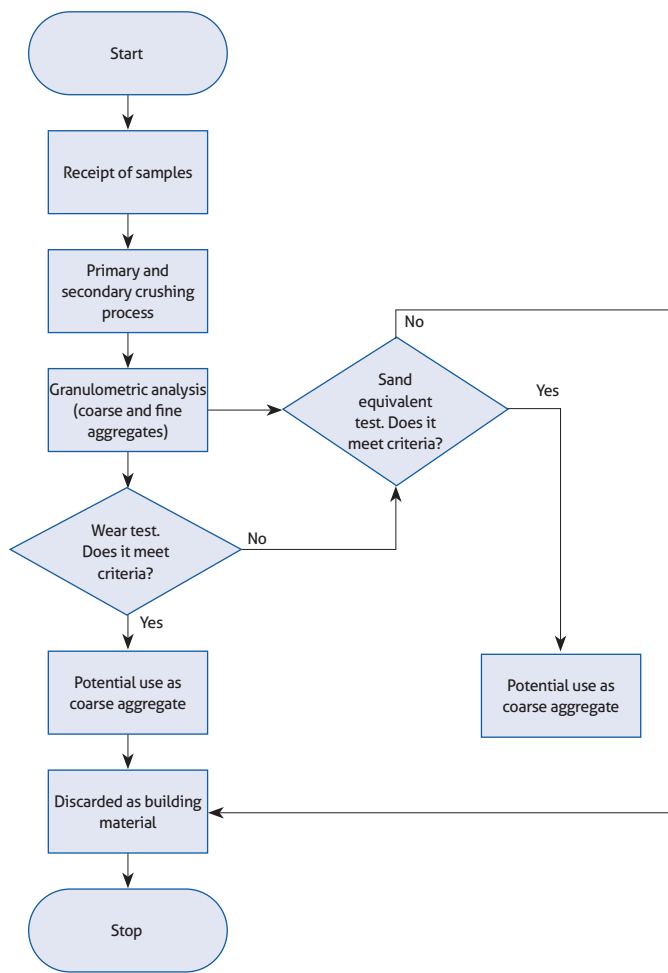


Figure 3. Process for geomechanical analysis of samples

Below is a flow chart that identifies the work stages (Figure 3).

3.1. Crushing process

The crushing process (Figures 4 and 5) is a physical transformation of stone materials without altering their mineralogical composition, hardness and durability and was necessary because the collected samples were larger than those required to perform laboratory tests (sizes between 75 and 0.075 mm).

Initially, the primary crushing was carried out by means of a jaw crusher made up of two plates facing each other, one fixed to the system and the other with a movement that oscillates back and forth. This first crushing reduced blocks or clasts of the rock up to 30 cm in size, as mentioned above. Due to the oscillatory movement of the plates, some samples tended to leave the aggregates with an elongated shape, for which a secondary crushing was necessary by means of an impact mill, made of rotating plates that hit the material against fixed plates, to correct and mold the aggregates into a cubic shape, which generates a better bond between aggregates and prevents them from fracturing easily due to the flat or elongated shape. Similarly, the impact mill reduced the size of the aggregates to produce coarse and medium sands.

3.2. Laboratory tests

The crushed samples were subjected to the geomechanical tests standardized by Inviás or the Colombian Institute of Technical Standards and Certification (Icontec) (Table 1).



Figure 4. Primary and secondary crushing laboratory of the Servicio Geológico Colombiano
a) Jaw crusher; b) impact mill.



Figure 5. Samples collected from the field and after the primary crushing process

Table 1. Laboratory tests performed

Property	Test	Norm
Distribution	Granulometric analysis of coarse and fine aggregates	INV E-213 NTC 77
Hardness	Resistance to degradation of coarse aggregates by means of the Los Angeles machine	INV E-218, INV E-219 NTC 93, NTC 98
Cleaning	Sand equivalent in soils and fine aggregate	INV E-133 NTC 6179

3.2.1. Granulometric analysis of coarse and fine aggregates

This test determines the percentage distribution of the sizes (Invías, 2013) of the materials that have undergone a crushing process (sizes of gravels, sands, silts, and clays), and that are

used as aggregates of granular materials, asphalt mixtures and hydraulic concrete. As mentioned above, the distribution of the crushed material in varied sizes or sieves was determined, 3", 2 1/2", 2", 1 1/2", 1", 3/4", 1/2", 3/8", #4, #10, #20, #40, and #200, with the #4 sieve dividing the gravel and sand portions and the #200 sieve dividing the sand and fine portions.

This size distribution is also necessary to obtain the fractions retained or the fractions that pass through a certain sieve, required for the execution of other tests (Figure 6).

3.2.2. Determination of the wear resistance of coarse aggregates

This test quantifies the loss of resistance of a material under an abrasive load and continuous movement and is the indicator of the material's hardness, an inherent property. This test is carried out in a machine called the Los Angeles machine (Figure 7), where a quantity of material classified by size and controlled weight is placed in a drum with an abrasive load for a time. Subsequently, the material is removed from the drum, and the sieving process is carried out: in this work, a sieve with an opening of 1.7 mm was used. Thus, the material disintegrated by the abrasive load was determined by the weight difference (Invías, 2013).

The parameters of the wear test, such as the type of granulometry, the amount of aggregate in a sieve, the number of revolutions and that of spheres that simulate the abrasive load, were defined in the test standard based on the predominant proportion of material that is retained in a range of sieves.

The granulometry that is further studied was chosen to be like that of the aggregate that will be used in the development



Figure 6. Granulometry test: Mechanical sieve, sieves and samples classified by size

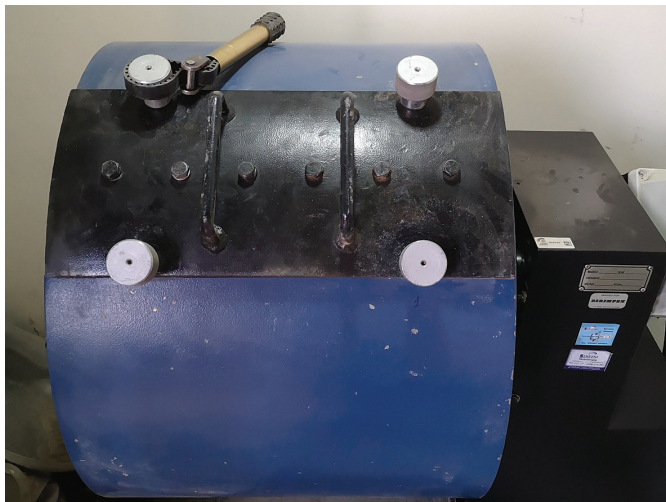


Figure 7. Wear test on the Los Angeles machine

This figure shows the spheres that simulate the abrasive load on the material, the material before the test and the disintegrated material once the test is performed.

of the infrastructure work. In our case, type A granulometry was defined, which represents the granulometries of granular materials, asphalt mixtures and hydraulic concrete established in the *General Construction Specifications* of Inviás.

To obtain the wear percentage, the dry mass after the test is subtracted from the mass of the initial dry sample, previously sieved by a 1.70 mm sieve in this work, and this product is divided by the initial mass (Inviás, 2013).

3.2.3. Sand equivalent in soils and fine aggregates

This test determines the relationship between the amount of sand, silts and clays present in a fine portion smaller than 4.75 mm (Figure 8). This represents the percentage of the fine silty sand portion in relation to the fine clay portion, which has a



Figure 8. Sand equivalent test

Specimens in the same test to determine an average value of sand equivalent readings

Table 2. Minimum requirements of the aggregates according to the use

Test	Affirmed (Art. 311)	Granular subbase (Art. 320), Class			Granular base (Art. 330), Class			Asphalt concrete (Art. 450) R/I/B			Hydraulic concrete (Art. 500)
		C	B	A	C	B	A	NT1	NT2	NT3	
Los Angeles machine wear (maximum%)	50	50	50	50	40	40	35	25/35/-	25/35/35	25/35/35	40
Sand equivalent (minimum%)	-	25	25	25	30	30	30		50	50	60

R: Surface layer, top layer of asphalt mix; I: Intermediate layer, middle layer of asphalt mix underlying the surface layer; B: Base layer, lower layer of asphalt mix underlying the intermediate layer; Class A: Material for transit NT3; Class B: Material for transit NT2; Class C: Material for transit NT1; NT3: NEE <500,000; NT2: 500,000 ≤ NEE ≤ 5,000,000; NT1: NEE > 5,000,000; NEE: Number of equivalent axles of 8.2 tons. Source: Adapted from General construction specifications (Invias, 2013).

harmful nature because the minerals present can generate volumetric changes during a change in the hydric state or due to accelerated weathering of the coarse and fine granular material or by interfering between anthropic chemical compounds (cement minerals), which can affect the quality and stability of the work where the material is used.

This test consists of taking a quantity of fine aggregates and a quantity of flocculating solution in a graduated cylinder and shaking the mixture so that the sand particles separate from the clay material. Subsequently, the mixture is irrigated with an additional amount of flocculating solution to force the clay material to remain in suspension. After a period of sedimentation, the heights of the flocculated clay material and the sand in the specimen are determined.

The sand equivalent is determined by dividing the sand reading by the clay reading (Invias, 2013).

3.3. Potential use

The initial criterion for analysis is resistance to degradation (wear), in which the sample must obtain a maximum wear value of 50% to be classified as a material suitable for construction. If the material does not meet this condition, through the granulometry results, it must be verified that the percentage that passes sieve #4 (4.75 mm) is greater than 60%, and the equivalent test of sand.

Once the results of the wear tests or sand equivalent have been obtained, the potential use is determined by verifying if the requirements established in the *General Construction Specifications* of Invías (Table 2) are met, classifying the coarse and fine aggregates suitable for the production of a hydraulic concrete, asphalt mixture (rolling, intermediate, and base types), granular base, granular subbase or affirmed material.

4. RESULTS

A total of 198 samples were processed, which were crushed and classified by size of gravels, sands, and fines by means of the granulometry test. Subsequently, wear and sand equivalent tests were carried out, depending on the matrix (coarse or fine) predominant in each sample.

Of these 198 samples, 131 corresponded to sedimentary rocks (66%), 36 to igneous rock samples (18%), 19 to metamorphic rocks (10%) and 12 to unconsolidated deposits, such as river alluvium (6%) (Figure 9).

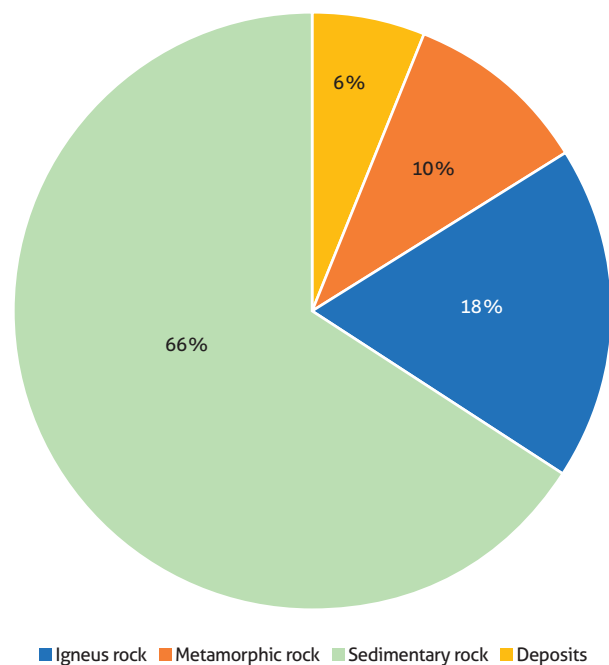


Figure 9. Distribution of the type of rocks in the sampling carried out

It is evident that 66% of the samples are sedimentary rocks because a large part of the pilot zone of Bogotá is in the eastern mountain range, formed by this type of rock.

Regarding the tests, 162 wear tests were carried out, of which 118 showed satisfactory preliminary results (wear less than 50%) to produce coarse aggregates suitable for use in granular subbases and bases, asphalt mixtures and hydraulic concrete (Appendix 1).

On the other hand, 37 sand equivalent tests were carried out, of which 19 showed satisfactory preliminary results (sand equivalent greater than 30%) to produce fine aggregates suitable for use in granular subbases and bases, asphalt mixtures and hydraulic concrete.

Appendices 1 and 2 show the location of the collected samples, the geological unit to which they belong, their classification by type of rock, and the results of the wear and sand equivalent tests.

5. DISCUSSION

In general, it was identified that the sedimentary rocks undergo the greatest loss of resistance measured by the wear test: of 102 samples evaluated of this type of rock, 35, which are equivalent to 34%, are not suitable for producing construction materials. The samples from unconsolidated deposits (27%), igneous rocks (16%) and metamorphic rocks (6%) follow in that order (Figure 10).

In terms of cleanliness (sand equivalent test), the sedimentary rocks are 50% unsuitable for fine aggregates due to the percentage of clay minerals that compose it, which are inadequate due to the quality of the sands (Figure 11).

For igneous rocks, saprolite samples were tested, and more than 50% do not comply due to the clay fraction product of the weathering of the feldspathic minerals.

On the other hand, the laboratory tests allowed us to classify the geological materials into coarse and fine aggregates suitable to produce asphalt mixtures, hydraulic concrete, and granular bases and subbases, in accordance with the requirements of the *General Construction Specifications* of Inviás. Table 3 shows the classification of all the samples analyzed.

In terms of hardness, it is evident that igneous and metamorphic rocks are more stable than sedimentary rocks, which have a wide variation in resistance. Regarding the cleaning property, no certain behavior is observed for any type of rock among the evaluated samples, furthermore, the number of samples to represent a specific behavior is limited.

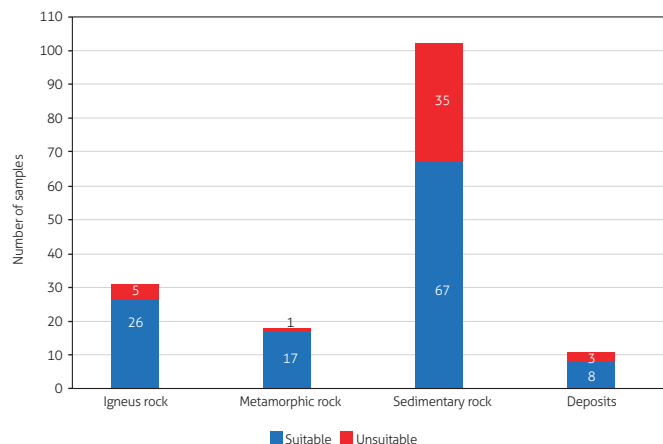


Figure 10. List of suitable and unsuitable samples of the wear test according to the type of rock

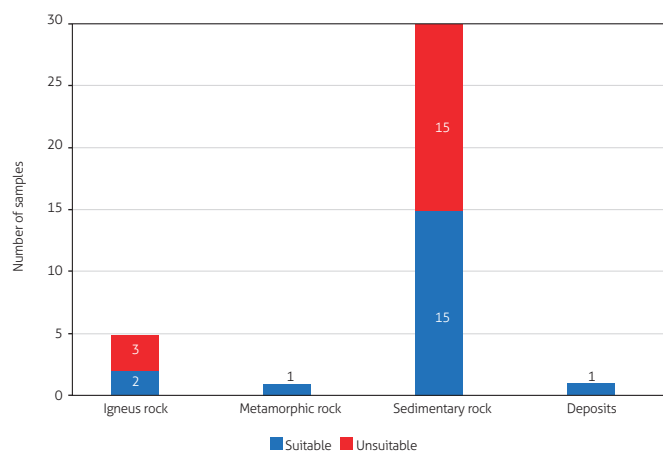


Figure 11. List of suitable and unsuitable samples of the sand equivalent test according to the type of rock

Table 3. Classification of samples based on their size, strength, or cleanliness

Classification according to material specifications	Percentage of samples
Coarse aggregate suitable to produce asphalt mixtures and hydraulic concrete	38%
Fine aggregate suitable to produce asphalt mixtures and hydraulic concrete	6%
Coarse aggregate suitable to produce granular base	15%
Fine aggregate suitable to produce granular base	2%
Coarse aggregate suitable to produce granular subbase or affirmed material	7%
Fine aggregate suitable to produce granular subbase	2%
Unsuitable material	30%

Regarding the type of rock, Figure 12 shows the classification of coarse aggregate samples based on the wear test results, and Figure 13 shows the classification of fine aggregate samples based on the sand equivalent results.

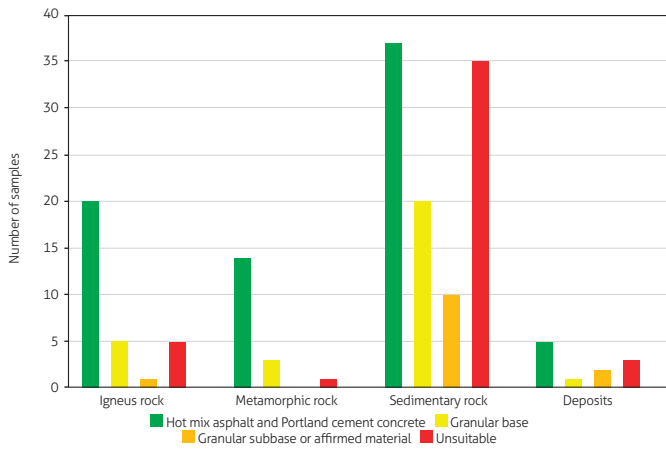


Figure 12. Distribution of coarse aggregate samples according to the wear result and the type of rock

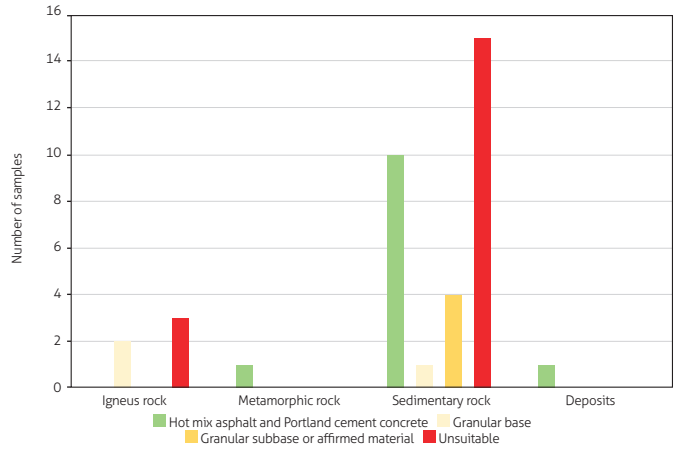


Figure 13. Distribution of fine aggregate samples as a function of the sand equivalent result and the type of rock

Figure 14 presents the location of the samples in the pilot zone of Bogotá, which is subdivided into four subzones formed as concentric circles (red dashed lines) around the city of Bogotá, to show the samples closest to the material consumption center.

It was identified that from the subzone between 50 and 100 km from the city of Bogotá, enough samples present favorable results to produce asphalt and hydraulic concrete and are thus suitable to produce granular materials (granular base, granular subbase and affirmed material).

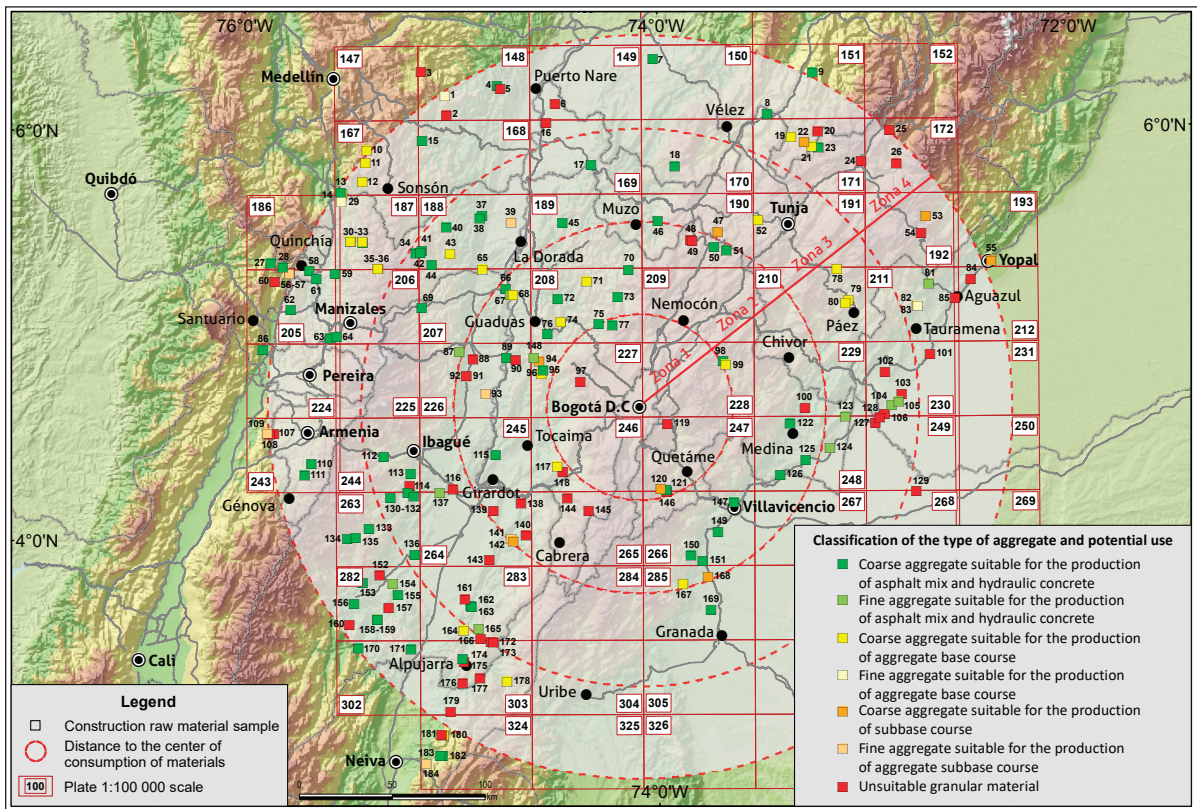


Figure 14. Potential use of the analyzed samples obtained in the pilot zone of Bogotá

6. CONCLUSIONS

According to the results obtained, igneous and metamorphic rocks are more resistant to wear in the Los Angeles machine.

Regarding the sand equivalent test, the samples that offer adequate cleanliness in the production of fine aggregates are weakly cemented clastic sedimentary rocks, with little clay matrix, and unconsolidated deposits (river sands).

Wear and sand equivalent tests show that 60% of the samples collected in the pilot zone of Bogotá can be used to produce aggregates for construction.

In the pilot zone of Bogotá, the subzone defined between 50 and 100 km from the city presents a convenient number of samples that present adequate results for the production of asphalt mixtures, hydraulic concrete and granular materials (granular base, subbase granular and affirmed material), which thus constitutes a possible area of interest for the production of construction materials that could be used in future infrastructure projects in this city and its surroundings.

7. ACKNOWLEDGMENTS

The authors thank Dr. Gloria Prieto Rincón, former director of the Directorate of Mineral Resources of the Servicio Geológico Colombiano (SGC), for the unconditional support of the activities carried out in the Project of Investigation and Exploration of Construction Materials in Colombia in the Pilot Zone of Bogotá;

to Mr. Miguel Ángel Chaves Camacho for the technical support in the execution of the geomechanical tests in the Geotechnical Laboratory required by our project; to the SIG engineer Hernán Guillermo Cifuentes, for the elaboration of the figures and location of the samples. Finally, we also thank the anonymous reviewers for their comments and suggestions.

SUPPLEMENTARY DATA

Supplementary data for this article can be found online at <https://doi.org/10.32685/0120-1425/bol.geol.49.2.2022.618>

REFERENCES

- Fuentes, L., Troncoso, J., Másmela, O., Páez, N., Quintero, L., & Terraza, R. (2020). *Protocolo para la prospección de materiales de construcción*. Servicio Geológico Colombiano.
- Gómez, J., Montes, N. Nivia, A., & Diederix, H. (2015). *Mapa geológico de Colombia*. Servicio Geológico Colombiano.
- Instituto Nacional de Vías. (2013). *Especificaciones generales de construcción de carreteras*. Invías.
- Instituto Nacional de Vías. (2013). *Manual de normas de ensayo de materiales para carreteras*. Invías.
- Montero, J., González, L., & López, J. (2009). *Estudio de fuentes de materiales de construcción en los alrededores de la sabana de Bogotá*. Proyecto SUB09-25, “Minerales industriales y materiales de construcción”. Ingeominas.



This work is distributed under the Creative Commons Attribution 4.0 License.

Received: October 29, 2021

Revision received: October 19, 2022

Accepted: October 31, 2022

Published online: December 28, 2022

Research article

The Upper Cretaceous (Santonian-Maastrichtian) phosphate deposits in the west of the Neiva subbasin, Upper Magdalena Valley, Colombia

El Cretácico Superior con fosfatos (Santoniano-Maastrichtiano) en el occidente de la subcuenca de Neiva, Valle Superior del Magdalena, Colombia

Claudia L. Martín Rincón¹, Roberto Terraza Melo¹, Nadia R. Rojas Parra¹, Germán A. Martínez Aparicio¹, Sandra Rojas Jiménez¹, Juan S. Hernández González¹

1. Dirección de Recursos Minerales, Servicio Geológico Colombiano, Bogotá, Colombia.

Corresponding author: Claudia Martín, cmartin@sgc.gov.co

ABSTRACT

It has long been known that economically exploitable phosphates in Colombia are contained within the Upper Cretaceous marine sedimentary successions (Cathcart and Zambrano, 1967; Mojica, 1987; Zambrano and Mojica, 1990). In the western region of the Neiva subbasin, which lies within the Upper Magdalena Valley (UMV), these layers are restricted to the Santonian-Maastrichtian interval, which is represented by the Lidita Inferior, Lidita Superior and Yaguará formations. The phosphates are laterally discontinuous and exhibit variations in the facies over short distances. The facies analysis and the stratigraphic correlations allowed us to infer that the facies in these units represent a very shallow marine environment that occurred at the transition between the offshore zones and the upper shoreface and included the lagoonal conditions identified within the Aico Formation. It is possible that paleotopographic variability and differential subsidence affected the lateral continuity and thickness of the Santonian-Maastrichtian lithostratigraphic units. Furthermore, subsequent tectonic events may have modified the spatial distribution of the phosphate deposits. The La Plata (Chusma) fault divides the study area into two structural domains. One is located in the west, in the hanging wall, where the oldest rocks of the pre-Cretaceous basement crop out, and the other domain is located in the east, within the footwall. This footwall is where the outcrops of the Cretaceous-Quaternary sedimentary sequences characteristic of the Neiva subbasin are found. In the footwall there are important folds, such as the Media Luna syncline and the San Francisco anticline to the north, the La Guagua anticline in the central area, and the La Hocha anticline and the El Vegón syncline to the south. Some of these folds are truncated by regional reverse faults with a dextral-strike component, such as the La Plata (Chusma), San Francisco and Betania faults.

Citation: Martín Rincón, C. L., Terraza Melo, R., Rojas Parra, N. R., Martínez Aparicio, G. A., Rojas Jiménez, S., & Hernández González, J. S. (2022). The Upper Cretaceous (Santonian-Maastrichtian) phosphate deposits in the west of the Neiva subbasin, Upper Magdalena Valley, Colombia. *Boletín Geológico*, 49(2), 75-96. <https://doi.org/10.32685/0120-1425/bol.geol.49.2.2022.621>

Keywords: Phosphates, Neiva subbasin, Upper Magdalena Valley, Upper Cretaceous, facies, stratigraphy.

RESUMEN

De tiempo atrás se conoce que los fosfatos económicamente explotables en Colombia se encuentran en sucesiones sedimentarias marinas del Cretácico Superior (Cathcart y Zambrano, 1967; Mojica, 1987; Zambrano y Mojica, 1990). En el occidente de la subcuenca de Neiva del Valle Superior del Magdalena (VSM), estos niveles están restringidos al intervalo Santoniano-Maastrichtiano, representado en las formaciones Lidita Inferior, Lidita Superior y Yaguará. Los fosfatos son lateralmente discontinuos y presentan variaciones faciales en distancias cortas. El análisis facial y las correlaciones estratigráficas permitieron inferir que las facies presentes en estas unidades representan un ambiente marino muy somero desde la zona de transición con el *offshore* hasta el *shoreface* superior, incluyendo condiciones de *laggon* para la Formación Aico. Posiblemente, la paleotopografía y la subsidencia diferencial han afectado la continuidad lateral y el espesor de las unidades litoestratigráficas del intervalo Santoniano-Maastrichtiano, y los eventos tectónicos posteriores han modificado la distribución espacial de los depósitos de fosfatos. La falla de La Plata (Chusma) divide la zona en cuestión en dos dominios estructurales: uno localizado en el occidente, en el bloque levantado, donde afloran las rocas más antiguas del basamento pre-Cretácico, y otro dominio localizado en el oriente, en el bloque hundido, donde aflora la secuencia sedimentaria cretácica-cuaternaria característica de la subcuenca de Neiva. En el bloque hundido se encuentran pliegues importantes, como el Sinclinal de Media Luna y el Anticlinal de San Francisco en el norte, el Anticlinal de La Guagua en la parte central, y el Anticlinal de La Hocha y el Sinclinal de El Vegón en el sur. Algunos de estos pliegues están truncados por fallas regionales inversas con componente de rumbo dextral, como las fallas de La Plata (Chusma), San Francisco y Betania.

Palabras clave: Fosfatos, subcuenca de Neiva, Valle Superior del Magdalena, Cretácico Superior, facies, estratigrafía.

1. INTRODUCTION

The essential chemical elements for the development of living organisms (e.g., plants and animals) are carbon, hydrogen, nitrogen, potassium, sulfur and phosphorus, being the last one used in fertilizer by the agroindustry. However, the availability of phosphorus, unlike calcium, nitrogen and potassium, is dependent solely on its extraction from rocks that contain phosphate (Soudry et al., 2006), which makes necessary its exploration. The main economically exploitable phosphate deposits worldwide were originated between the Upper Cretaceous and Eocene in the South Tethyan Phosphogenic Province (STPP), which extends from Colombia to Venezuela and from the northern and northwestern regions of Africa into the Middle East (Notholt, 1985; Follmi et al., 1992; Pufahl et al., 2003). These deposits are characteristic of an epicontinental sea on a carbonate dominated platform that extended along the margin of the STPP (Follmi et al., 1992) and constitute the largest known accumulation of sedimentary phosphorites, which is host of the 66% of the global phosphate reserves (Grimm, 1997; USGS, 2000; Pufahl et al., 2003).

In Colombia, the STPP consists of phosphate deposits that extend through the Eastern Cordillera and the southeastern

end of the Central Cordillera and involves rocks from the Catumbo, Middle and Upper Magdalena Valley, Eastern Cordillera and Caguán-Putumayo basins. Furthermore, these deposits are located in the departments of Norte de Santander, Santander, Boyacá, Cundinamarca, Tolima, Huila and part of the departments of Putumayo and Cauca (Zambrano and Mojica, 1990; Mojica, 1987; Terraza et al., 2016, 2019).

Phosphate deposits are found in the Cretaceous sedimentary successions, which initially (i.e., the Early Cretaceous) accumulated in a *rift*-type basin with an extensional tectonic regime inherited from the Jurassic (Julivert, 1970; Bayona et al., 1994; Sarmiento, 2019). Later, at the end of the Late Cretaceous, this regime transitioned to a compressional regime and the basin was fully closed (Bayona, 2018; Zapata et al., 2019; Sarmiento, 2019).

In the western part of the Neiva subbasin in the Upper Magdalena Valley (UMV), potentially exploitable phosphate levels appear in the Lidita Inferior, Aico, Aipe, Lidita Superior and Yaguará formations (*sensu* Terraza et al., 2019) which were deposited between the Santonian and the Maastrichtian. Most of these deposits have not been characterized in detail. However, considering their economic importance for the country's agroindustry, the national government issued Conpes 3577 do-

cument in 2009, which instructed the Servicio Geológico Colombiano (SGC) to identify new potential mineral sources for the production of fertilizers, which phosphates are essential. The objective is that, in the medium term, the country will be able to manufacture and market phosphorous-based agrochemicals at more affordable prices for Colombian farmers.

For this purpose, the results of the geological exploration carried out in the western sector of the Neiva subbasin are presented, which included geological mapping at 1:25 000 scale and detailed stratigraphic descriptions of eleven stratigraphic sections. These works allowed us a better understanding of the phosphate-bearing lithostratigraphic units and to better understand the accumulation processes. Additionally, based on the comparison of those stratigraphic sections, as well as on the facies analyses and sedimentary environment analyses, we propose an outline of the possible basin paleotopography during the Santonian-Maastrichtian interval.

2. REGIONAL GEOLOGICAL FRAMEWORK

The UMV basin corresponds to a structural depression that is oriented along the SSW-NNE direction and is bounded on its eastern and western sides by compressive and transpressive faults (Roncancio and Martínez, 2010). In the Mesozoic, extensional tectonic events were predominant, and compressional events dominated in the Cenozoic (Mojica and Franco, 1990; Horton et al., 2010). The Cretaceous sedimentary succession was deposited in a retroarc basin that formed in the Jurassic (Bayona et al., 1994), which at the end of the Early Cretaceous transitioned from an extensional tectonic regime to a compressional regime due to the oblique subduction and accretion of oceanic crust along the continental margin (Horton et al., 2010; Bayona, 2018; Zapata et al., 2019). Subsequent tectonic events gave rise to new structures, geometric changes occurred in the preexisting structures, and some of these structures were eroded or further deformed (Roncancio and Martínez, 2010; Jiménez et al., 2012).

The Natagaima Arch, or Alto de Patá, divides the UMV in two parts: the Neiva subbasin, located in the southern part, and the Girardot subbasin, located in the northern part (Beltrán and Gallo, 1968). In the case of the Neiva subbasin, the Garzón-Suaza fault together with the western foothills of the Garzón Massif mark the eastern limit, and the La Plata (Chusma) fault together with the eastern foothills of the Central Cordillera delimit the western limit (Figure 1). The paleotopography of

the basement affected the geometric configuration of the surface structures, which is reflected in the curvilinear outline of the major fold axes, such as by the Tesalia syncline and the La Hocha anticline (Jiménez et al., 2012).

The study area is comprised of Jurassic, plutonic and volcanic igneous rocks, whose compositions vary from felsic to intermediate (i.e., Saldaña Formation, Ibagué Batholith and related igneous bodies) (Bustamante et al., 2016; Rodríguez et al., 2018; Hernández and Urueña, 2017; Villamizar et al., 2021). Unconformably on the basement, sedimentary rocks from the basal Cretaceous crop out, composed of siliciclastic sediments that range in size from sand to gravel, accumulated in a depositional environment likely consisted of alluvial fans and fluvial systems (i.e., Yaví and Alpujarra formations) (Flórez and Carrillo, 1994; Etayo, 1994).

The remaining Cretaceous sequence, deposited in transitional and shallow marine environments (Etayo, 1994), corresponds to mixed sedimentary rocks or fine texture calcareous rocks and is enriched with organic matter and planktonic or benthic foraminifera. This sequence is contained within the El Ocal, Tetuán, Bambucá, Hondita, Loma Gorda, Lidita Inferior, Aico, Lidita Superior and Yaguará formations (*sensu* Terraza et al., 2019).

The Cretaceous sequence is unconformably covered by a thick succession of Paleogene and Neogene sedimentary rocks that are predominantly fluvial in origin and are dominated by conglomerates and sandstones (from the upper part of the Seca Formation, Chicoral and Doima Formations and Honda Group), with mudstone and claystone intercalations (found in the lower part of the Seca, Potrerillo and Barzalosa formations) (Terraza et al., 2019; Villamizar et al., 2021).

3. METHODOLOGY

The topography used as the basis for the geological map was compiled from digital and analog sources provided by the Instituto Geográfico Agustín Codazzi (IGAC) at a 1:25 000 scale. Field trips were carried out transversally to the geological structures with four or more control points for each linear kilometer. This allowed for the different outcropping units to be described in greater detail, for the lateral variations in facies to be more accurately assessed, and for a more reliable interpretation of the geological structures. For the systematic monitoring of regional structures (faults and folds) and competent and incompetent lithostratigraphic levels or units, a 30 m resolution digital terrain

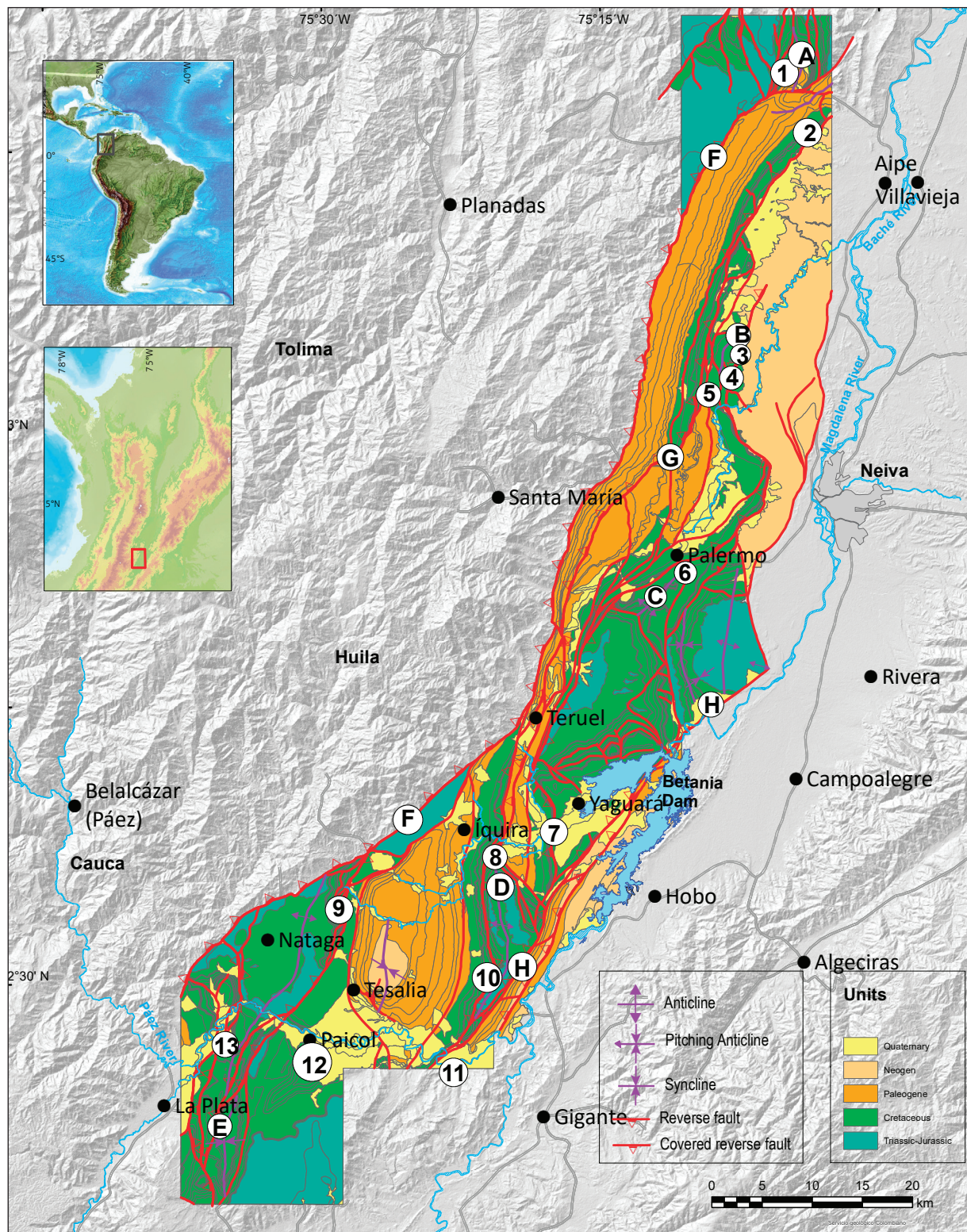


Figure 1. Regional geology of the study area
 Numbers 1 to 13 show the locations of the stratigraphic sections referenced in this article: 1 = Bambucá creek, 2 = Aipe River, 3 = La Honda creek, 4 = La Tribuna, 5 = Yaya River, 6 = El Boquerón creek, 7 = Yaguará River, 8 = Íquira River, 9 = Yaguaracito River, 10 = El Caney creek, 11 = La Juanita, 12 = Divino Niño, 13 = Itaibe creek. Letters A to H: A = Media Luna Syncline, B = San Francisco Anticline, C = La Guagua Anticline, D = La Hocha Anticline, E = El Vegón Syncline, F = La Plata (Chusma) Fault, G = San Francisco Fault, H = Betania Fault

model was used, as were aerial photographs at a scale between approximately 1:22 000 and 1:43 000, which were acquired along NS-oriented flight paths, and from Google Earth imagery.

Stratigraphic columns were measured with a “Jacob’s staff”. The main rock features (color, texture, composition, layer shapes, sedimentary structures, fossils and degree of bioturbation) were recorded at 1:100 or 1:200 scales consistent with the previously discussed field formats. Field lithological descriptions were complemented by microscopic analyses of thin sections. Strike and dip data were taken with a structural type Brunton compass. Control points and sampling locations were georeferenced with a Garmin GPSmap 62s. To visualize very thin lithostratigraphic units on the geological map, such as from the Lidita Inferior and Lidita Superior formations of the Olini Group, it was necessary to exaggerate their thicknesses.

For the lithological description of the rock outcrops, by either hand samples or thin sections, the following protocols were used: 1) to determine the thickness of layers and sheets, the methods established by Ingram (1954) and Campbell (1967) and adapted by Reineck and Singh (1980) were followed; 2) to determine the type of contact between layers (sharp or gradational), geometry (tabular or wedge-shaped) and partition, the methods from Wilkins (2011) were used; 3) diagrams proposed by Krumbein and Sloss (1969) were used to identify sedimentary particle shape; 4) diagrams proposed by Compton (1985) were used to identify particles in sediments or clastic sedimentary rocks; 5) the classification of calcareous rocks was done according to Dunham (1962) and Folk (1962); 6) in order to classify terrigenous rocks according to their texture and composition, the methods described by Folk (1951, 1954, 1959, 1962, 1974) were followed; 6) the degree of bioturbation was assessed with Moore and Scruton (1957) systematics; 7) the roundness of sedimentary particles was determined by following the Powers (1953) diagram; 8) Reineck and Wunderlich (1968) diagrams were used to distinguish between lenticular and *flasser* stratification; 9) rock colors (for either wet or dry samples) were determined according to the color chart provided by The Geological Society of America (1995); 10) “mixed” rocks (i.e., rocks with a mixture of terrigenes and authigenic siliceous and calcareous components) were identified in accordance with the general classification of sedimentary rocks established by Williams et al. (1954); 11) the macroscopic description of siliceous rocks (i.e., with > 50% diagenetic or primary silica, such as cherts and porcelanites, or impure cherts) was supported by the Dunham (1962) textural classi-

fication system, e.g., chert with 10-50% of benthic foraminifera is described as fossiliferous chert of benthic foraminifera with wackestone texture; 12) phosphate rocks and phosphorites were classified according to the systematics proposed by Ptáček (2016) and Cook et al. (1986) (in Cook and Shergold, 1986), which was based on Dunham’s (1962) classification of calcareous rocks but modified for phosphorites, e.g., a phosphorite composed of peloids and fish remains with a packstone texture would represent a rock with peloids and fish fragments in a proportion >50%, whose texture resembles that of a packstone texture limestone; 13) for the identification of the phosphorus element in the samples, a qualitative chemical test was carried out with 30% HNO₃ and ammonium molybdate in excess (Swanson, 1981); if phosphorus is present, a yellow precipitate of ammonium phosphomolybdate is produced, the color intensity indicated that either a low, medium or high concentration of this element is present.

Lithological and facies comparison (lithocorrelation) was performed on the Upper Cretaceous stratigraphic sections of interest for the identification of phosphates. A total of eleven stratigraphic sections were developed, and the stratigraphic sections from the Itaibe creek studied by Mendivelso (1982, 1993) and the Bambucá creek described during the SGC-UNAL Agreement (2018) were included, which allowed establishing the chronostratigraphic positions of the phosphate intervals. Additionally, we relied on the advice of Professor Fernando Etayo Serna, both in the laboratory and in the field, who assisted in determining the stratigraphic positions of the different mapped lithostratigraphic units. Sections were all drawn at the same scale, and a common reference stratigraphic level was taken (e.g., the contact between the Yaguará or La Tabla formations and Seca Formation [see Figures 8, 10 and 11]) to a better analysis of the spatial distribution (lateral and vertical) of phosphate levels and visualize their relationships with other regional structures (faults and folds) and the basement. The locations of these sections are shown in Figure 1.

For the interpretation of the sedimentary environments, petrographic analyses and the main features of the layers were considered. Additionally, the grain size and composition, geometry, thickness, type of contact, sedimentary structures, fossil content, degree of bioturbation, and some paleoenvironmental indicators, such as glauconite or siderite, were also considered. The methods and techniques followed can be found in Reineck and Singh (1980), Van Wagoner et al. (1990), Kamola and Van Wagoner (1995) and Hampson and Storms (2003).

4. RESULTS

4.1. Description of the main folds and faults

The most important structures are the Media Luna syncline, the San Francisco anticline and the San Francisco fault in the north; the La Guagua anticline in the central part; and the La Hocha anticline and the El Vegón syncline to the south. Finally, the La Plata (Chusma) fault and the Betania fault are regional structures that cross the study area from south to north (see Figure 1 for their locations).

Media Luna syncline. This syncline is a fold isolated by faulting and surrounded by the pre-Cretaceous basement located in the hanging wall of the La Plata (Chusma) fault. It is a subvertical and open fold whose axial plane presents a dip greater than 80° to the west and a moderate dip to the SW. It follows an elongated “S” shape and ends to the north against the Jurassic basement of the Saldaña Formation and to the SW against the La Plata (Chusma) fault. At the core are rocks from the Seca Formation and on its flanks Cretaceous rocks are outcropping, from the Alpujarra Formation to La Tabla Formation (Figures 2a, 2b).

San Francisco anticline. Is a complex fold that varies from subvertical and open to sloping and asymmetric, with moderate dipping in both the NE and south; its axis is slightly sinuous and curved along a NE and SE direction. It is truncated by some thrust faults with a dextral-strike component that produce axial displacement. The Baché fault abruptly cuts the eastern flank and the southern end of the fold, and the western flank is cut by the San Francisco fault (Figure 2c). Rocks from the Loma Gorda Formation crop out in the core and rocks from the Olini Group and Yaguará Formation crop out on the flanks.

La Guagua anticline. This anticline consists of a smooth vertical fold, dipping weakly to the NNE and a general NNE orientation. Geographically, the anticline is confined between the Upar and Baché faults to the west and La Boa fault to the east. Jurassic plutons crop out in the center of the structure and the entire Cretaceous succession and part of the Paleogene succession overlay those plutons.

La Hocha anticline. This anticline consists of a vertical fold with structural closures to the south and is slightly more open to the north. It dips weakly to both the north and to the south. It extends 21 km with N-S to SSW-NNE orientation and is

confined between the La Hocha and Betania faults. To the north, it is cut by an unnamed reverse fault that follows a NE-SW direction, and to the south, it is cut by the Betania fault. The Saldaña Formation is located at its core, and the entire Cretaceous succession outcrops on its west flank, including the Olini Group and the Yaguará Formation, which have important phosphate layers (Figure 2e).

El Vegón syncline. This structure is smooth and has a vertical fold that dips weakly to both the SSW and to the north. The axis, both to the south and to the NNE, is cut by the Pacarní fault. Rocks from the Yaguará Formation comprise the outcrop in the core, and on the flanks, rocks from the Loma Gorda Formation and the Olini Group have a significant amount of phosphate levels.

La Plata (Chusma) fault. This is a high-angle reverse regional fault with SE tectonic transport. The hanging wall contains rocks from the Saldaña Formation and Jurassic plutons (e.g., Ibagué Batholith); this tectonic block rises over the Cretaceous and Paleogene sedimentary units (Figure 2f). The fault has 113 km length and is NE ($29^\circ \pm 12^\circ$) oriented, with an average inclination of 40° - 60° to the west and presents reverse-dextral-strike movement. This fault truncates important folds, such as the Nátaga anticline to the south and the Media Luna syncline to the north. It is recognized as the geological boundary between the Central Cordillera and the Neiva subbasin in the UMV (Butler and Schammel, 1988).

San Francisco fault. It is a low- to moderate-angle regional reverse fault ($<45^\circ$ W), with a general NE orientation (10° - 50°). The initial section brings into contact the Paleogene rocks of the Seca Formation and the Olini Group (in the hanging wall) with rocks from the Potrerillo Formation (in the footwall). To the north of the study area, the fault consists of fossilized Neogene rocks from the Honda Group. In the San Francisco fault, Cretaceous rocks of the Hondita Formation (in the hanging wall) are in contact with the rocks of the Yaguará Formation (in the footwall).

Betania fault. This regional reverse fault has a high dip angle ($> 45^\circ$ NW), and its main line follows a NE direction of $40^\circ \pm 10^\circ$. It extends for approximately 53 km, truncates the La Hocha anticline, and brings into contact rocks from the Saldaña Formation with Cretaceous and Paleogene-Neogene sedimentary rocks (Figure 2d).

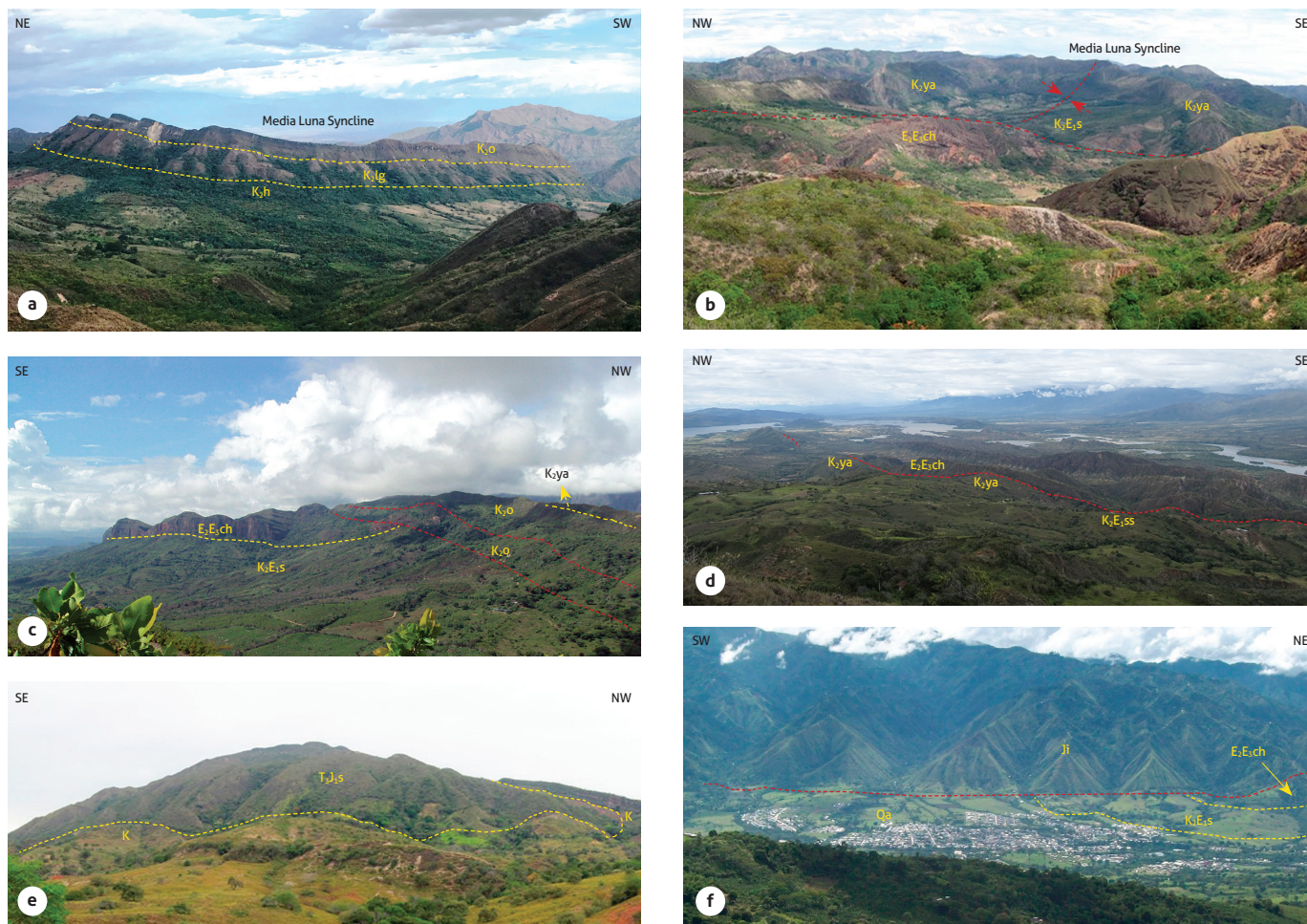


Figure 2. Main structures of the study area

a) Structural of the Media Luna syncline; rocks from the Hondita (K2h), Loma Gorda (K2lg) and Olini Group (K2o) formations are observed. b) La Plata (Chusma) fault, which truncates the continuity of the Media Luna syncline to the SSW and connects the Yaguará (K2ya) and Seca (K2E1s) formations to the Chicoral Formation (E2E3ch). c) San Francisco fault; which is where the Seca-Member Teruel formations (K2E1st) and Chicoral Formation (E2E3ch) connect with the Olini Group (K2o). d) Betania fault, which correspond to the contact between the Yaguará (K2ya) and Seca-Member San Francisco (K2E1ss) formations against the Chicoral Formation (E2E3ch). e) La Hocha anticline; rocks from the Saldaña Formation (T3J1s) crop out at the center of the structure and is covered by the basal Cretaceous succession (K). f) La Plata (Chusma) fault; is the tectonic contact between rocks from the Jurassic Ibagué Batholith (Ji) with rocks from the Seca (K2E1s) and Chicoral (E2E3ch) formations and is in the vicinity of the municipality of La Plata. Source: Terraza et al. (2019).

4.2. Phosphate-bearing Upper Cretaceous lithostratigraphic units

The potential phosphate deposits are associated with the Lidita Inferior, Lidita Superior and Yaguará formations (*sensu* Terraza et al., 2019). Mapping these units is difficult due to the overlapping of tectonic events that caused strong deformation and impacted their geographic distribution and lateral continuity.

Olini Group (K2o): Early Santonian-Campanian. This group is widely distributed across the study area. Morphologically it stands out from the underlying Loma Gorda Formation, in the

sites where the overlying unit is the Yaguará Formation this stands out over the Olini Group (Figure 3). These features facilitated the geological mapping of this feature. The Olini Group was mapped along the Yaguaracito River (which lies on the eastern flank of the Nátaga anticline), from the north of Yaguará to Palermo (on both flanks of the La Hocha anticline), at the NE termination of the La Guagua anticline and to the SW of its eastern flank, in the center of the Nazareth syncline, on the western flank of the Media Luna syncline, and on its eastern flank, along the Aipe-Río Patá road. There is an outcrop associated with this group to the north and east of Paicol, in

the vicinity of the Paéz River. Additional outcrops are visible in narrow strips that follow a NE and NW direction located to the west and NW of Neiva, and in NNE-SSW direction from near Neiva and extending to the Aipe River, in the vicinity of the municipality of Aipe.

From bottom to top, the Olini Group consists of the Lidita Inferior Formation, the Aipe or Aico formations (*sensu* Terraza et al., 2019) and the Lidita Superior Formation.

In general, the Olini Group overlies the Loma Gorda formation and underlies the Yaguará formations with a sharp and conformable contact. The upper and lower contacts of the constituent formations (Lidita Inferior, Aipe or Aico and Lidita Superior) are also conformable and sharp.

Yaguará Formation (K2ya): late Campanian-early Maastrichtian. Outcrops of this formation are present on the eastern flank of the Nátaga anticline (Yaguaracito riverbed) and extends to the south toward the municipality of El Pital. This formation is also apparent in the center of the Itaibe syncline, which is located on the flanks of the La Hocha anticline and at the NE termination of the La Guagua anticline (which runs from the north of Yaguará to Palermo) where it continues to the SW of its eastern flank. It also crops out to the north and east of Paicol (in the vicinity of the Paéz River), to the west of Yaguará, to the west and NW of Neiva, and from the NW of Neiva to the Aipe River.

The Yaguará Formation was described in the stratigraphic section from the Yaguará River, where it presents an excellent exposure. Lithologically, it is composed of quartz-arenites that vary in texture from fine to very fine, and in color between brown, gray and yellow, with intercalations of mudstones,



Figure 3. Typical escarpments of the Yaguará Formation (K2ya) that overlie the Lidita Superior (K2ls) and Aico (K2ai) formations that comprise the Olini Group and underlie the Seca Formation
Source: Terraza et al. (2019).

phosphates, porcelanites or quartz siltstones with glauconite, phosphate remains and dissolved calcareous concretions.

The Yaguará Formation underlies the Seca Formation, overlies the Lidita Superior Formation in sharp and concordant contact, and generates a prominent escarpment between these two units (see Figure 3). The Yaguará-Seca contact is considered a paraconformity (*sensu* Howe, 1997).

Buscavida (K2b) and La Tabla (K2lt) formations: late Campanian-early Maastrichtian. These formations emerge to the east of the La Plata (Chusma) fault in the area of the Media Luna syncline, which includes the Bambucá creek, where they have been previously described (SGC-UNAL Agreement, 2018). The morphological expression of the Buscavida Formation is of a narrow valley between the Lidita Superior and the La Tabla Formation, while the La Tabla Formation forms strong escarpments that are accentuated by the smooth landforms and topographic depressions generated by the mudstones and claystones of the overlying Seca formation.

To the south of the Bambucá creek, the exposed facies of the Buscavida (*sensu* Guerrero et al., 2000) and La Tabla formations change to the predominantly quartz-sandstone terrigenous lithofacies of the Yaguará Formation.

The Buscavida Formation overlies the Lidita Superior Formation and is in conformable sharp contact. Similarly, The Seca Formation overlies in concordant and sharp (paraconformable) contact the La Tabla Formation.

4.3. Phosphate-bearing Upper Cretaceous lithofacies

Table 1 shows the different facies in the Upper Cretaceous lithostratigraphic units that contain phosphates and correspond to the Santonian-Maastrichtian stratigraphic interval.

5. DISCUSSION

5.1. Facies characterization of the Santonian-Maastrichtian interval that contains phosphates

Lidita Inferior Formation. There is a predominance of chert facies to the north (Bambucá creek), where chert comprises 48% of the unit (Figure 4a). Toward the south, 35% of the unit consists of porcelanites with mudstone texture and phosphorites with peloids with packstone texture, while 12% of the unit consists of fish remains and phosphate clasts (Figure 4b). The phosphorite deposits are located toward the top of the unit. These phosphorite intervals can reach up to 90 cm in thick-

Table 1. Facies in the lithostratigraphic units that contain phosphates from the Upper Cretaceous (Santonian-Maastrichtian)

Unit	Facies and lamination	Stratification	Remarks	Associated Ichnofacies
Yaguará Formation	Very fine - fine grained sand, homogeneous appearance	Thick and very thick, Even nonparallel	Phosphates	<i>Teredolites, Thalassinoides</i>
	Very fine - fine grained sandstone, discontinuous wavy nonparallel	Thick and very thick. Even nonparallel	Calcareous	<i>Skolithos</i>
	Fossiliferous sands of medium grain, homogeneous appearance	Thick and very thick Curved, nonparallel	Calcareous with strong dissolution	<i>Thalassinoides</i>
	Very coarse-grained sandstone slightly conglomerate, cross-laminated, tangential to the base	Thick and very thick Curved, nonparallel		
	Quartz siltstones, Even parallel lamination	Medium and coarse, even parallel	Silicified	<i>Planolites</i>
	Porcelanite with Wackestone - mudstone texture, even parallel lamination	Thin and medium, even parallel	Fossiliferous-benthic foraminifera	
	Cherts with mudstone - wackestone texture, even parallel lamination	Thin, even parallel	Diagenetic Fossiliferous-Foraminifera Benthic Chert	
	Phosphorites with packstone and wackestone texture, homogeneous appearance	Thick and very thick, even nonparallel	Pellets, peloids, fish remains, phosphate intraclasts, benthic and planktonic foraminifera	
	Biosparites with grainstone-packstone texture, homogeneous appearance	Thick and very thick, curved parallel	Thick-shelled bivalves (ostreids), orientation of bioclasts	
	Biomicrorites with packstone texture, discontinuous, even nonparallel lamination	Medium and coarse, even nonparallel	Benthic foraminifera, bioclasts, peloids	
Sandy biosparites with wackestone texture, Discontinuous, even nonparallel lamination	Coarse to very coarse, discontinuous, curved nonparallel	Remains of thick-shelled bivalves (ostreidae)		
La Tabla Formation	Fine-grained sands, cross-laminated, tangential to the base	Very thick, even parallel	Clayey	
	Medium-grained sands, cross-laminated, tangential to the base	Coarse to very coarse, Curved, nonparallel		
	Coarse to very coarse-grained sands, cross-laminated, tangential to the base	Coarse to very coarse, Curved, nonparallel		
Buscavida Formation	Terrigenous Mudstones, Even parallel lamination	Thin and medium, Even parallel		
	Fossiliferous sandy lodolites, Wavy, nonparallel lamination	Thin to medium Even parallel	Calcareous	<i>Planolites</i>
	Siltstones, Wavy, nonparallel lamination	Thin to medium, Even parallel		<i>Thalassinoides</i>
Lidita Superior Formation	Cherts with mudstone- wackestone texture, Even parallel lamination	Thin, Even parallel	Diagenetic chert, benthic foraminifera	
	Phosphorites with packstone and wackestone texture, homogeneous appearance	Coarse to very coarse, Wavy, parallel to discontinuous, curved, nonparallel	Pellets, peloids, fish remains, phosphate intraclasts, benthic and planktonic foraminifera	
	Porcelanite with wackestone - mudstone texture, Even parallel lamination	Thin and medium, Even parallel		
	Quartz siltstones, continuous Even parallel lamination	Thin, even parallel	Silicified, calcareous	
	Wackestone biomicrorites, Wavy, parallel lamination	Thick, Wavy, parallel	Benthic and planktonic foraminifera, fish remains and peloids	
Aico Formation	Claystone with Discontinuous, wavy, nonparallel lamination	Thin and medium Discontinuous, even parallel	Pyritized Radiolaria	
	Terrigenous Mudstones with wavy nonparallel and discontinuous lamination	Thin even parallel		
	Porcelanite with wackestone texture, Discontinuous, even parallel lamination	Medium, even parallel	Phosphates	
	Fine-grained sandstones with Wavy, nonparallel lamination	Medium, even parallel	Calcareous	<i>Palaeophycus</i>
Aipe Formation	Very fine and fine-grained sands, Wavy, nonparallel lamination	Thick and very thick, Even nonparallel	Locally lithic	
	Quartz siltstones, Even parallel lamination	Thin Even parallel	Silicified-calcareous	
Lidita Inferior Formation	Porcelanite with mudstone texture, continuous parallel flat laminations	Continuous parallel plane, medium		
	Chert with mudstone -wackestone texture, even parallel lamination	Thin even parallel	Diagenetic chert, planktonic foraminifera	
	Phosphorites with wackestone and packstone texture, homogeneous appearance	Medium and coarse, even parallel	Pellets, peloids, fish remains, phosphate intraclasts, benthic and planktonic foraminifera	
	Terrigenous Mudstones, even parallel lamination	Thin and medium even parallel	Silicified	

ness. In the southern part, they can be up to 30 cm thick (e.g., sections of El Caney, Río Íquira and Río Yaguarcito). The Lidita Inferior Formation in the Itaibe creek was correlated with

the upper middle part of the layer N-14 described by Mendivelso (1982, 1993, Figure 3) and has a thickness of approximately 3 m.

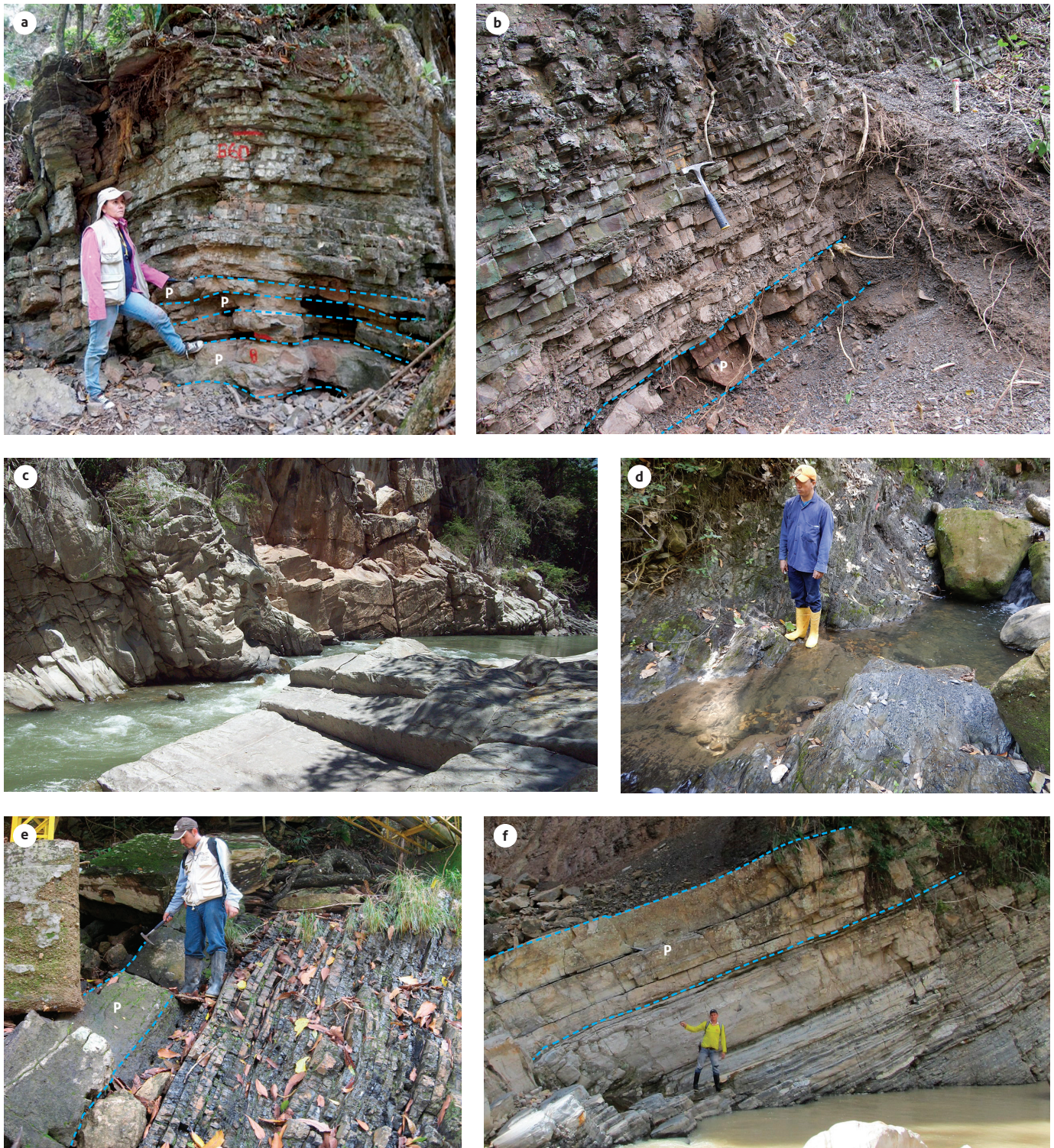


Figure 4. Characteristics of the Olini Group in some stratigraphic sections

a) Lidita Inferior Formation in the Yaya River stratigraphic section; porcelanites and cherts with phosphorite intercalations (P). b) Lidita Inferior Formation in the Íquira River stratigraphic section; thin layers of tabular porcelanite with a thin tabular layer of phosphorite (P) at the base. c) Aipe Formation in the Aipe River stratigraphic section comprised of very thick layers of quartz-arenites. d) Aico formation in the El Caney creek stratigraphic section, with fissile mudstones arranged in thin layers. e) Lidita Superior Formation in the Aipe River stratigraphic section; thin and medium subtabular layers of porcelanite with a thick wedged-shaped layer of phosphorite (P) interbedded. f) Lidita Superior Formation in the Íquira River stratigraphic section; medium layers of cherts with layers of phosphorite (P) on top. Source: Terraza et al. (2019).

Aipe Formation. The dominant facies of this formation (94% of the unit) consist of very thick layers of sandstone comprised of terrigenous sand (Figure 4c). However, the unit does not contain representative phosphate deposits. The thickness of the Aipe Formation in the Yaguaracito River is 26.3 m, and in the Aipe River, it is 76.6 m, displaying a thickening trend toward the north.

Aico formation. Typical clay facies represent 87% of this unit. However, fissile mudstones appear to a lesser extent, and occasionally hard levels of phosphatic porcelanite, very fine-grained sandstones and massive sandy limestone with packstone texture (Figure 4d). The Aico Formation is 20 m thick in the Caney creek, and 46.3 m thick in the Íquira River. Outcrops are mainly located in the southern part of the study area and in the east of the San Francisco fault. This unit was described in the stratigraphic sections from El Caney, Río Íquira, and partially in the Yaguará River. This unit represents a facial change for the Aipe Formation where these units are considered contemporary and heterotopic. The outcrops of the Aico Formation are 50 m thick in the Itaibe creek and correlate with the top of layer N14 described by Mendivelso (1982, 1993, Figure 3). The unit shows a tendency to thickening toward the SE (Figure 7).

Lidita Superior Formation. Chert facies with wackestone texture represent 38% of the unit, followed by peloidal phosphorites, which represent 29%, with packstone texture and wackestone, fish remains, planktonic and benthic foraminifera, layered with subtabular and canaliform shapes (Figures 4e and 4f). These facies do not exhibit internal laminations except at the base of the layers, where continuous nonparallel wavy laminations are seen. These have elongated and imbricated micritic intraclasts and decimetric chert nodules, spherical and ellipsoidal in size. Porcelanites, quartz-siltstones and some limestones compose 22% of the unit. The porcelanites are slightly calcareous, have wackestone and mudstone textures, and contain benthic and planktonic foraminifera arranged in very thin sheets. Additionally, phosphatic porcelanite with wackestone texture with benthic and planktonic foraminifera-bearing, peloids and fish remains are also found.

These beds are recurrent and are especially associated with phosphate levels. The laminations are interrupted by spherical chert nodules a centimeter in diameter and decimeter-scale ellipsoidal micritic concretions. Toward the top, it is common to observe phosphorite layers up to 70 cm thick with wackestone and packstone textures and wavy bases, which represent the most important accumulations of phosphates at the regional setting.

This unit shows a NE to SW thinning trend and has 31.6 m in thickness in the Bambucá creek and 9.4 m in the El Caney creek. In general, all the Upper Cretaceous units show this tendency; however, there is no correlation with the phosphate facies, as they are thicker toward the SW, possibly due to the proximity of the source area of the phosphate material.

Yaguará Formation. A total of 68.9% of the terrigenous facies are composed of quartz arenites; phosphatic quartz-arenites with peloids, phosphate clasts, glauconite and hydrocarbon inclusions; and fossiliferous friable quartz-arenites with centimeter-scale gastropod and bivalve remains and peloids (Figures 5a and 5b). Up to 24% of the terrigenous facies consist of phosphatic porcelanite and porcelanites with a mudstone and packstone texture, chert with a wackestone texture (with benthic and planktonic foraminifera) and siliceous siltstone (containing planktonic foraminifera and disseminated pyrite). Additionally, these units contain phosphatic siltstones that grade to very fine-textured phosphatic quartz-arenites, with siliceous cement, peloids and muscovite (Figure 5c). Regarding the relevant phosphate deposits, in the Divino Niño section to the NE of Paicol, there is a layer more than 2 m thick, which contains sandy phosphorite with a packstone texture (Figure 5d).

On the road between Hobo and Paicol, near the La Juanita phosphate mine, the La Juanita Member crops out, which is composed of calcareous facies likely deposited in a high energy environment. These facies consist of bivalve grainstone and fossilized sandy packstone, with sparitic cement, bivalve massif grainstone with articulated ostreid shells and sandy wackestone with weathered pale yellowish orange sparitic cement. Furthermore, all the beds in these facies are either conformable or oriented obliquely to the stratigraphy. These facies represent approximately 20% of the unit in this section (Figures 5e and 5f).



Figure 5. Main characteristics of the Yaguará Formation in some stratigraphic sections
 a) Aipe River stratigraphic section; thick and very thick layers of quartz-arenites in which cavities are observed due to the dissolution of calcareous concretions. b) The Yaguará River stratigraphic section; thick and very thick layers of phosphatic quartz-arenites in which cavities were formed due to dissolution of calcareous concretions and interspersed with thin layers of porcelanite and siltstones. c) Íquira River stratigraphic section; very fine-textured quartz-arenites overlaid by siliceous siltstones. d) Divino Niño stratigraphic section; phosphorites (P) with packstone texture. e) La Juanita stratigraphic section; bivalve grainstones in thick and solid layers in the middle part of the La Juanita Member. f) La Juanita stratigraphic section; grainstone to packstone containing ostreidae shown in detail at the bottom of the La Juanita Member. Source: Terraza et al. (2019).

Thickness of the Yaguará Formation is variable. This formation is thicker to the east of the study area. It is 134 m thick in the El Boquerón creek (Palermo municipality), 99 m in the typical section of the Yaguará River and 78 m in the Íquira River. The narrowest parts of the formation were registered in the Yaguaracito River, where it was on 19 m wide. In the Itai-be creek, the Yaguará Formation is approximately 150 m thick

and is correlated with the N-12 to N-5 layers of the Campanian and N-4 to N-1 of the Maastrichtian, as designated by Mendivelso (1982, 1993, Figure 3) for the Guadalupe Group.

The Yaguará Formation represents the facies change of the Buscavida and La Tabla formations, and for this reason it is assigned an equivalent age to these two units, which varies between the late Campanian and the early Maastrichtian.

5.2. Facies analysis of the Santonian-Maastrichtian interval that contains phosphates

Based on the interpretation of the facies and the lithocorrelations that have been carried out, the possible hydrodynamic conditions that prevailed on the sea floor during the accumulation of the phosphate-rich sediments in the Santonian-Maastrichtian period are inferred. For this interpretation, a generic morphological profile of a modern ramp-type coastal depositional system was taken as a reference, compiled from the published specialized literature (Figure 6).

The sediments observed in the facies from the Lidita Inferior and Lidita Superior formations accumulated on very low sloping sea floors, which is reflected in the parallel flat stratification of these units, and under low-energy and dysoxic conditions. This conclusion is suggested by the predominance of thinly laminated fine-granular facies arranged in a parallel and flat sequence and the absence of any bioturbation. Thus, these sediments belonged to a medium carbonate ramp environment, and were below the fair-weather wave action but above the baseline of storm-driven waves.

In the Lidita Inferior and Lidita Superior formations, sedimentation was influenced by waves and bottom currents,

which is expressed within the phosphate lithofacies. These lithofacies present slightly wavy stratification and lamination, parallel and nonparallel, canaliform layers, decreases in grain size, a low to moderate degree of bioturbation, and rounded and imbricated particles. The observed lithofacial characteristics support reworking processes by unidirectional marine currents induced by tides, normal waves and the energetic action of storm waves. In the case of the Lidita Inferior Formation, an enrichment in organic matter is observed (>1%), which suggests that accumulation occurred with minimal benthic oxygen levels (e.g., at the sediment-water interface, or a few centimeters below), which would have prevented oxidation and subsequent bacterial destruction. The appearance of benthic foraminifera is an indication of shallower conditions in the sedimentary environment, possibly toward the upper part of the middle ramp (upper offshore).

The Aipe and La Tabla formations, represented by clayey to silty sandstone, with grain sizes that vary from very fine to granule, correspond to moderate to high energy environments. Additionally, these environments contained active benthic organisms (with high degrees of bioturbation), had wavy to sloped laminations, and thick to very thick layers. These characteristics

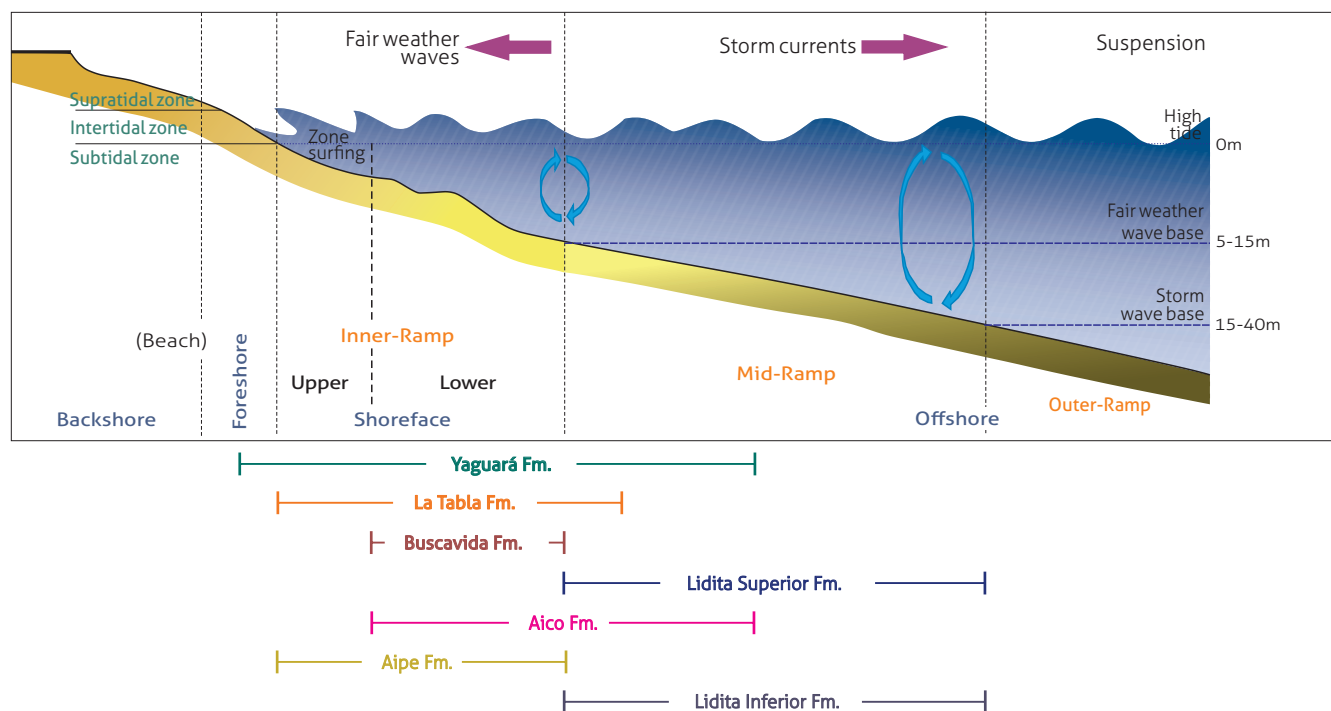


Figure 6. Interpreted sedimentary environment corresponding to the different Upper Cretaceous facies Based on Flügel and Munnecke (2010), Reineck and Singh (1980); Walker and Plint (1992); Evoy and Moslow (1995); Zelazny et al. (2018).

indicate an upper to lower shoreface depositional environment on an oxygenated bottom along the internal ramp.

The Buscavida Formation is characterized by facies that indicate environments with moderate to low energies, possibly indicative of hydrodynamic conditions along an internal ramp environment in the lower shoreface (Reineck and Singh, 1980). This interpretation is based on heterolytic laminations, the abundance of benthic foraminifera and the presence of burrows. Furthermore, it is common for sandstones and mudstones to be associated with calcareous deposits during periods of low terrigenous contribution. The hydrodynamic conditions inferred from the facies of the Aico Formation are similar, albeit shallower, to those of the Lidita Superior and Lidita Inferior formations, as evidenced by the benthic fauna and the sedimentary structures observed, probably associated with a lagoonal environment.

Finally, the Yaguará Formation presents facial variations that indicate variable hydrodynamic energy. With a predominance of sandstone facies with grain sizes that vary from very fine to fine, wavy laminations, layers with textural variations between coarse and very coarse, and evidence of high degrees of bioturbation (indicating locally complete disturbance) by the vigorous action of benthic organisms within the substrate. The energy of this environment ranged from moderate to high and likely represents a lower to upper shoreface configuration on an oxygenated bottom on the internal ramp. The fine-granular facies were thinly laminated, in parallel, and interspersed with siltstones, which suggests accumulation occurred in the middle ramp on a sea floor with low levels of hydrodynamic energy and below the action of the waves during good weather.

The La Juanita Member of the Yaguará Formation contains large accumulations of bioclastic carbonates (grainstone and packstone) and canaliform layers of disarticulated ostreids, with its long axis parallel to the stratification, which suggests that accumulation occurred in high energy areas with intense biological activity that were subjected to waves and unidirectional currents. This area was possibly a well oxygenated intertidal and subtidal zone that was located between the upper shoreface and the foreshore (Reineck and Singh, 1980).

5.3. Basin paleotopography for the phosphate-bearing Santonian-Maastrichtian interval

Based on the lithocorrelation of the Upper Cretaceous stratigraphic sections (Figures 7 and 8), for which a baseline was taken at the contact between the Yaguará and Seca formations,

the possible paleotopography of the basin in the western sector of the Neiva subbasin of the UMV that corresponds to the Santonian and Maastrichtian periods, is inferred.

The distribution, shape and thickness of the observed facies, as well as the lithostratigraphic units involved, allow us to suggest that tectonism conditioned the landforms of the basin floor. This tectonic activity was probably related to the uplift pulses of the ancient Central Cordillera during the Campanian and Maastrichtian periods (Salazar, 1992; Villamil, 1998; Velozza et al., 2008; Roncancio and Martínez, 2010; Bayona, 2018; Villamizar et al., 2021).

The uplift triggered a subsidence deformation mechanics that led to the creation of foreland basins (Jordan, 1995; Flemings and Jordan, 1990, Horton et al., 2010) and facilitated deposition within a tectonic post-graben environment (Föllmi et al., 1992, Horton et al., 2010). This dynamic tectonic framework allowed certain faults to control the accommodation space and the sediment accumulation conditions along the bottoms as well as the paleotopographic configuration of the sedimentary environments of the units studied here. This resulted in zones with differential subsidence essentially controlled by regional tectonics. As a product of this tectonism, there are synchronous and heterotopic lithostratigraphic units that show marked variability in terms of thickness and facies, as is the case of the Aipe vs. Aico and the Yaguará vs. Buscavida and La Tabla formations.

Depending on the intensity and periodicity of the tectonic uplift, there were periods in which the sedimentation was relatively more stable, which added to the relative eustatic sea level conditions and allowed the Lidita Inferior and Lidita Superior formations to be deposited in less dynamic environments. These units present facies associated with a relative rise in sea level with low rates of sharp accumulation of sediments under low energy conditions, as evidenced by their sedimentary structures.

Concomitantly, physicochemical mechanisms were developed that favored the supply and mobilization of nutrients, which led to the increase in bioproductivity that was necessary for phosphogenesis. Subsequently, the pristine phosphate generated was remobilized and concentrated by waves and bottom currents in layers of “granular” phosphates (sensu Glenn et al., 1994) or “allochthonous” phosphates (sensu Föllmi et al., 1992; Föllmi, 1996) in the Lidita Superior and Lidita Inferior Formations. The most likely accumulation mechanism would have occurred through storm-induced gravity sediment

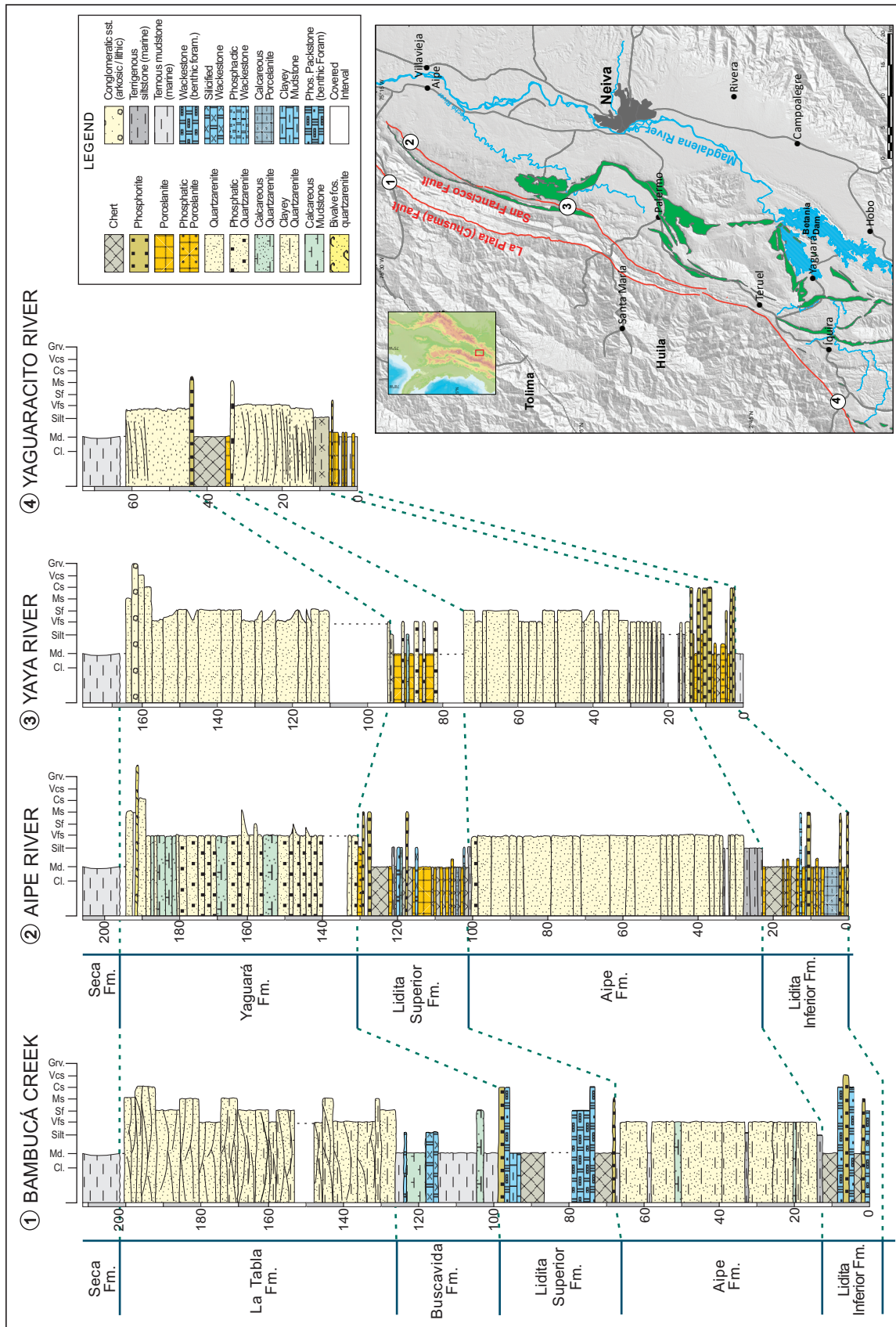


Figure 7. Lithocorrelation in the NE-SW direction within the western portion of the study area

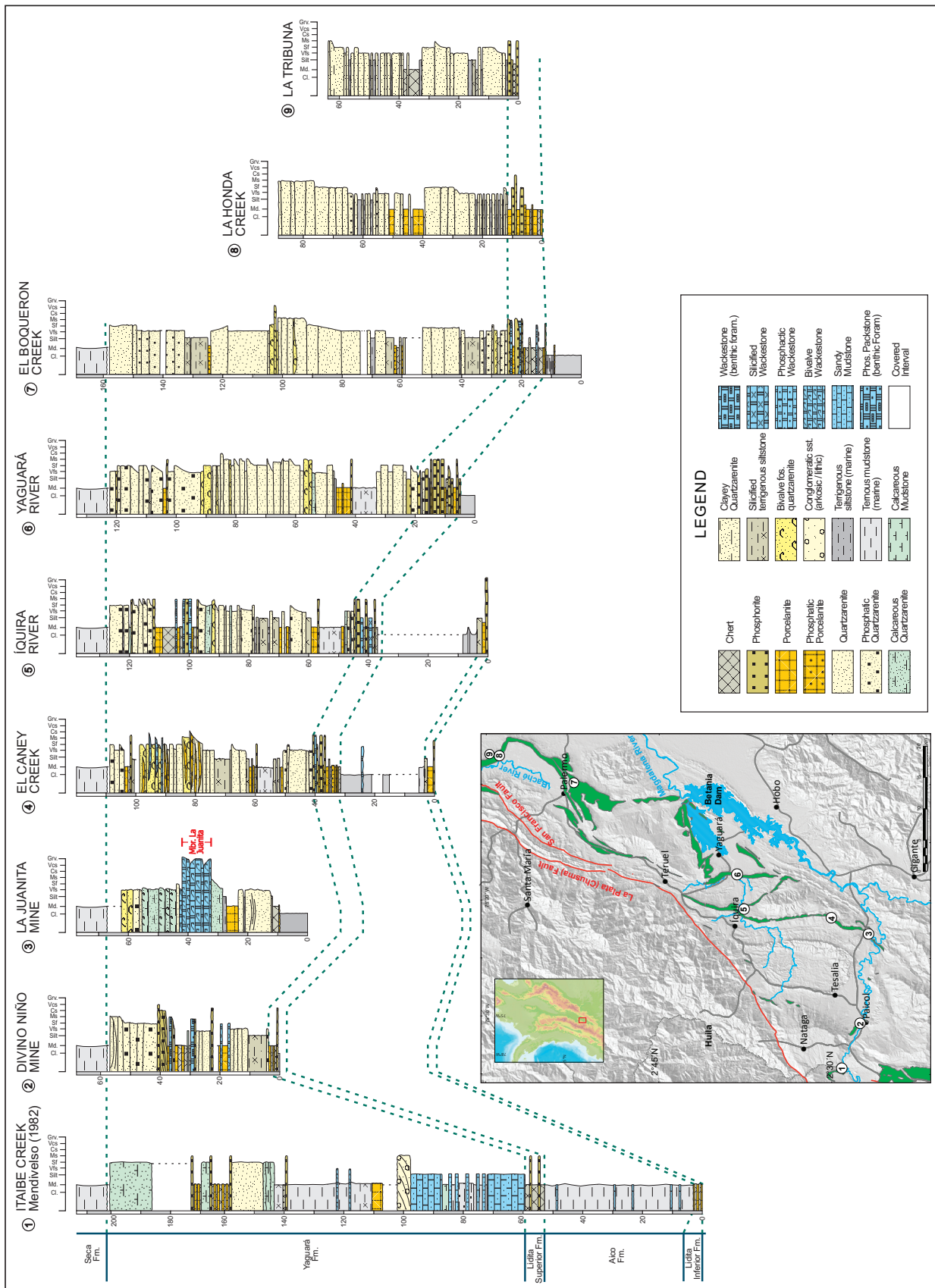


Figure 8. Lithocorrelation along the west to east orientation in the study area

flows. These flows were generated between the base level of the waves in both calm and stormy weather. Then, the flows amalgamated successively to form the layers of granular or allochthonous phosphate, which are the thickest and most economically interesting phosphate deposits in Colombia and worldwide (Grimm, 2000; Pufahl et al., 2003).

The accumulation mechanism of phosphorites associated with quartz-arenite rocks, such as those found in the Yaguará Formation (e.g., in the Divino Niño stratigraphic section, in NE Paicol, see Figure 4d), was possibly similar; the difference is in the hydrodynamic and depth conditions. To explain these coastal phosphorites, a rapid accumulation of granular phosphates is inferred in littoral areas due to storms, a process analogous to that described by Brenner and Davis (1973) to explain underdeveloped sand bars in intertidal plains. This type of deposit shows little lateral continuity, as confirmed by the geological mapping carried out in the surroundings of the El Divino Niño phosphate mine to the NE of Paicol. Furthermore, these deposits were specifically conditioned by the morphology of the bottom and the dynamics of the flow that mobilized them.

By comparing the thicknesses of the Upper Cretaceous lithostratigraphic units in the SN direction in the west of the study area (Figure 7), a thickening is observed oriented along the NE direction, which varies from slightly more than 60 m in the Yaguaracito River section to more than 200 m in the Bambucá creek section. This thickening trend is evident throughout the entire UMV basin, as reported by Vergara (1997) and Mora (2003), who affirm that the increase in accommodation space in the units to the north of the basin is notable, which allows for a greater accumulation of sediment.

It is feasible to consider that the sea floor on which these units were deposited did not present a continuous form but instead showed landforms, or a paleotopography, that would have controlled the thickness and distribution of the sediments, as well as the hydrodynamic conditions that impacted the sediments and the sedimentary environments. These interpretations can be inferred from the lithocorrelation that was carried out in the study area along the east to west orientation, (Figure 8).

It is inferred that toward the end of the Maastrichtian, there was a paraconformity (*sensu* Howe, 1997) between the deposits within the Yaguará or La Tabla formations and the Seca Formation. This is evidenced by the marked change from the fluvial environments in the Seca Formation to the reddish mudstones

and claystones of the marine facies from the upper shoreface as shown by the Yaguará or La Tabla Formations. Geological mapping shows that the Yaguará Formation, on the western flank of the La Hocha anticline, is gradually losing thickness along the north-south direction because the uppermost layers of the unit are progressively eroding, which confirms the proposed hypothesis. Roncancio and Martínez (2010) related this event to the first uplift pulses of the Central Cordillera, which initiated the folding of the sedimentary sequence in the UMV basin.

6. CONCLUSIONS

The detailed geological mapping and stratigraphic descriptions made it possible to specify that the Upper Cretaceous Lidita Inferior, Lidita Superior and Yaguará formations contain the phosphate layers of major economic interest, which correspond to phosphorites with packstone texture. The vertical and lateral distribution of these layers is conditioned by the compressive and transpressive structural style with dominant tectonic transport toward the east. This gave rise to the folding of the lithostratigraphic units of the Santonian-Maastrichtian interval where the phosphates are hosted. Furthermore, the deposits are truncated by regional faults, such as the La Plata (Chusma) and San Francisco faults, which complicate the modeling of these deposits.

The La Plata (Chusma) fault is considered the geological limit between the Central Cordillera and the Neiva subbasin in the UMV. The San Francisco fault is another important structure that truncates folds and the lithostratigraphic units where the phosphate deposits are found. Some of the main fold axes are curvilinear (e.g., the Tesalia syncline and La Hocha anticline) because the pre-Cretaceous basement affects the geomorphology of the structures.

The sedimentary components, textures and structures observed in the phosphorites suggest that sediment transport and accumulation was influenced by bottom currents and storm-induced waves through gravity flows or rapid accumulation of sediments in littoral sand bars in medium to very shallow marine environments. Likewise, the Upper Cretaceous facies (Santonian-Maastrichtian period) represented in the Lidita Inferior, Aipe, Aico, Lidita Superior, Yaguará, Buscavida and La Tabla formations suggest a shallow, ramp-like marine environment, with the seabed less than 40 m below the surface. Additionally, accumulation occurred from the transition zone to the upper shoreface to the middle ramp offshore. High ener-

gy storms, such as hurricanes and typhoons, syndepositionally reworked the pristine phosphate lithofacies, which later accumulated as allochthonous phosphorites (Föllmi et al., 1992; Föllmi, 1996) or granular phosphorites (Glenn et al., 1994).

The successive amalgamation of granular, or allochthonous, phosphate layers produced thicker deposits of greater economic interest (Grimm, 2000; Pufahl et al., 2003). These types of layers are the ones that appear in the study area and must have formed during the periods of maximum storm activity, thus generating phosphorites with packstone texture.

The distribution, shape and thickness of the facies observed in the Upper Cretaceous units that correspond to the Santonian-Maastrichtian interval, which appear as outcrops in the western regions of the Neiva subbasin, allow us to infer tectonism and exhumation of the source areas concomitant with sedimentation. This type of dynamic environment allowed certain faults to control the sediment accommodation space, the hydrodynamic conditions of the seafloor and the paleotopography of the basin, which resulted in zones with differential subsidence essentially controlled by regional tectonics.

ACKNOWLEDGMENTS

This research was carried out as part of the Phosphates and Magnesium Prospecting and Exploration project, code: 1001615, Dirección de Recursos Minerales of the SGC. The authors express their gratitude to Dr. Gloria Prieto Rincón for her full support and to Dr. Fernando Etayo Serna for his advice on the chronostratigraphy of the different lithostratigraphic units that were mapped. We thank the anonymous reviewers and the Editorial Committee of the *Boletín Geológico* of the SGC for their comments and suggestions. Finally, we thank the geographer Hernán Cifuentes for his determined technical support to the working group.

REFERENCES

- Bayona, G., García, D., & Mora, G. (1994). La Formación Saldaña: producto de la actividad de estratovolcanes continentales en un dominio retro-arco. In F. Etayo Serna (dir.), *Estudios geológicos del Valle Superior del Magdalena*. Universidad Nacional de Colombia. W. Taller Editorial Ltda.
- Bayona, G. (2018). El inicio de la emergencia en los Andes del norte: una perspectiva a partir del registro tectónico-sedimentológico del Coniaciano al Paleoceno. *Revista de la Academia Colombiana de Ciencias Exactas, Físicas y Naturales*, 42(165), 364-378. <http://dx.doi.org/10.18257/raccefyn.632>
- Beltrán, N., & Gallo, J. (1968). *The geology of Neiva Sub-Basin Upper Magdalena Basin, southern portion*. Ninth Annual Field Conference. Colombian Society of Petroleum Geologists and Geophysicists.
- Brenner, R. L., & Davis, K. D. (1973). Storm-generated coquina sandstone: Genesis of high-energy marine sediments from the Upper Jurassic of Wyoming and Montana. *GSA Bulletin*, 84(5), 1685-1698. [https://doi.org/10.1130/0016-7606\(1973\)84<1685:SCSGOH>2.0.CO;2](https://doi.org/10.1130/0016-7606(1973)84<1685:SCSGOH>2.0.CO;2)
- Bürgl, H., & Botero, D. (1967). Las capas fosfáticas de la cordillera Oriental. *Boletín Geológico*, 15(1-3), 7-44. <https://doi.org/10.32685/0120-1425/bolgeol15.1-3.1967.88>
- Bustamante, C., Archanjo, C. J., Cardona, A., & Vervoort, J. D. (2016). Late Jurassic to Early Cretaceous plutonism in the Colombian Andes: A record of long-term arc maturity. *GSA Bulletin*, 128(11-12), 1762-1779. <https://doi.org/10.1130/B31307.1>
- Butler, K., & Schamel, S. (1988). Structure along the eastern margin of the Central Cordillera, Upper Magdalena Valley, Colombia. *Journal of South American Earth Sciences*, 1(1), 109-120. [https://doi.org/10.1016/0895-9811\(88\)90019-3](https://doi.org/10.1016/0895-9811(88)90019-3)
- Cáceres, C., Cediel, F., & Etayo, F. (2003). *Mapas de distribución de facies sedimentarias y almacén tectónico de Colombia a través del Proterozoico y del Fanerozoico*. Ingeominas.
- Campbell, C. (1967). Lamina, laminaset, bed and bedset. *Sedimentology*, 8(1), 7-26. <https://doi.org/10.1111/j.1365-3091.1967.tb01301.x>
- Compton, R. (1985). *Geology in the field*. John Wiley & Sons, Inc.
- Conpes 3577 (2009). *Política nacional para la racionalización del componente de costos de producción asociado a los fertilizantes en el sector agropecuario*. Departamento Nacional de Planeación.
- Conpes 3577 (2009). *Política nacional para la racionalización del componente de costos de producción asociado a los fertilizantes en el sector agropecuario*. Departamento Nacional de Planeación.
- Cathcart, J., & Zambrano, F. (1967). Roca fosfática en Colombia, con una sección sobre fosfatos de Turmequé, Boyacá. *Boletín Geológico*, 15(1-3), 65-162. <https://doi.org/10.32685/0120-1425/bolgeol15.1-3.1967.210>
- Cook, P., & Shergold, J. (1986). Proterozoic and Cambrian phosphorites: An introduction. In *Phosphate deposits of the*

- World, vol. 1: Proterozoic and Cambrian phosphorites. Cambridge University Press.
- Dunham, R. (1962). Classification of carbonate rocks according to depositional texture. In W. E. Ham (ed.), *Classification of Carbonate Rocks, a Symposium* (pp. 108-121). American Association of Petroleum Geologists. <https://doi.org/10.1306/M1357>
- Etayo, F. (1994). A modo de historia geológica del Cretácico en el valle superior del Magdalena. In F. Etayo Serna (dir.), *Estudios geológicos del Valle Superior del Magdalena*. Universidad Nacional de Colombia.
- Evoy, R. W., & Moslow, T. F. (1995). Lithofacies associations and depositional environments in the Middle Triassic Doig Formation, Buick Creek Field, northeastern British Columbia. *Bulletin of Canadian Petroleum Geology*, 43(4), 461-475. <https://doi.org/10.35767/gscpgbull.43.4.461>
- Flemings, P. B., & Jordan, T. E. (1990). Stratigraphic modeling of foreland basins: Interpreting thrust deformation and lithospheric rheology. *Geology*, 18(5), 430-435. [https://doi.org/10.1130/0091-7613\(1990\)018<0430:SMOFBI>2.3.CO;2](https://doi.org/10.1130/0091-7613(1990)018<0430:SMOFBI>2.3.CO;2)
- Flórez, M., & Carrillo, G. (1994). Estratigrafía de la sucesión litológica basal del Cretácico del valle superior del Magdalena. In F. Etayo Serna (dir.), *Estudios geológicos del valle superior del Magdalena*. Universidad Nacional de Colombia.
- Flügel, E., & Munnecke, A. (2010). *Microfacies of carbonate rocks: Analysis, interpretation and application*. Springer.
- Folk, R. (1951). Stages of textural maturity in sedimentary rocks. *Journal of Sedimentary Research*, 21(3), 127-130. <https://doi.org/10.2110/jsr.21.127>
- Folk, R. (1954). The distinction between grain size and mineral composition in sedimentary-rock nomenclature. *The Journal of Geology*, 62(4), 344-359. <https://doi.org/10.1086/626171>
- Folk, R. (1959). Practical petrographic classification of limestones. *The American Association of Petroleum Geologists Bulletin*, 43(1), 1-38. <https://doi.org/10.1306/0BDA5C36-16BD-11D7-8645000102C1865D>
- Folk, R. (1962). Spectral subdivision of limestone types. In W. E. Ham (ed.), *Classification of Carbonate Rocks, a Symposium* (pp. 62-84). American Association of Petroleum Geologists. <https://doi.org/10.1306/M1357>
- Folk, R., & Siedlecka, A. (1974). The "schizohaline" environment: its sedimentary and diagenetic fabrics as exemplified by Late Paleozoic rocks of Bear Island, Svalbard. *Sedimentary Geology*, 11(1), 1-15. [https://doi.org/10.1016/0037-0738\(74\)90002-5](https://doi.org/10.1016/0037-0738(74)90002-5)
- Folk, R. (1980). *Petrology of sedimentary rocks*. Hemphill Publishing Co.
- Föllmi, K. B. (1990). Condensation and phosphogenesis: Example of the Helvetic mid-Cretaceous (northern Tethyan margin). Special Publications, vol. 52. Geological Society of London. <https://doi.org/10.1144/GSL.SP.1990.052.01.17>
- Föllmi, K. B. (1996). The phosphorus cycle, phosphogenesis and marine phosphate-rich deposits. *Earth-Science Review*, 40(1-2), 55-124. [https://doi.org/10.1016/0012-8252\(95\)00049-6](https://doi.org/10.1016/0012-8252(95)00049-6)
- Föllmi, K. B., Garrison, R. E., Ramírez, P. C., Zambrano Ortiz, F., Kennedy, W. J., & Lehner, B. L. (1992). Cyclic phosphate-rich successions in the Upper Cretaceous of Colombia. *Palaeogeography, Palaeoclimatology, Palaeoecology*, 93(3-4), 151-182. [https://doi.org/10.1016/0031-0182\(92\)90095-M](https://doi.org/10.1016/0031-0182(92)90095-M)
- Fürsich, F. (1995). Shell concentrations. *Eclogae Geologicae Helveticae*, 88(3), 643-655.
- Glenn, C., Föllmi, K., Riggs, S., Baturin, G., Grimm, K., Trappe, J., Abed, A., Galli-Olivier, C., Garrison, R., Ilyin, A., Jehl, C., Rohrlich, V., Rushdi, Sadaqah, R., Schidrowski, M., Sheldon, R., & Siegmund, H. (1994). Phosphorus and phosphorites: Sedimentology and environments of formation. *Eclogae Geologicae Helveticae*, 87(3), 747-788.
- Grimm, K. A. (1997). Phosphorites feed people. *Farm Folk/City Folk's Newsletter*, (13), 4-5.
- Grimm, K. A. (2000). Stratigraphic condensation and the redeposition of economic phosphorite: Allostratigraphy of Oligo-Miocene shelfal sediments, Baja California Sur, Mexico. In C. R. Glenn, L. Prévôt-Lucas & J. Lucas (eds.), *Marine Authigenesis: From Global to Microbial*. Society for Sedimentary Geology. <https://doi.org/10.2110/pec.00.66.0325>
- Guerrero, J., Sarmiento, G., & Navarrete, R. (2000). The stratigraphy of the W. side of the Cretaceous Colombian Basin in the Upper Magdalena Valley: Reevaluation of selected areas and type localities including Aipe, Guaduas, Ortega, and Piedras. *Geología Colombiana*, 25, 45-110.
- Hampson, G., & Storms, J. E. (2003). Geomorphological and sequence stratigraphic variability in wave-dominated, shoreface-shelf parasequences. *Sedimentology*, 50(4), 667-701. <https://doi.org/10.1046/j.1365-3091.2003.00570.x>
- Hernández, J., & Urueña, C. (2017). Aspectos geocronológicos y petrogenéticos del Complejo Aleluya: implicaciones en la exploración de Mg en el norte del departamento del Huila, Colombia. *Memorias XVI Congreso Colombiano de Geología*, Santa Marta, August 28 to September 1, 2017.

- Horton, B. K., Saylor, J. E., Nie, J., Mora, A., Parra, M., Reyes-Harker, A., & Stockli, D. F. (2010). Linking sedimentation in the northern Andes to basement configuration, Mesozoic extension, and Cenozoic shortening: Evidence from detrital zircon U-Pb ages, Eastern Cordillera, Colombia. *GSA Bulletin*, 122(9-10), 1423-1442. <https://doi.org/10.1130/B30118.1>
- Howe, R. (1997). Geologic contacts. *Journal of Geoscience Education*, 45(2), 133-136. <https://doi.org/10.5408/1089-9995-45.2.133>
- Ingram, R. (1954). Terminology for the thickness of stratification and parting units in sedimentary rocks. *GSA Bulletin*, 65(9), 937-938. [https://doi.org/10.1130/0016-7606\(1954\)65\[937:TFTTOS\]2.0.CO;2](https://doi.org/10.1130/0016-7606(1954)65[937:TFTTOS]2.0.CO;2)
- Jiménez, G., Rico, J., Bayona, G., Montes, C., Rosero, A., & Sierra, D. (2012). Analysis of curved folds and fault/fold terminations in the southern Upper Magdalena Valley of Colombia. *Journal of South American Earth Sciences*, 39, 184-201. <https://doi.org/10.1016/j.jsames.2012.04.006>
- Jordan, T. E. (1995). Retroarc Foreland and related basins. In C. J. Busby & R. V. Ingersoll (eds.), *Tectonics of sedimentary basins* (pp. 331-362). Blackwell Science.
- Julivert, M. (1970). Cover and basement tectonics in the Cordillera Oriental of Colombia, South America, and a comparison with some other folded chains. *GSA Bulletin*, 81(12), 3623-3646. [https://doi.org/10.1130/0016-7606\(1970\)81\[3623:CAB-TIT\]2.0.CO;2](https://doi.org/10.1130/0016-7606(1970)81[3623:CAB-TIT]2.0.CO;2)
- Kamola, D., & Van Wagoner, J. (1995). Stratigraphy and facies architecture of parasequences with examples from the Spring Canyon Member, Blackhawk Formation, Utah. In *Sequence Stratigraphy of Foreland Basin Deposits: Outcrop and Subsurface Examples from the Cretaceous of North America*, AAPG Memories vol. 64. American Association of Petroleum Geologists. <https://doi.org/10.1306/M64594C3>
- Kammer, A., Piraquive, A., Gómez, C., Mora, A., & Velásquez, A. (2020). Structural styles of the Eastern Cordillera of Colombia. In *The geology of Colombia*, vol. 3. Servicio Geológico Colombiano. <https://doi.org/10.32685/pub.esp.37.2019.06>
- Krumbein, W., & Sloss, L. (1969). *Estratigrafía y sedimentación*. Uteha.
- Mendivelso, D. (1982). *Aspectos fotogeológicos y estratigráficos del Cretáceo en la región de Itaiibe (valle superior del Magdalena)* (Bachelor thesis). Universidad Nacional de Colombia.
- Mendivelso, D. (1993). Aspectos fotogeológicos y estratigráficos del Cretáceo por la quebrada Itaiibe, valle superior del río Magdalena, Colombia. *Revista Cipres*, 14(1), 67-84.
- Miall, A. D. (1984). Variations in fluvial style in the lower Cenozoic synorogenic sediments of the Canadian Arctic Islands. *Sedimentary Geology*, 38(1-4), 499-523. [https://doi.org/10.1016/0037-0738\(84\)90091-5](https://doi.org/10.1016/0037-0738(84)90091-5)
- Mojica, P. (1987). Fosfatos. In *Recursos minerales de Colombia* (t. II, pp. 856-893). Ingeominas.
- Mojica, J., & Franco, R. (1990). Estructura y evolución tectónica del valle medio y superior del Magdalena, Colombia. *Geología Colombiana*, 17, 41-64.
- Moore, D., & Scruton, P. (1957). Minor internal structures of some recent unconsolidated sediments. *American Association of Petroleum Geologists Bulletin*, 41(12), 2723-2751. <https://doi.org/10.1306/0bda59db-16bd-11d7-8645000102c1865d>
- Mora, A. (2003). *Modelo estratigráfico para el Cretácico Basal (Aptiano-Albiano) en el norte de la subcuenca de Neiva, valle superior del Magdalena, Colombia*. 8.º Simposio Bolivariano, Exploración Petrolera en las Cuencas Subandinas. European Association of Geoscientists and Engineers.
- Morales, C., Caicedo, J., Velandia, F., & Núñez, T. (2001). *Geología de la plancha 345, Campoalegre: Memoria explicativa*. Ingeominas.
- Nichols, G. (1999). *Sedimentology and Stratigraphy*. Blackwell Science.
- Notholt, A. J. G. (1985). Phosphorite resources in the Mediterranean (Tethyan) phosphogenic province: A progress report. *Sciences Géologiques, Bulletins et Mémoires*, 77(1), 9-17.
- Powers, M. (1953). A new roundness scale for sedimentary particles. *Journal of Sedimentary Research*, 23(2), 117-119. <https://doi.org/10.1306/0bda59db-16bd-11d7-8645000102c1865d>
- Ptáček, P. (2016). Phosphate rocks. En *Apatites and their synthetic analogues: Synthesis, structure, properties and applications*. IntechOpen. <https://doi.org/10.5772/59882>
- Pufahl, P. K., Grimm, K. A., Abed, A. M., & Sadaqah, R. M. (2003). Upper Cretaceous (Campanian) phosphorites in Jordan: Implications for the formation of a south Tethyan phosphorite giant. *Sedimentary Geology*, 161(3-4), 175-205. [https://doi.org/10.1016/S0037-0738\(03\)00070-8](https://doi.org/10.1016/S0037-0738(03)00070-8)
- Reineck, H., & Singh, I. (1980). *Depositional sedimentary environments (with reference to terrigenous clastics)* (2.ª ed.). Springer-Verlag.
- Reineck, H., & Wunderlich, F. (1968). Classification and origin of flaser and lenticular bedding. *Sedimentology*, 11(1-2), 99-104. <https://doi.org/10.1111/j.1365-3091.1968.tb00843.x>
- Rodríguez, G., Arango, M. I., Zapata, G., & Bermúdez, J. G. (2018). Petrotectonic characteristics, geochemistry, and U-Pb geochronology of Jurassic plutons in the Upper Magdalena

- Valley-Colombia: Implications on the evolution of magmatic arcs in the NW Andes. *Journal of South American Earth Sciences*, 81, 10-30. <https://doi.org/10.1016/j.jsames.2017.10.012>
- Roncancio, J., & Martínez, M. (2010). Upper Magdalena Basin. In F. Cediél & F. Colmenares (eds.), *Petroleum geology of Colombia*, vol. 14. Agencia Nacional de Hidrocarburos.
- Salazar, A. (1992). *Depositional and paleotectonic settings of the Cretaceous sequence, Upper Magdalena Valley, Colombia* S. A. (Ph. D. thesis). University of South Carolina.
- Sarmiento Rojas L. F. (2019). Cretaceous stratigraphy and paleo-facies maps of Northwestern South America. In F. Cediél & R. P. Shaw (eds.), *Geology and tectonics of Northwestern South America*. Frontiers in Earth Sciences. Springer. https://doi.org/10.1007/978-3-319-76132-9_10
- Servicio Geológico Colombiano, & Universidad Nacional de Colombia. (2018). Convenio Especial de Cooperación n.º 13 de 2017. Potencial de fosfatos en un sector del valle superior del Magdalena mediante el estudio estratigráfico de las rocas cretácicas, haciendo énfasis en el Cretáceo superior.
- Soudry, D., Glenn, C. R., Nathan, Y., Segal, I., & VonderHaar, D. (2006). Evolution of Tethyan phosphogenesis along the Northern edges of the Arabian-African shield during the Cretaceous-Eocene as deduced from temporal variations of Ca and Nd isotopes and rates of P accumulation. *Earth-Science Reviews*, 78(1-2), 27-57. <https://doi.org/10.1016/j.earscirev.2006.03.005>
- Swanson, R. (1981). *Sample examination manual*. AAPG Methods in Exploration Series, vol. 1. The American Association of Petroleum Geologists. <https://doi.org/10.1306/Mth1413>
- Terraza, R. (2019). "Formación La Luna": expresión espuria en la geología colombiana. In F. Etayo-Serna (dir.), *Estudios geológicos y paleontológicos sobre el Cretácico en la región del embalse del río Sogamoso, Valle Medio del Magdalena*. Compilación de los Estudios Geológicos Oficiales en Colombia, vol. XXIII. Servicio Geológico Colombiano. <https://doi.org/10.32685/9789585231788-5>
- Terraza, R., Martín, C., Martínez, G., & Rojas, N. (2016). *Exploración geológica de fosfatos en el Bloque Boyacá, planchas 191 y 210*. Informe técnico. Servicio Geológico Colombiano.
- Terraza, R., Martín, C., Martínez, G., Rojas, S., & Rojas, N. (2019). *Exploración geológica de fosfatos en el departamento del Huila, costado occidental del río Magdalena. Planchas 302, 323, 344, 345 y 366*. Informe técnico. Servicio Geológico Colombiano.
- Terraza Melo, R., Martín Rincón, C. L., Martínez Aparicio, G. A., Rojas Jiménez, S. T., Rojas Parra, N. R., & Hernández González, J. S. (2019). *Litoestratigrafía estandarizada para el valle superior del Magdalena, subcuenca de Neiva, costado W del río Magdalena*. Publicaciones Especiales del Servicio Geológico Colombiano.
- The Geological Society of America. (1995). *Rock-color chart*. Prepared by The Rock-Color Chart Committee, 8th printing.
- United States Geological Survey-USGS. (2022). *Mineral commodity summaries 2022*. U.S. Geological Survey, 202 p. <https://doi.org/10.3133/mcs2022>
- Van Wagoner, J., Mitchum, R., Campion, K., & Rahmanian, V. (1990). Siliciclastic sequence stratigraphy in well logs, cores and outcrops: Concepts for high-resolution correlation of time and fades. *AAPG Methods in Exploration Series*, (7), 55.
- Veloza, G, Mora, A., De Freitas, M., & Mantilla, M. (2008). Dislocación de facies en el tope de la secuencia cretácica de la subcuenca de Neiva, valle superior del Magdalena, y sus implicaciones en el modelo estratigráfico secuencial colombiano. *Boletín de Geología*, 30(1), 29-44.
- Vergara, L. (1997). Stratigraphy, foraminiferal assemblages and paleoenvironments in the late Cretaceous of the Upper Magdalena Valley, Colombia (part I). *Journal of South American Earth Sciences*, 10(2), 111-132. [https://doi.org/10.1016/S0895-9811\(97\)00010-2](https://doi.org/10.1016/S0895-9811(97)00010-2)
- Villamil, T. (1998). Chronology, relative sea-level history and a new sequence stratigraphic model for basinal Cretaceous facies of Colombia. In L. James & C. D. Pindell (eds.), *Paleogeographic Evolution and Non-Glacial Eustasy, Northern South America* (pp. 161-216). Special publication vol. 58. SEPM Society for Sedimentary Geology.
- Villamizar, N., Bernet, M., Urueña, C., Hernández, J. S., Terraza, R., Roncancio, J., & Piraquive, A. (2021). Thermal history of the Southern Central Cordillera and its exhumation record in the Cenozoic deposits of the Upper Magdalena Valley, Colombia. *Journal of South American Earth Sciences*, 107, 103-105. <https://doi.org/10.1016/j.jsames.2020.103105>
- Walker, R. G., & Plint, A. G. (1992). Wave and storm dominated shallow marine systems. In R. G. Walker & N. P. James (eds.), *Facies models: Response to sea-level change* (pp. 219-238). Geological Association of Canada.
- Wilkins, A. D. (2011). *Terminology and the classification of fine-grained sedimentary rocks: Is there a difference between a claystone, a mudstone and a shale?* University of Aberdeen.

- Williams, H., Turner, F., & Gilbert, C. (1954). *Petrography: An introduction to the study of rocks in thin sections*. W. H. Freeman & Company, Inc.
- Zapata, S., Cardona, A., Jaramillo, J. S., Patiño, A., Valencia, V., León, S., Mejía, D., Pardo-Trujillo, A., & Castañeda, J. (2019). Cretaceous extensional and compressional tectonics in the Northwestern Andes, prior to the collision with the Caribbean oceanic plateau. *Gondwana Research*, 66, 207-226. <https://doi.org/10.1016/j.gr.2018.10.008>
- Zambrano, F., & Mojica, P. (1990). Characteristics of Colombian phosphate deposits. In G. E. Ericksen, M. T. Cañas Pinochet & J. A. Reinemund (eds.), *Geology of the Andes and its relation to hydrocarbon and mineral resources*. Circum-Pacific Council for Energy and Mineral Resources Earth Science Series, v. 11.
- Zelazny, I. V., Gegolick, A., Zonneveld, J. P., Playter, T., & Moslow, T. F. (2018). Sedimentology, stratigraphy and geochemistry of Sulphur Mountain (Montney equivalent) Formation outcrop in south central Rocky Mountains, Alberta, Canada. *Bulletin of Canadian Petroleum Geology*, 66(1), 288-317.

Corrigendum

Corrigendum to "Interpretation of Palaeozoic geofoms with the use of seismic attributes in a region of the Eastern Plains, Colombia" [*Boletín Geológico*, 49(1), 2022]

Laura Carolina Esquivel¹, Fanny Villamizar², Indira Molina¹

¹ University of the Andes. Now at Servicio Geológico Colombiano, Bogotá, Colombia.

² Servicio Geológico Colombiano, Bogotá, Colombia.

Corresponding author: Laura Carolina Esquivel, lc.esquivel10@uniandes.edu.co

Original article: 2022, 49(1) : <https://doi.org/10.32685/0120-1425/bol.geol.49.1.2022.557>

First published: April 24, 2022

DOI: <https://doi.org/10.32685/0120-1425/bol.geol.49.2.2022.686>

The authors regret the error in the map of figure 1 where the location of the area was incorrectly shown, and the error in figure 5 where the connection of well-3 with the Paleozoic was omitted.

The authors wish to apologize for any inconvenience caused. The correct figures are the following:



Figure 1. Location of the study area in the Eastern Plains basin in Colombia

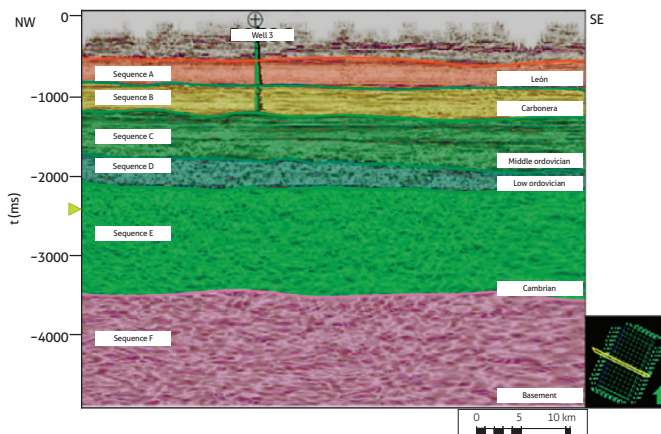


Figure 5. Sequences established for the study area (*Inline: 650*)

Boletín Geológico

Editorial Policy and Author Guidelines

The Editorial Policy and the Author Guidelines are available online in the web page of the journal:
<https://revistas.sgc.gov.co/index.php/boletingeo/index>

CONTENTS

3 Editorial

Mario Maya

Data article

5 **Macroseismic intensity data and effects of significant earthquakes in Colombia based on historical seismicity studies**

Ana Milena Sarabia Gómez, Diana Rocío Barbosa Castro, María Mónica Arcila Rivera

Review article

15 **Evolution of arc magmatic cycles from the Carboniferous to the Early Cretaceous in the western paleomargin of Gondwana, north of the Andes**

Gabriel Rodríguez García, Ana María Correa Martínez, Juan Pablo Zapata, Diego Armando Ramírez, Carlos Andrés Sabrica

Research article

45 **Potential and prospects for hydrogeological exploration according to lithostructural criteria in Antioquia department, Colombia**

Teresita Betancur, Cristina Martínez

Research article

65 **Geomechanical characterization of samples in the pilot zone of Bogotá, Colombia, to determine its potential as aggregates for construction**

Juan Ricardo Troncoso Rivera, Nelly Páez Fonseca, Óscar René Másmela Rodríguez, Leonardo Fuentes Aldana and Roberto Terraza Melo

Research article

75 **The Upper Cretaceous (Santonian-Maastrichtian) phosphate deposits in the west of the Neiva subbasin, Upper Magdalena Valley, Colombia**

Claudia L. Martín Rincón, Roberto Terraza Melo, Nadia R. Rojas Parra, Germán A. Martínez Aparicio, Sandra Rojas Jiménez, Juan S. Hernández González

97 Corrigendum

Corrigendum to "Interpretation of Palaeozoic geofoms with the use of seismic attributes in a region of the Eastern Plains, Colombia" [Boletín Geológico, 49(1), 2022]

Laura Carolina Esquivel, Fanny Villamizar, Indira Molina



MINISTERIO DE MINAS Y
ENERGÍA

